Projecte Final de Carrera

Microstrip Patch Antenna Design with Artificial Material Loadings

Irena CALAFELL RUEDA

Dirigit per:

José Mª. GONZÁLEZ-ARBESÚ
Pere J. FERRER

Microstrip Patch Antenna Design with Artificial Material Loadings

Irena Calafell Rueda

February 19, 2009

Agraïments

Primer de tot i sobretot gràcies als meus pares. Sí, per haver-me suportat tots aquest anys..., tot i que això no sigui garantia de no haver-me de suportar més temps! Sense aquest suport, és tipic però és veritat, no seria on sóc ara. També gràcies al meu germà Roger, que sempre em fa riure fins i tot quan m'enfado amb ell. I gràcies a l'Enric, per haver-me trobat.

Gràcies a tots els companys i companyes que han esdevingut amics importants en el transcurs d'aquests anys: Raquel, Tamara, Silvia, Cristina S., Marta, Mari, Mireia M., Cris B., Esther P., Miriam, Alberto, Rubén, Raúl, Carlos, David, Javi G., Juan, Marc V., Pau, Xavi..., hem compartit classes, pràctiques, dinars al Polipuaj (però de tàper eh, amb la salut no fem broma! I aquesta música de la Soraya...), cues per agafar lloc a la biblioteca, cues per agafar lloc al laboratori de DCISE (tot i que això més que compartir era competència bruta), cues per anar al labavo a plorar després de sortir d'un exàmen (això era broma..., o no?), i fins i tot sopars, festes...

Gràcies als meus tutors Pere J. Ferrer i Chema González pel seu transvassament de coneixements, la seva paciència, i per haver-me donat l'oportunitat d'aprendre realitzant el projecte que en aquest treball presento.

També gràcies als qui, d'una manera o altra, m'han ajudat en el dia a dia al departament: Benji (sí, al final t'he posat als agraiments!), Javi A., Dani M.,Vero, Cristina, Isaac, Bea, Santi...

Abstract

Conventional microstrip patch antennas can be easily miniaturized by increasing the substrate electric permittivity (ε_r) although the fractional bandwith (FBW) is dramatically decreased. In this work, the use of metamaterials as artificial antenna substrates is studied as an alternative method to efficiently miniaturize patch antennas, accounting not only electric permittivity ε_r but also magnetic permeability μ_r.

In addition, a compact FBW formulation proposed by Yaghjian et al. [10] is applied to compute the maximum achievable bandwidth of patch antennas with both homogeneous and dispersive material substrates.

Several prototypes with artificial metasubstrates have been fabricated to assess the simulations results, leading to a proper patch antenna miniaturization while maintaining its FBW.

Contents

Chapter 1

Introduction

Modern communication systems, from wireless to space communications, require compact and light weight components. One important component is the antenna, which, in addition, is required to have sufficiently high gain, wide bandwidth, high efficiency and to be easy to fabricate. Patch antennas are commonly used in these aplications, since they inherently have low profile and low weigth apart from having a low fabrication cost. Printed antennas, thanks to their planar geometry, are usually integrated in devices mounted on a platform (for example in a mobile telephone). However, printed antennas on substrates which have a metallic ground plane possess a limited bandwidth and efficiency.

Figure 1.1: Evolution of the mobile handsets (top) and laptops (bottom). The trend is to miniaturize those devices in order to offer more portability.

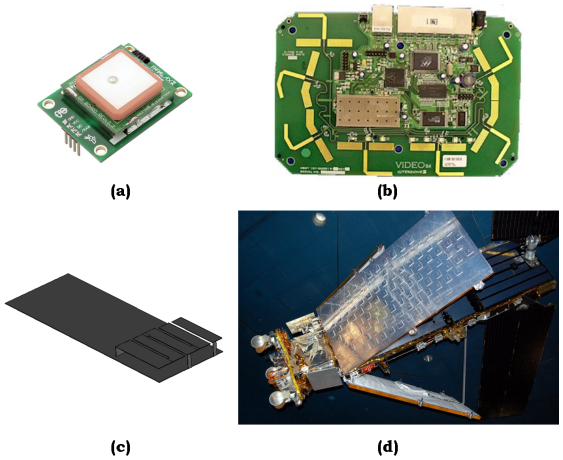

Figure 1.2: Examples of the use of microstrip patch antennas: (a) GPS receiver module with a ceramic microstrip patch antenna, (b) internal view of a wireless router with a patch array, (c) sketch of a patch antenna for a cellular phone, and (d) satellite with a patch antenna array (silver pannels; the solar pannels are the black ones).

A rapid increase in the use of personal communication devices forces to adapt the technology to new user's necessities. Portable communication devices have to adapt to different communication protocols in orther to have access to the huge variety of communication possibilities that nowadays exist. The trend is to evolve to a new model of mobility: a mobile phone, a laptop or a PDA must be capable to be always connected. The localization of its user can change rapidly, but it has to be guaranteed its capability to be connected to one of the existing data communication networks. This implies that not only the software, where media independent handover services are becoming to be developed (IEEE 802.21), but also the hardware has to be designed thinking in the concept of multiband operational devices. Those varying scenarios demand also high gain antennas in order to receive a signal that is broadcasted to a great amount of users and hence has a limited power of emission.

If we focus in the bandwidth required in GSM, WiFi and other systems a typical patch antenna can meet with the bandwidth specifications. The problem stems from the antenna miniaturization. Compact devices need miniaturized antennas. Nevertheless when an antenna is shrunk its bandwidth dramatically decreases. The challenge is to engineer miniaturized antennas maintaining the original bandwidth or even improving it. In additon, an antenna can not be made arbitrarily small because its dimensions are related with its resonant frequency.

Metamaterials can help in antenna miniaturisation due to their novel and amazing electromagnetic properties that do not exist in nature.

1.1 Definition of Metamaterial

A metamaterial, or artificial material, is an artificial structure that can be designed to obtain controllable electromagnetic properties which are not found in nature. The majority of the metamaterials have

the period much smaller than the signal wavelength: $p << \lambda$, being p the period and λ the wavelength at the working frequency. Our study will be focused on sub-wavelength periodical metamaterials whose electromagnetic properties can be obtained from an homogenization of effective media procedure. They are usually constituted through the alignement of dielectric substrates with periodical metal patterns printed on them and/or metallic inclusions. Some examples can be seen in Fig. 1.3.

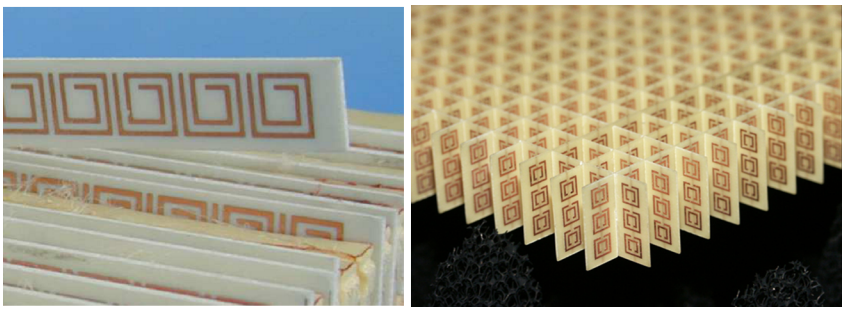

Figure 1.3: Metamaterials fabricated by printing metallic patterns on a dielectric substrate [1, 2].

Since the metamaterials fabricated are not physically homogeneous (they neither are homogeneous in electromagnetic properties terms) a novel terminology has appeared when referring to them: metasurfaces.

1.2 Historical Review of Metamaterials

Theoretical double negative (DNG) materials, which have $\varepsilon < 0$, $\mu < 0$, were firstly analyzed in the 60's by V.G. Veselago [3]. He was the first researcher who demonstrated that, in such media, the magnetic and the electromagnetic fields ($\overrightarrow{E}$, $\overrightarrow{H}$) and the propagation vector ($\overrightarrow{\beta}$) form a triad that follow the left-hand rule instead of the traditional right-hand rule. Precisely for that reason Veselago called this kind of materials Left Handed Materials (LHM), oppositely to the classical Right Handed Materials (RHM). Veselago stated that the LHM possess surprising physical properties such as the propagation of the wave in the direction contrary to the direction of the propagation of the energy, the negative refraction and the reversal Doppler's effect and Snell's law, among others.

The investigation carried out by Veselago was forgotten for decades because of non apparent practical application until J.B. Pendry et al. demonstrated the feasability of this materials [4]. They proposed an artificial media formed by arrangements of split-ring resonators (SRRs) and Swiss Roll Capacitors which working at a given frequency range possess a negative effective permeability $\mu < 0$.

A year later D.R. Smith et al. fabricated the first artificial media having both negative permeability (μ) and permittivity (ε) [1]. This material was based in Pendry's SRRs that provides $\mu < 0$ combined with metallic rods, that provides an effective $\varepsilon < 0$.

After the work of the pioneers, and from 2000 to present days, a huge number of theoretical and practical studies have been carried out focused on the posibilities that these new materials can offer when applied to antennas and microwave systems.

1.3 Main properties

The electromagnetic properties of the materials, the dielectric permittivity (ε) and the magnetic permeability (μ) determine how the electromagnetic waves propagate through a material. Depending on its sign metamaterials can be classified into four regions, as it can be seen in Fig. 1.4.

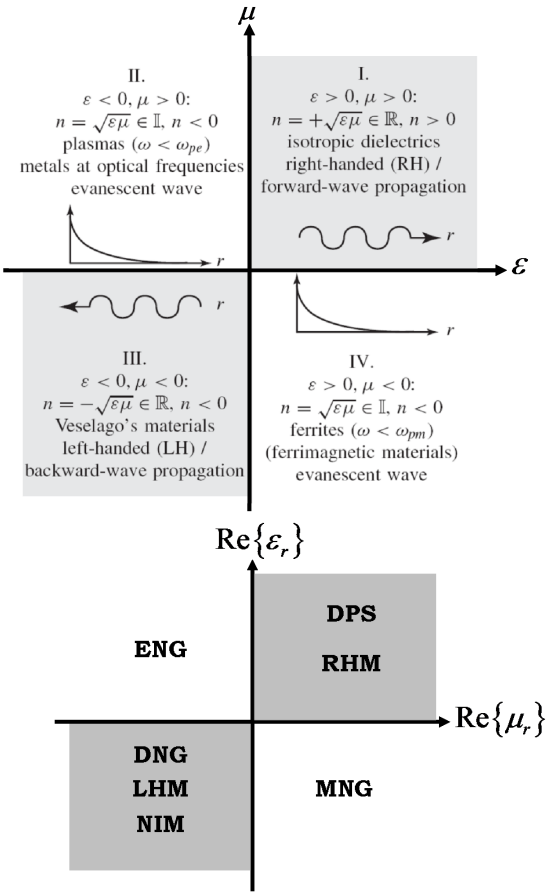

Figure 1.4: Classification of metamaterials depending on the sign of ε and μ. ω is the angular frequency, and ω_p and ω_{pm} are the electric and magnetic plasma frequencies, respectively. ENG stands for Epsilon NeGative, DPS for Double PoSitive, RHM for Right Handed Material, DNG for Double NeGative, LHM for Left Handed Material, NIM for Negative Index Medium and MNG for Mu NeGative [6].

Combinations I, II and IV are well known in conventional materials. In the group III are included the DNG, which are a new class of materials. Propagation only occurs in type I materials (or RHM) as

forward-wave propagation, and in type III materials (or LHM) as backward-wave propagation, whereas in the other types, the waves do not propagate since they are evanescent, and hence, they are attenuated.

Unfortunatelly, metamaterial structures are frequency dependent. Hence, the analytical design of its resonant (or operational) frequency band is very important. In this way, the constitutive parameters (ε and μ) are related with the refractive index n as:

$$n(\omega) = \pm\sqrt{\varepsilon(\omega)\mu(\omega)} \tag{1.1}$$

The refractive index is related with the propagating wave function by Eq. 1.2. Therefore, a change in the refractive index sign implies a change in the normal wave propagation.

$$e^{\pm j\beta} = e^{\pm jk_0 n} \tag{1.2}$$

Several physics phenomena change or reverse their behaviour with DNG metamaterials. Some of them are going to be briefly introduced in the following subsection.

1.3.1 Negative Refraction Index

When the refractive index in Eq. 1.1 has negative value (Veselago's materials) the field equations are affected in this way:

$$\overrightarrow{\beta} \times \overrightarrow{E} = \omega\mu\overrightarrow{H} \tag{1.3}$$

$$\overrightarrow{\beta} \times \overrightarrow{H} = -\omega\varepsilon\overrightarrow{E} \tag{1.4}$$

The Poynting vector, which indicates the direction of the energy flux (Eq. 1.5), becomes antiparallel to the propagating vector $\overrightarrow{\beta}$, while in a normal situation would be parallel.

$$\overrightarrow{S} = \overrightarrow{E} \times \overrightarrow{H} \tag{1.5}$$

This means that the vectors $\overrightarrow{E}$, $\overrightarrow{H}$ and $\overrightarrow{\beta}$ follow a left-handed rule instead of following a right-handed rule (see Fig. 1.5).

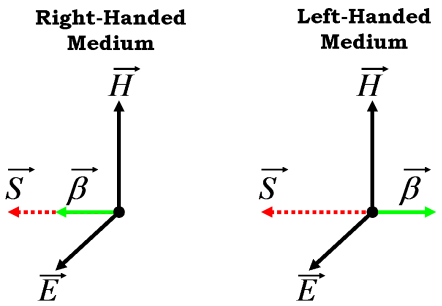

Figure 1.5: RH media (left) and LH media (right).

As it has been said before, metamaterials have a frequency dependent behaviour. These materials do not possess their metamaterial characteristics in the whole frequency domain, but their behaviour changes when working at one frequency or another. For example, the effective parameters of a metamaterial can be the ones depicted in Fig. 1.6.

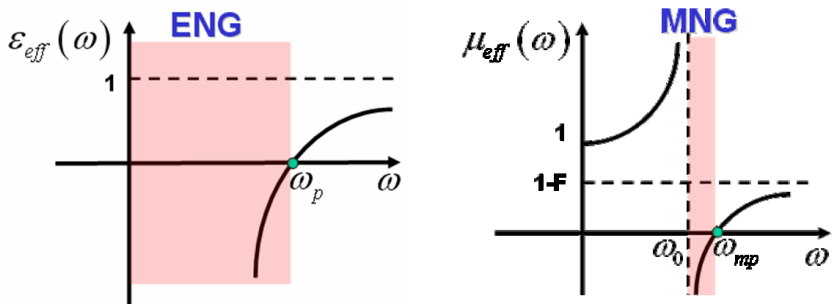

Figure 1.6: Frequency dependent effective parameters of an arbitrary metamaterial. A material is ENG until ω_p (left), a material is MNG in the range between ω_0 and ω_{mp}. ω_p: plasma frequency, ω_{mp}: magnetic plasma frequncy, ω_0: divergence frequency and F: fractional area (0<F<1) [7].

In that case the metamaterial acts as a LHM only in the intersection of the frequency bandwidths $0<\omega<\omega_p$ $\omega_0<\omega<\omega_{mp}$, this is, where ε and μ are both negative.

With a negative refractive index the Snell's law is also modified. This implies that an incident wave coming from a RHM will not be refracted as expected, but in an unusual direction. To exemplify the situation, imagine a scenario like the one depicted in Fig. 1.7, where the light of a lantern incides in the glass of a window coming from the outside of a house. On the left part of the figure the scheme of a normal refraction is depicted. That follows the Snell's law. A person situated in the point A would project a shadow behind him/herself, while one in B would not. On the right part of the figure, imagine that behind the glass that separates the outside of the house there is not simply a normal room, but a LHM filling that space. In that case the light will be refracted in a strange way, and a person in point A would not have a shadow while a person in B would have it! This is the meaning of the reverse Snell's law.

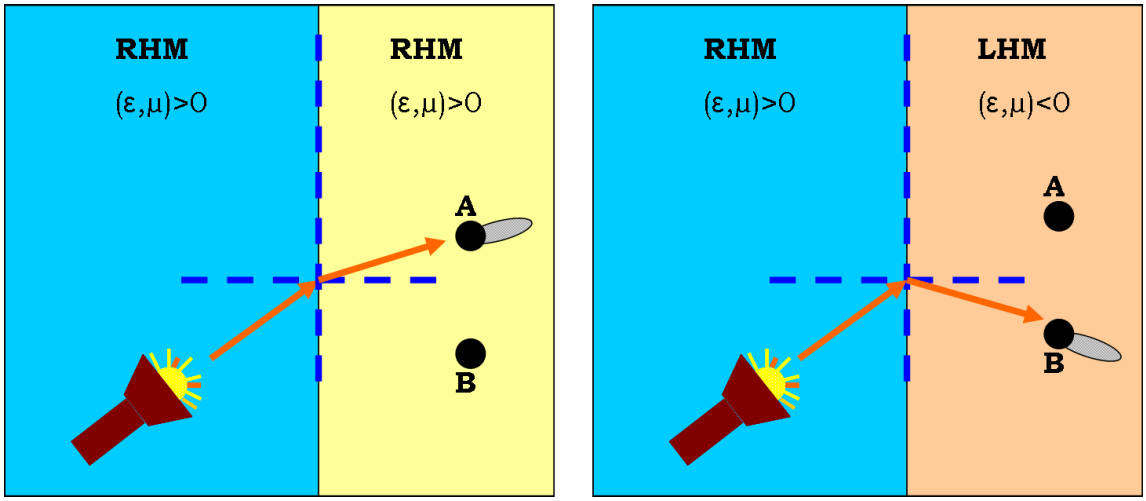

Figure 1.7: RHM-RHM and RHM-LHM interfaces.

1.4 Applications

A couple of examples are going to be introduced to give an idea of what are the potential applications of metamaterials aside from the one described in this work.

1.4.1 Artificial Magnetic Conductors (AMC)

PEC (Perfect Electric Conductor) surfaces are used as a backing material in many antenna applications to assure that the antenna radiates towards one direction only. They have a broadband 180^{o} phase reflection, which means that the incident electric field is reflected out of a wide frequency range. A PEC is an electrical reflector. An antenna should be placed at a distance of $\frac{\lambda}{4}$ from the reflector to enhance the field radiated by the antenna.

An AMC is a kind of metamaterial which has the property of a PMC (Perfect Magnetic Conductor), which means a 0^{o} phase reflection of the electric field. An AMC is a magnetic reflector. If AMC are used instead of PEC materials, the antenna can be placed closer to the surface maintaining its radiation properties. This leads to compact and low profile antennas. However, contrarily to the PEC screens made by metal, magnetic screens do not exist in nature. In Fig. 1.8 a fabricated AMC is shown.

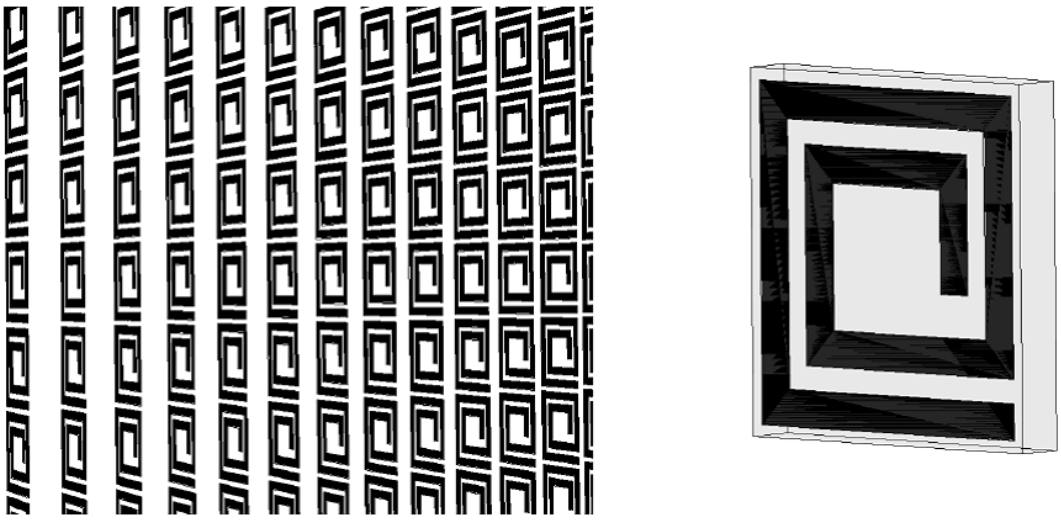

Figure 1.8: AMC surface: infinite array (left) and single element (right) [1].

1.4.2 Electromagnetic Cloaking

The most recent application of metamaterials is the electromagnetic cloak. It has been proposed by J.B. Pendry et al. to make metallic objects invisible at microwave frequencies [8].

In Fig. 1.9-left the idea of the functioning of the electromagnetic cloak is shown: to control the paths of electromagnetic waves within a metamaterial by means of varying the spatial variation in the constitutive parameters (i.e. the magnetic resonators). In the rigth part of the figure a fabricated cloak is shown. The fabricated cloak is cylindrical instead of spherical for easiness of fabrication.

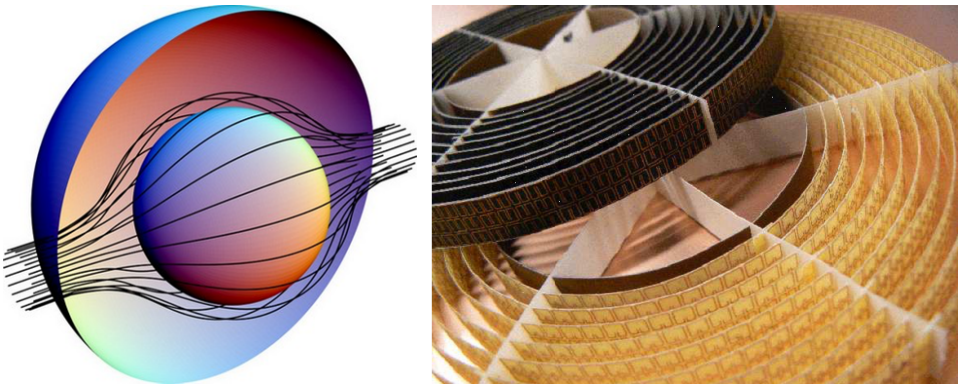

Figure 1.9: Electromagnetic cloak phenomenon (left) and fabricated cloak (right) [8, 9].

The novelty in this area is the cloaking carpet, which has been designed to hide 3D objects from the electromagnetic waves at microwave frequencies.

The news talk about hiding objects in visible light, showing images like the ones in Fig. 1.10. The image on the left shows a man wearing special clothing with unusual optical properties. These properties are due to the negative refractive index property of some kinds of metamaterials. The image on the right shows a fictitious scenario where the cloaking carpet effect is shown.

Figure 1.10: Images shown in the news when introducing the metamaterial application of cloaking: cloaking at visible light (left) and the novel cloaking carpet concept (right).

1.5 Objectives

In this work metamaterials are going to be applied to reduce the physical size of microstrip patch antennas working at approximately 2.45GHz in order to demonstrate that the electrical size reduction of patch antennas is possible. The typical patch antenna miniaturization using dielectric substrates trade-off is that the antenna bandwidth decreases. One of the objectives is to reduce the size of the antennas without reducing their fractional bandwidth. Another important objective is to apply a novel formulation to compute the FBW of an antenna and assess whether it can be used to predict the maximum reachable antenna FBW in its designing stage.

In Chapter 2 some basic concepts to understand how patch antennas can be miniaturized are introduced, and a new formula (Yaghjian's formula [10]) to analyze the fractional bandwidth is presented in order to apply it to the antennas which are going to be studied. In Chapter 3 a theoretical study on how metamaterials affect to the basic antenna parameters is carried out. In Chapter 4 a more realistic model of metamaterial is used to study how artificial materials can help to miniaturize patch antennas and some prototypes are fabricated. Finally, in Chapter 5 the conclusions reached at the light of the results obtained in this work are gathered and some future lines are proposed.

Chapter 2

Miniaturization and Bandwidth Study of Microstrip Patch Antennas

Modern communication systems require smaller and lighter devices in order to satisfy the consumer's needs. One of the basic components of these devices is the antenna. Consequently antennas have to be miniaturized. Different methods applied to obtain miniaturized patch antennas are briefly explained in the following sections of this Chapter. The majority of them are based on the increase of the permittivity value of the antenna substrate.

However, miniaturization leads to decrease the antenna operational bandwidth. To explain this performance the Chu's fundamental limit that relates the antenna size and its bandwidth is presented.

Hansen and Burke's FBW formaula opens a new possibility in antenna miniaturization: high permeability substrates can lead to an efficient miniaturisation, without a decrease in the antenna bandwidth[1]. The state of the art in metamaterials applied to patch antenna miniaturization is revised.

The maximum bandwidth obtained for a given antenna can be computed using different methods. The standard method (or direct measurement) is compared with a new and compact formulation proposed by Yaghjian.

2.1 Preliminary Definitions

Basic definitions of some properties and concepts related with patch antenna technology that are used throughout the rest of the work are required for a quick and easy comprehension of more fundamental ideas.

[1] Contrary to the BW decrease when using high dielectric substrates.

2.1.1 Electromagnetic properties of the materials

The physical insight of the main EM properties of the materials that will be studied are presented.

The *dielectric constant* or *relative permittivity,* ε_r, is the parameter which defines the relative charge or energy (relative compared to free space) storage capabilities of a dielectric material. High-ε_r values indicate that the dielectric material has high ability in storing charge (or energy). The free space permittivity has the value $\varepsilon_0 = (1/36\pi)$ x10^{-9}F/m. The *static permittivity* of a medium is $\varepsilon = \varepsilon_0\varepsilon_r$.

There is even another parameter; the *effective dielectric constant* or *effective relative permittivity*, ε_{reff}. It is defined when the dielectric material which fills a volume is divided in different parts having different relative permittivities. Then, the effective permittivity of the material in that volume is defined.

For a microstrip line with air above the substrate, the effective dielectric constant has values in the range $1 < \varepsilon_{reff} < \varepsilon_r$. In most applications where the ε_r of the substrate is $\varepsilon_r \gg 1$ the value of the ε_{reff} will be closer to the value of the actual dielectric constant of the substrate, ε_r. The effective dielectric constant is also a function of frequency. However, for typical substrates the variation with the frequency is almost constant at low frequencies. This value increases monotonically with frequency eventually approaching the values of the ε_r of the substrate [11]. The frequency dispersion in the ε_{reff} will be studied in Chapter 4.

The *magnetic constant* or *relative permeability*, μ_r, is the parameter which defines the relation between the magnetic flux density and the magnetic field intensity. The free space permeability, $\mu_0 = 4\pi$x10^{-7} H/m, is related with the *static permeability* of a medium by: $\mu = \mu_0\mu_r$. As in the dielectric medium, an *effective magnetic constant* or *effective relative permeability*, μ_{reff}, is defined. This μ_{reff} also varies with frequency.

The above mentioned material properties are the ones in which all the studies of this work are based. Their value variation when considering different materials loading a patch antenna is the basis of an exhaustive study to determine how antenna radiation parameters change.

Subsequently, and for the sake of simplicity, the relative permittivity is going to be mentioned simply as permittivity or ε_r and the relative permeability as permeability or μ_r. This can be done because the material properties that are varied in our studies are the relative ones. Nevertheless in Chapter 4 frequency dispersion will be taken into account when studying artificial materials, and the relative effective parameters, ε_{reff} and μ_{reff} will be considered.

2.1.2 Microstrip Patch Antenna Modelling

The main models are based in the transmission line equivalent circuit (useful to obtain the antenna impedance) and considering the patch antenna similar to a resonant cavity (useful to obtain the radiation pattern).

In Fig. 2.1 the side view of a microstrip patch antenna is depicted. In this case, a rectangular microstrip antenna fed by a coaxial transmision line is used. The electromagnetic waves which are guided through the coaxial feed spread out under the patch and by reaching it (the patch constitutes a boundary for them) some of them are reflected back while others are radiated into free space.

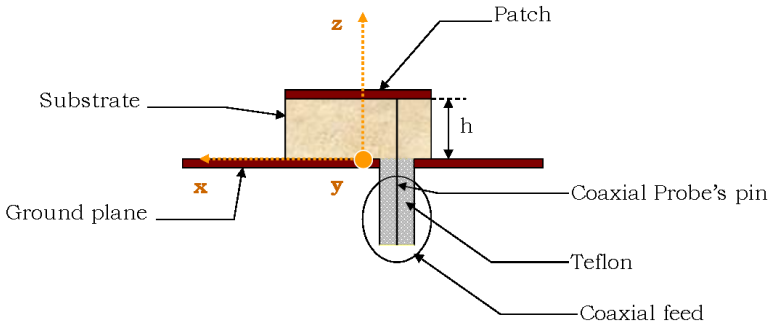

Figure 2.1: Coaxial fed microstrip patch antenna having a patch-sized substrate.

From this principle of operation, the different methods of analysis are derived. When the objective is to determine the antenna radiated fields it can be done either finding the current distributions along the antenna structure (exact model), thus obtaining the radiation fields from these current sources, or finding the fields at the exit region (cavity model), the apertures which act as equivalent sources hence obtaining the radiation fields from them.

In the cavity model the rectangular patch antenna is analyzed as two equivalent radiating slots. Each of them has a width W and a height h being separated the patch length, L. It has to be assumed that the substrate height is much less than a wavelength, and then it can be stated that:

- $\overrightarrow{E}$ has only $\hat{z}$ component (when the antenna is oriented like in Fig.2.1) and $\overrightarrow{H}$ has only transverse components in the region limited by the patch and the ground plane. However this does not holds for the area near the edge, because of the fringing fields.
- In the region bounded by the patch and the ground plane, $\overrightarrow{E}$ and $\overrightarrow{H}$ do not vary with $\hat{z}$.
- The electric current in the microstrip line must not have a component normal to the edge and hence the $H_{\perp}$ component along the edge is negligible, following Maxwell's equations.

It is through the former observations that the region limited by the patch and the ground plane of the microstrip antenna is considered as a cavity bounded by electric walls on the top and bottom and by magnetic walls on the side.

It is not our objective to reproduce theories, but to know their existence and their basis. Hence, more information about these methods can be found in [12, 13].

2.1.3 Resonance and matching of a patch antenna

An antenna is designed to have the desired response at a desired frequency of operation, f_0. The antenna is properly designed when: its power pattern at f_0 is the desired one, its radiation efficiency has an acceptable value and its impedance is matched to a generator or load. Depending on the application of the antenna, other characteristics like the impedance bandwidth or the directivity must meet specifications.

Different methods to adjust the antenna size can be followed depending on whether the f_0 is defined as the antenna resonant frequency or the antenna matching frequency. An *antiresonant* patch antenna at f_0 has zero reactance and maximum input resistance at this frequency. The resonant and antiresonant regions in the patch antenna impedance are indicated in Fig. 2.2.

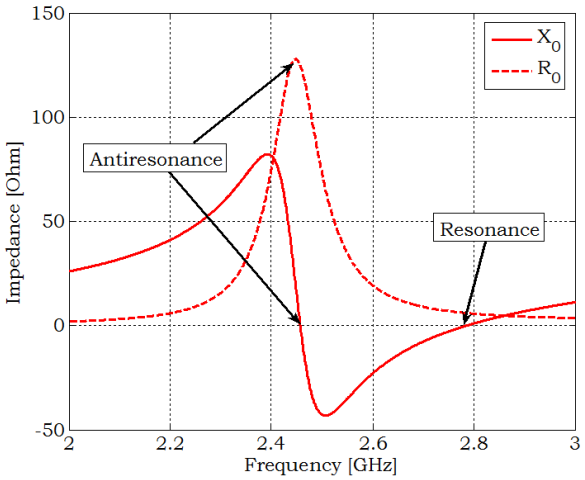

Figure 2.2: Resonace and antiresonance of a patch antenna with air filling tuned to f_0=2.45GHz.

Nonetheless, what is called *resonant* in patch antennas is actually the formerly described antiresonance, where the slope of the reactance is negative ($X(f_0) = 0$, $X'(f_0) < 0$). Hereinafter, for simplicity, an antenna designed to be *antiresonant* at f_0 will be called as a *resonant* antenna at f_0.

Observe that it is not the same an antenna *tuned* at f_0 than an antenna *resonant* at f_0. A tuned antenna has $X(f_0) = 0$ at a frequency where the antenna resistance does not have to be in its maximum value. In Fig. 2.3 a patch antenna filled with air is tuned using a series reactive component (a capacitor, in the example).

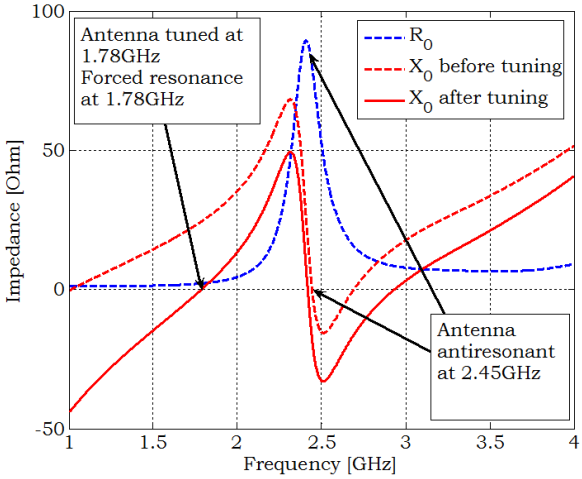

Figure 2.3: Tuned antenna at 1.78GHz.

The antenna is forced to be resonant at 1.78GHz, hence having an *artificial* resonance at this frequency. Nevertheless, its *antiresonance* at 2.45GHz is scarcely modified from its initial value.

A *matched* antenna has maximum *return loss* at f_0 (or minimum *reflection coefficient* at f_0). Return losses are defined referred to Z_{ref}, typically 50Ω.

The return loss parameter and the reflection coefficient are related by the Eq. 2.1, and Eq. 2.2 defines the reflection coefficient expressed in dB and the reflection coefficient is related with the reference impedance by Eq. 2.3.

$$RL = -\Gamma \tag{2.1}$$

$$\Gamma \equiv S_{11} \mid_{dB} = 20log_{10}(|\rho|) \tag{2.2}$$

$$\rho \equiv S_{11} = \frac{Z_0 - Z_{ref}}{Z_0 + Z_{ref}} \tag{2.3}$$

Where Z_0 is the antenna impedance and Z_{ref} the characteristic impedance of the circuit at which the antenna is connected (or directly the feedline). Ideally, the reflection coefficient should be zero and the reflection coefficient has to be $-\infty$ (there is no reflected signal, hence no power is reflected back to the transmitter) when perfect matching between the antenna and the feedline is achieved.

The antenna is considered to be properly matched when the reflection coefficient is under a threshold of $-L_{dB}$. Normally, the threshold taken as a reference is $L = 3dB$, $L = 6dB$ (this value is typical when considering mobile communication devices) or $L = 10dB$.

In Fig. 2.4 the magnitude of the reflection coefficient of an antenna correctly matched to 50Ω is plotted.

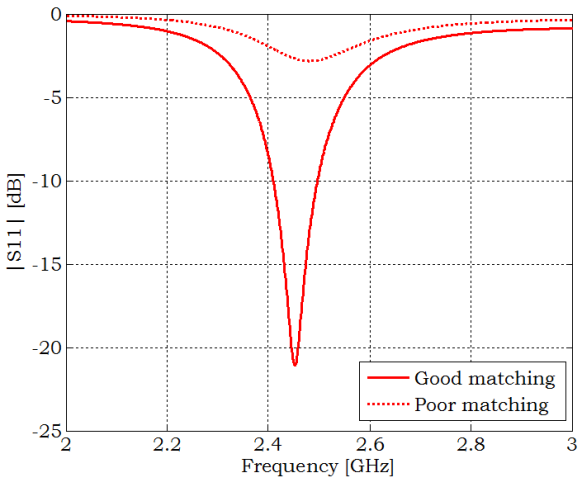

Figure 2.4: Patch antenna reflection coefficient S11 (magnitude) when the same patch antenna is matched to 50Ω in a good and in a poor way.

2.1.4 How to Calculate BW/FBW

The bandwidth of an antenna is the parameter which informs about the frequency range where a given requirement is fulfilled. The parameters which can fix the requirements are the side lobe level gain, the radiation efficiency and the input impedance, among others. Usually, the common bandwidths are the *radiation pattern bandwidth* and the *impedance bandwidth* [12].

Bandwidth can also be specified as a percentage, and is called *fractional bandwidth FBW[%]*. In fact, the FBW is a figure of merit like the Q parameter and the radiation efficiency; because they give a reference value which can be used to compare different antennas.

The $VSWR$ is a parameter related with the reflection coefficient through Eq. 2.4:

$$VSWR = \frac{1+|\rho|}{1-|\rho|} \tag{2.4}$$

For a $VSWR<S$, the fractional impedance bandwidth is defined through Eq. 2.5 :

$$FBW = \frac{100\,(S-1)}{Q_T\sqrt{S}} \tag{2.5}$$

A common $VSWR$ value to define the impedance bandwidth is $S=2$, equivalent to a return loss value of $\Gamma \approx 10dB$. In that case, the operational bandwidth of the antenna is related to the total Q factor as:

$$FBW = \frac{100}{Q_T \sqrt{2}}$$

However, this is not a universal definition, and some authors [12] define the bandwidth as:

$$BW = \frac{1}{Q_T} \tag{2.6}$$

Nevertheless, the former equation is less useful because it does not take into account the impedance matching of the antenna.

For an antenna under test, the fractional bandwidth can be measured from the magnitude of the reflection coefficient of the antenna:

$$FBW\,[\%] = \frac{f_2 - f_1}{f_0}\,100 \tag{2.7}$$

Where f_1 and f_2 are the cut-off frequencies for a given magnitude of the reflection coefficient, and f_0 is the operational frequency. The f_0 can also be defined from f_1 and f_2 as:

$$f_0 = \begin{cases} \frac{f_1+f_2}{2} & arithmetic\,mean \\ \sqrt{f_1 f_2} & geometric\,mean \end{cases}$$

Normally, a certain value of the measured 50Ω match is set from the magnitude of the reflection coefficient and the f_0 value can be considered as the arithmetic/geometric mean or simply as the frequency where the magnitude of the reflection coefficient is minimum[2].

2.1.5 Microstrip Patch Antenna Typical Performance

Microstrip patch antennas are designed to have a hemispherical radiation pattern. Theoretically the patch does not radiate under the ground plane because is considered infinite in size. However, practical designs over finite ground planes radiate as it can be observed in Fig. 2.5.

[2]In that case multiple resonances or resonances leading to non-symmetrical $|S_{11}|_{dB}$ curves can lead to a wrong result. However, in narrow band applications the error would be practically imperceptible.

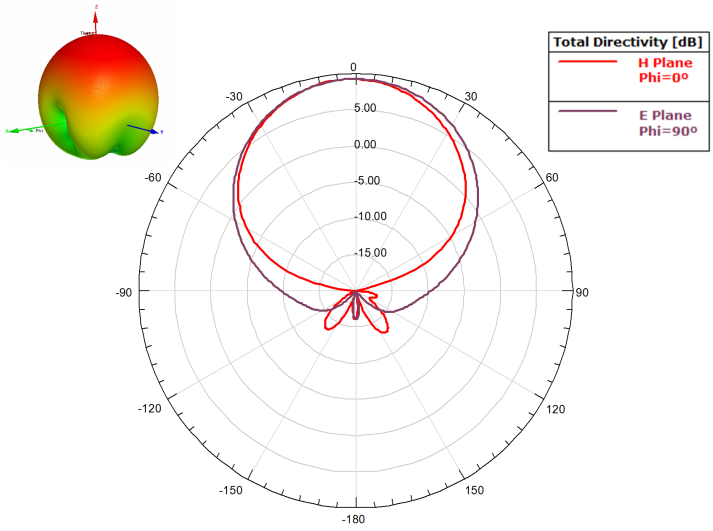

Figure 2.5: Typical directivity radiation pattern shape of a microstrip patch antenna.

One important parameter in microstrip patch antenna design is the front-to-back radiation ratio. For mobile handset applications this parameter must be the minimum possible in order to protect the user from the antenna radiation.

As can be observed in Fig. 2.5, conventional patch antenna directivity values are between 7 and 10dB for the broadside direction of radiation. Typically, the FBW_{-10dB} of a patch antenna filled with air is between a 3% and a 5%.

2.2 Patch Antennas Miniaturisation

Microstrip patch antennas offer many advantages: simple fabrication, low cost and light weight are among them. Their planar geometry makes them compatible with the increasingly demanded planar and compact circuitry.

They are used in popular devices like mobile phones thanks to their low profile and mainly unidirectional radiation pattern and in other wireless communication systems or space communication modules under the form of array. However, these applications demand high gain, high impedance bandwidth and miniaturized components. The challenge is to obtain antenna miniaturization while efficiently maintaining or even increasing the bandwidth at the same time. In general efficient miniaturization means that the rest of the antenna radiation features are not degraded.

In this way one of the microstrip patch antenna constraints use to be the impedance bandwidth, which for a typical patch antenna is very limited. Since the bandwidth and the radiation efficiency are inversely related, increasing means decreasing the gain due to radiation efficiency degradation.

Moreover, another constraint is related with the antenna miniaturization. An antenna can not be made tinier capriciously. For a given working frequency f_0 the microstrip patch antenna size is defined by Eq. 2.8. Thus, the size is related with the frequency ($\lambda_0 = c/f_0$, c=$3{\cdot}10^8$ m/s) but also with the substrate parameters: the relative permittivity (ε_r) and the relative permeability (μ_r).

$$L = \frac{\lambda_0}{2n} = \frac{\lambda_0}{2\sqrt{\varepsilon_r \mu_r}} \tag{2.8}$$

Therefore, the effort to miniaturize the antenna has to be concentrated in achieving a high-$\varepsilon_r\mu_r$ value.

2.2.1 Theoretical BW limitations

As mentioned before, the antenna size depends on the working frequency. But then one has to think if there is any limit which relates the antenna size and its bandwidth. There exists, and it was introduced by Chu [14] for electrically small antennas.

In Fig. 2.6 the electrically small antenna definition conditions are depicted in two situations. The first one represents a dipole antenna (it can be any other antenna) circumscribed in a sphere of radius a. This sphere is the minimum sphere that encloses the antenna. The parameter k_0 is the wave number at the working frequency; $k_0 = 2\pi/\lambda_0$. In the second situation, the condition for an antenna which is situated above a ground plane is depicted. In that case a is the radius of the hemisphere. As it can be observed in the figure, the radius a does not take into account the size of the ground plane. Hence, the condition to be fulfilled for a microstrip patch antenna to be considered an electrically small antenna is: $k_0{\cdot}a < 0.5$.

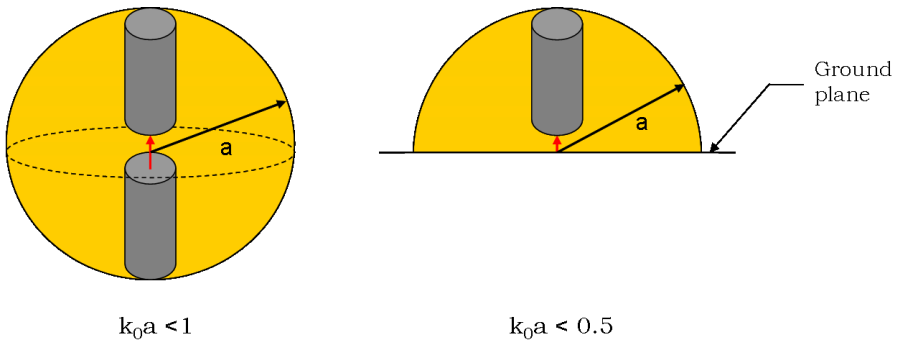

Figure 2.6: Electrically small antenna definition.

For an electrically small antenna with linear polarisation the Q and FBW are defined as:

$$Q_{Chu} \geq \frac{1}{k_0 a} + \frac{1}{(k_0 a)^3} \sim (k_0 a)^{-3} \tag{2.9}$$

$$FBW_{Chu} = \frac{1}{Q_{Chu}} \sim (k_0 a)^3 \tag{2.10}$$

The antenna quality factor increases (FBW decreases) as the antenna shrinks, hence not allowing proper antenna miniaturisation with high FBW values ($\equiv$ low Q).

The objective would be to be as near as possible to the Chu's limit. A more realistic criterion for the FBW of electrically small antennas would consider a Q_{Chu} limit incremented 10 times [15] and the FBW limit for a return loss of 10dB:

$$FBW_{max} = 100\frac{1}{\sqrt{2}Q_T}$$

The Q_{Chu} limit is depicted in Fig. 2.6 and compared with the more realistic criterion: Q=10·Q_{Chu}. In addition, the FBW_{Chu} limit along with the FBW when Q=10·Q_{Chu} are shown in Fig. 2.8.

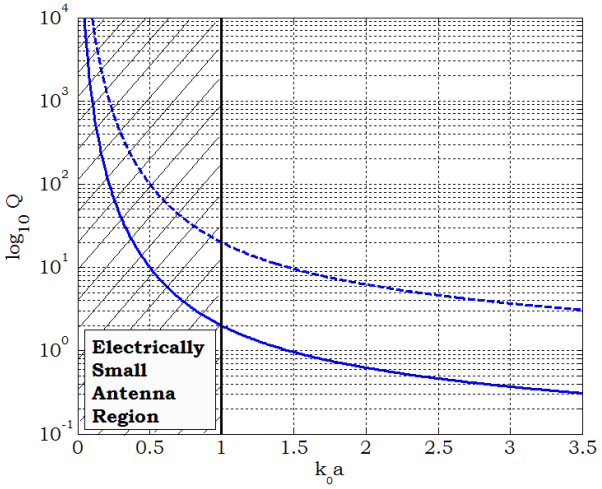

Figure 2.7: Chu's limit. Solid line for Q_{Chu}, dashed line for $10Q_{Chu}$. The quality factor results very low for realistic electrically small antennas.

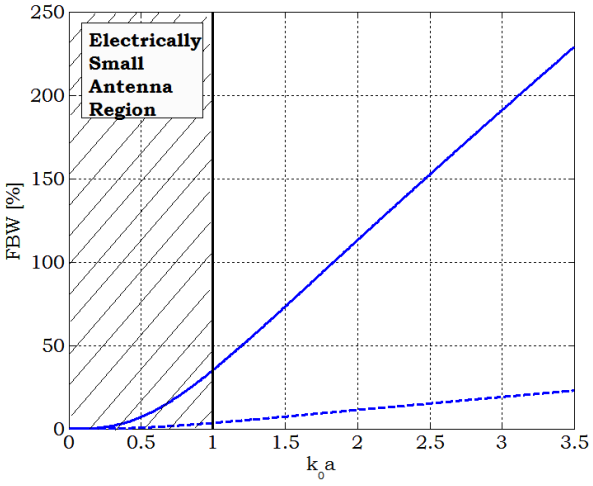

Figure 2.8: Solid line for the FBW_{Chu} and dashed line for the $FBW|_{Q=10Q_{Chu}}$, a more practical limit for electrically small antennas.

The Chu's limit is a fundamental limit, which means that can not be surpased. Given an antenna electrical size, a lower Q value than the Q predicted by Chu's limit can not be obtained.

2.2.2 Background in patch antennas miniaturisation

Many different techniques have been used to reduce the size of patch antennas. In this section we focus our attention in the miniaturization of rectangular patch antennas. A typical approach consists of loading the radiator with high-ε_r substrates. This leads to a lower resonant frequency, from Eq. 2.8. To tune back the antenna to its original resonant frequency the antenna size has to be reduced, thus miniaturizing the antenna.

One drawback of this approach is that antennas loaded with dielectrics are prone to surface wave excitation, consequently decreasing the antenna efficiency. In addition, more energy delivered to the antenna is trapped in substrates with high-ε_r because of the strong electromagnetic coupling between the patch and the ground plane. This increases the antenna Q, therefore reducing the antenna impedance bandwidth.

To miniaturize antennas the use of inductive or capacitive loadings and/or meandered lines has also been attempted, but these methods cause an increase in the losses and the bandwidth also suffers. An example of each of those techniques can be observed in Fig. 2.9.

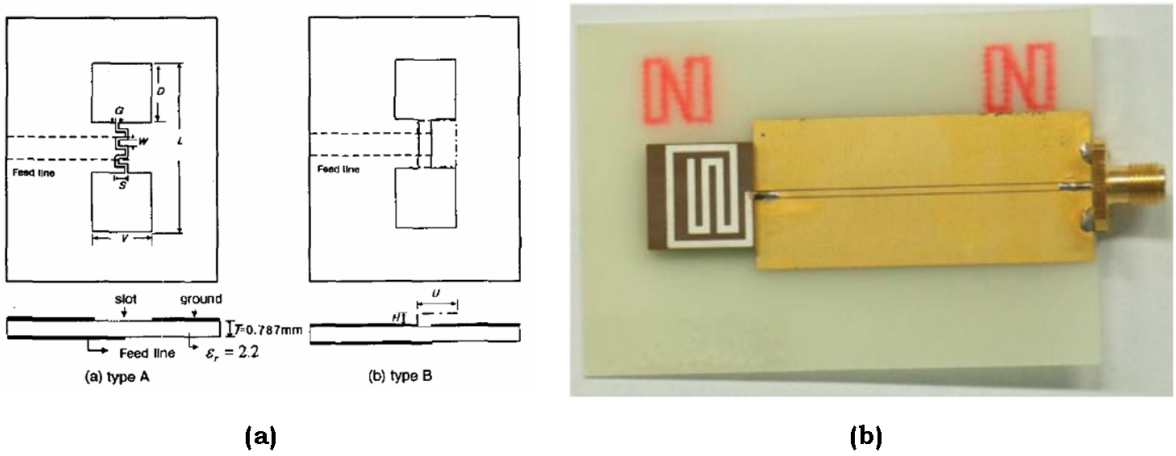

Figure 2.9: Examples of antenna miniaturization using: (a) inductive-capacitive loading [16] and (b) meandered lines [17].

In Fig. 2.9 (a) two different types of inductive and capacitive (at the same time) loaded antenna proposed by G.Y. Lee et al. [16], whilst in Fig. 2.9 (b) the meandered antenna designed, fabricated and measured by H. Liu et al. [17] is shown.

Another approach to miniaturize patch antennas is the use of lumped reactive loads, as done by Bhuiyan et al. [18]. In their work, varactor diodes are used to reduce the size of the antenna. A disadvantage of this design is that the cross-polarization and the directivity are worsened. In addition, varactor diodes need to be fed and this is another disadvantage of this approach.

2.2.3 Hansen and Burke BW Formula

Increasing the ε_r of the substrate in a patch antenna leads to its miniaturization, because the ε_r and the L are inversely related (Eq. 2.8). Nevertheless, ε_r is also inversely related with the impedance bandwidth of the antenna [12]. For that reason increasing the ε_r value is not an efficient way to shrink the antenna size if the objective is maintaining a certain value of the impedance bandwidth.

Hansen and Burke [19] defined a *zero-order BW formula* to obtain the bandwidth of resonant patch antennas loaded with magneto-dielectrics. Their objective was to provide a simple equation to have an instant comprehension on how the bandwidth varies with the patch antenna physical parameters. The general FBW of a rectangular patch antenna is defined in Eq. 2.11 as:

$$FBW\,[\%] = \frac{96}{\sqrt{2}} \frac{\sqrt{\frac{\mu_r}{\varepsilon_r}}}{[4 + 17\sqrt{\mu_r \varepsilon_r}]} \frac{h}{\lambda_0} 100 \tag{2.11}$$

Which is told to be valid for $1 \leq \mu_r \varepsilon_r \leq 10$, and considering $VSWR{=}2$ (equivalent to $\Gamma \approx -10dB$).

Eq. 2.11 opens new possibilities in antenna miniaturization: the relative material permeability μ_r is inversely proportional to the antenna size but directly proportional to the bandwidth of the antenna.

Hansen and Burke conclude that significant bandwidth improvement results only when μ_r is large and ε_r is close to one. A substrate with large μ_r allows only a small increase in bandwidth over the same patch with $\mu_r = 1$. However, unlike ε_r, μ_r does not reduce the patch BW. In addition, the patch resonant length is reduced by $\sqrt{\mu_r}$. The advantage is that with μ_r a much smaller patch will have roughly the same bandwidth as a patch with ε_r only. Nevertheless, materials with high permeability values are not easy to find in nature.

Fig. 2.10 shows that, using the Eq. 2.11, higher FBW vales are achieved having high-μ_r materials than having high-ε_r materials (obtaining the same antenna miniaturization factor). The enhancement in the FBW value when comparing a material having $\varepsilon_r = 3$ with one having $\varepsilon_r\mu_r = 3$ is around a 2.1%, which is a worthwhile improvement. To maintain the antenna FBW value (and even improve it) while miniaturizing the antenna is not easy. This happens when using high-μ_r materials. In addition, if the FBW values having $\varepsilon_r = 2$ and $\mu_r = 2$ are compared, the improvement is around a 4.2%.

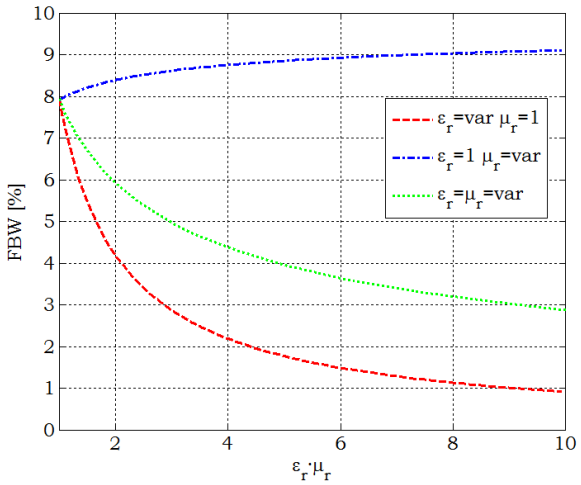

Figure 2.10: $FBW(\varepsilon_r\mu_r)$ computed through the Hansen and Burke equation.

Briefly, the conclusion is that the best results in antenna miniaturisation while retaining or improving the FBW would be achieved using a magneto-dielectric having $\mu > 1$, $\varepsilon = 1$.

2.2.4 State of the art in metamaterials applied to patch antenna miniaturization

The idea presented by Hansen and Burke [19] in its FBW formulation opened new doors in antenna miniaturization design. From their study it was extracted that using a magneto-dielectric substrate ($\mu > 1$, $\mu > \varepsilon$) some drawbacks of the patch antenna on high permittivity substrates can be overcome.

Some of the recent approaches to miniaturize patch antennas are described below.

2.2.4.1 Ikonen et al. [20] miniaturization approach

To miniaturize a microstrip patch antenna with strip line feeding, Ikonen et. al. [20] proposed a metasolenoid as an artificial magnetic media at microwave frequencies.

After having studied the material properties, they assert that if the material resonates inside the operational band of the antenna (realizable materials have dispersive EM properties), a multiresonant antenna is achieved. Otherwise, if the material resonates at a considerably higher frequency than the operational frequency of the loaded antenna, inside the operational band of the radiator the material presents high μ_r over a wide frequency band. Simulations and measurements were carried out to assess the improvement in the FBW using magnetodielectrics when trying to miniaturize the antenna and also to investigate the influence of the dispersion on the FBW when trying to miniaturize the antenna.

They firstly analyzed the dispersion-free situation, comparing the cases referred in Table 2.1.

Material	ε_{eff}=1	μ_{eff}
Air	1	1
High - μ	1	8.3
High - ε	6.75	1
Magneto - Dielectric	2.65	2.65

Table 2.1: Considered lossless and dispersion-free material parameters in the first case of analysis.

In order to compare the different antenna performance, they matched to 50Ω the antennas for every filling substrate. The results for the first simulations are depicted in Fig. 2.11.

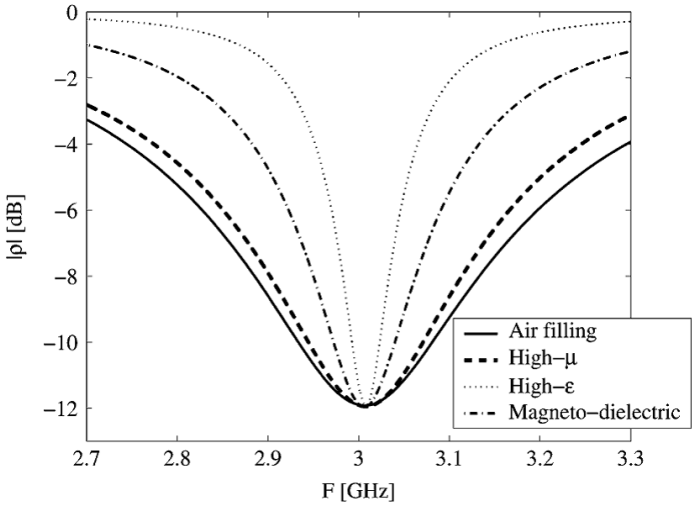

Figure 2.11: Calculated reflection coefficient with different material fillings. Dispersion-free μ_{eff} [20].

The results show how the high-μ_{eff} material improves the bandwidth behaviour of the high-ε_{eff} material, with the magneto-dielectric allowing a moderate improvement in the bandwidth when compared with the high-ε_{eff} material. However, none of the proposed materials performs a better bandwidth than the air.

Secondly, dispersion was taken into account. The dispersive behaviour of the realizable substrate is depicted in Fig. 2.12.

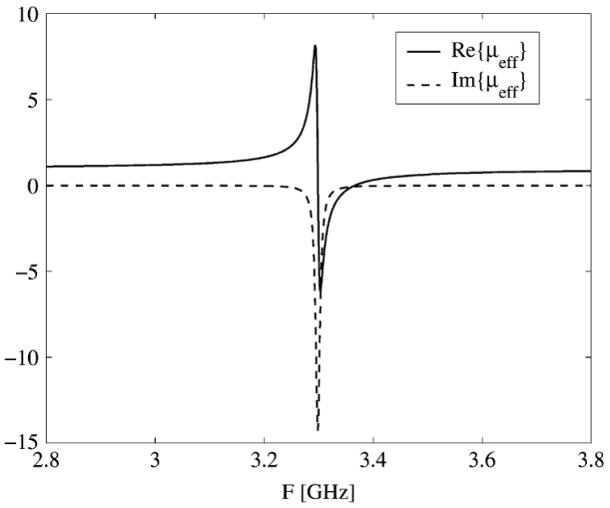

Figure 2.12: Dispersive behaviour of μ_{eff} of a realizable substrate. Figure from [20].

The considered substrates are shown in Table 2.2.

Material	ε_{eff}=1	μ_{eff}
Air	1	1
Magneto-Dielectric	1	From the dispersive μ_{eff} figure
Reference dielectric	10.1(1-j0.001)	1
Dispersion-free μ	1.21(1-j0.0024)	8.5(1-j0.001)

Table 2.2: Considered material parameters in the second case of analysis.

The magneto-dielectric has a narrower bandwidth than the reference dielectric, which in its turn has a narrower bandwidth than the dispersion-free μ substrates. None of them are better than the air case.

Comparing a material having a static $Re\{\mu_{eff}\} = 2$ and $\varepsilon_{eff} = 1$ (the dispersive behaviour of μ_{eff} is the same as depicted in 2.12) with a reference dielectric substrate having $\varepsilon_{eff} = 2.14(1 - j0.001)$, the improvement of the bandwidth with magneto-dielectrics in front of dielectric substrates is shown.

Hence, authors deduce that magneto-dielectrics are only useful when the frequency dispersion in μ_{eff} is very weak (working below the resonance of the substrate).

Finally, an antenna filled with a metasolenoid material was fabricated:

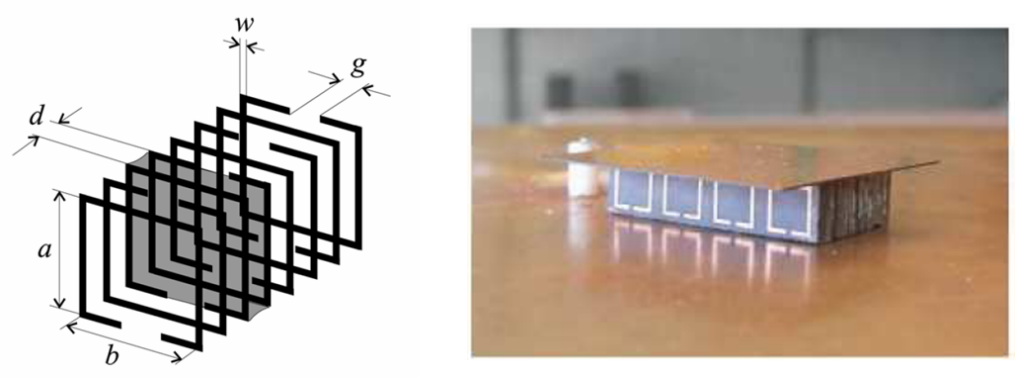

Figure 2.13: Schematic ilustration of the metasolenoid and manufactured prototype antenna [20].

The material resonance was at approximately 2.3GHz, and the operational frequency of the loaded antenna was 2.07GHz. They estimate that $Re\{\mu_{eff}\} = 1.25$ while $Re\{\varepsilon_{eff}\} = 8.5$ (the relative effective permittivity was considered real, while the relative effective permeability is real at the operational frequency of the loaded antenna). The reference dielectric has $\varepsilon_r^{ref} = 10.8(1 - j0.0037)$. The measured reflection can be observed in Fig. 2.14.

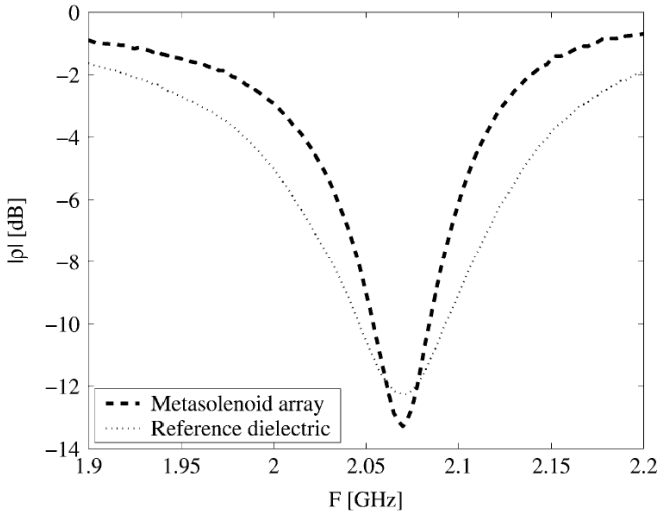

Figure 2.14: Measured reflection coefficient with different material fillings. Figure from [20].

The conclusion was very clear for the same matching figures: the μ_{eff} dispersive behaviour of realizable magnetodielectric materials caused the bandwidth reduction in front of the traditional high-ε_{eff} materials.

2.2.4.2 Mosallaei et al. [21] miniaturization approach

Mosallaei et al. used an anisotropic metamaterial with a dense periodic array of miniaturized embedded-circuit loops which presented a relatively high ε_{eff} and μ_{eff} values at the working frequency. The geometry of the magnetodielectric and the effective constitutive parameters of the metamaterial are shown in Fig. 2.15.

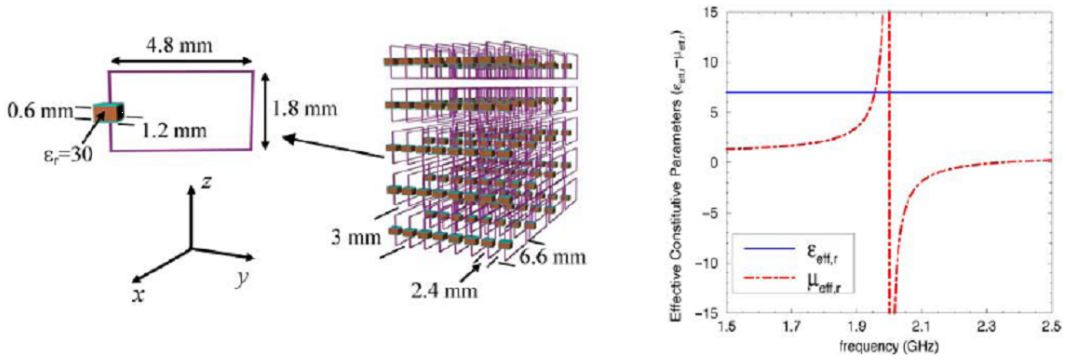

Figure 2.15: (Left) Sketch of the unit cell. (Center) Geometry of the magneto-dielectric embedded-circuit medium. (Right) Effective constitutive parameters of the metamaterial; where $\varepsilon_{eff} = 7\varepsilon_0$. Figure from [21].

The reference patch length was 2.16 cm and 1.80 cm width, printed on a substrate with $\varepsilon_r = 13.92$ and a thickness of 3 mm. The ground plane was 3.96 cm x 3.84 cm. This antenna was compared with the one in Fig. 2.16.

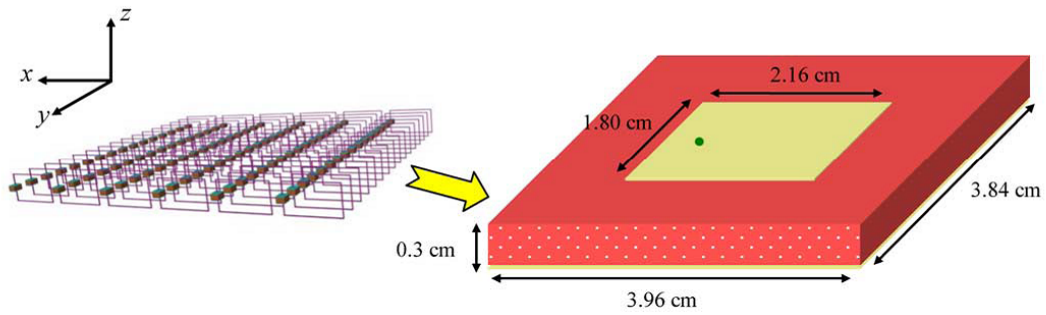

Figure 2.16: Patch antenna printed on the embedded-circuit metasubstrate with effective parameters given in Fig.2.15. The loop circuits are embedded inside the host medium with $\varepsilon_r = 4.5$ [21].

FDTD was the numerical technique used to characterize the structure. Return losses can be observed in Fig. 2.17. A resonance at $f_0 = 1.74GHz$ (miniaturization factor of 4) and a narrow bandwidth of 0.6% are observed for the dielectric substrate case, while for the metasubstrate case the bandwidth is increased to about a 1%.

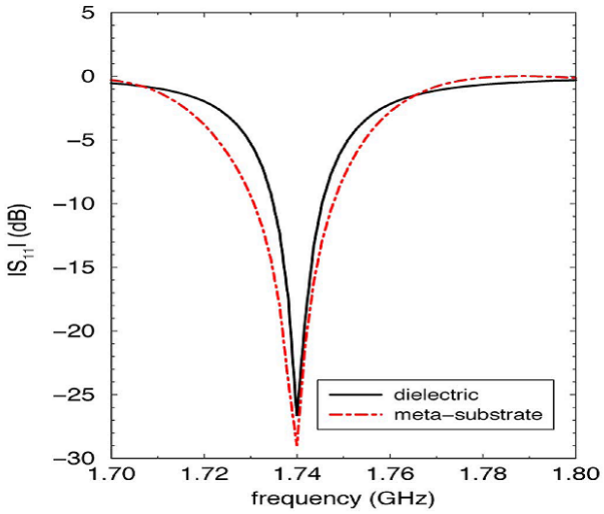

Figure 2.17: $|S_{11}|$ of antenna printed on dielectric and embedded-circuit substrates. The metasubstrate clearly provides larger bandwidth. Figure from [21].

The radiation patterns for both antenna fillings are similar. The simulated radiation efficiency is 76% for the antenna printed on the metasubstrate, in front of the 78% presented by the antenna printed on the dielectric material.

In conclusion, to achieve a high radiation performance and sufficient impedance bandwidth is possible. However the antenna must operate below the resonant frequency of the metasubstrate in the spectral range where there is a weak dispersion characteristic of the material, low loss behaviour and an acceptable high permeability value.

These results seem to contradict the Ikonen et al. ones. However there are some reasons explained in [22] that lead to the different conclusions extracted by Mosallaei et al.

2.2.4.3 Abdouni et al. [23] miniaturization approach

With the use of a metasolenoid as an artificial magneto-dielectric substrate, Abdouni et al. designed a compact patch antenna operating around 5 GHz for the Wi-Fi applications.

The unit cell used to simulate the material behaviour is depicted in Fig. 2.18, which reproduces with the maximum accuracy the physical realisation (its top view can be observed in Fig. 2.19- right).

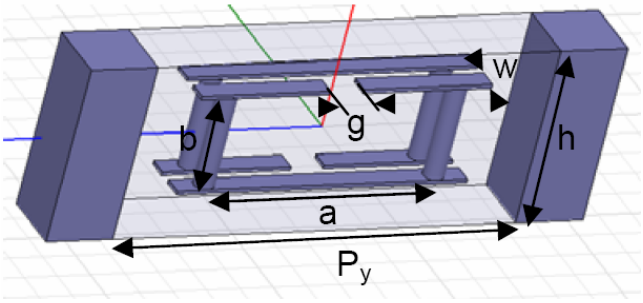

Figure 2.18: Simulated unit cell. The host substrate has a permittivity value of $\varepsilon_r = 2.22(1 - j0.0009)$, the unit cell height is h=3mm and the distance $P_y = 6mm$. The SRR measures are: a=3.4mm, b=1.575mm, g=0.5mm, w=0.32mm and d=0.2mm [23].

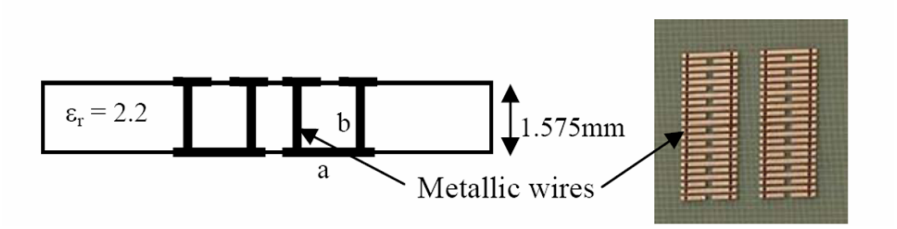

Figure 2.19: Cross section (left) and top view (right) of the metasolenoids of Abdouni et al. [23].

They simulated and measured the reflection coefficient of the antenna. The results in Fig. 2.20 show a multiresonant behaviour of the antenna, due to the combination of the resonant nature of the material with the resonant nature of the patch antenna (note that the resonance of the material, around 4.5 GHz, is very near the resonance of the considered patch antenna, 5 GHz). The theoretical resonance frequencies observed were $f_{1The} = 4.391\,GHz$, $f_{2The} = 4.973\,GHz$, $f_{3The} = 5.461\,GHz$ and $f_{4The} = 7.573\,GHz$. The simulated and measured results are in a good agreement.

They concluded that the frequency of resonance of the patch antenna printed in metamaterial substrate is reduced by 52% for f_{1The} and by 17% for f_{4The} compared to a patch printed on a single dielectric of permittivity $\varepsilon_r = 2.2$ (without metasolenoids) with a 9.2GHz resonance frequency.

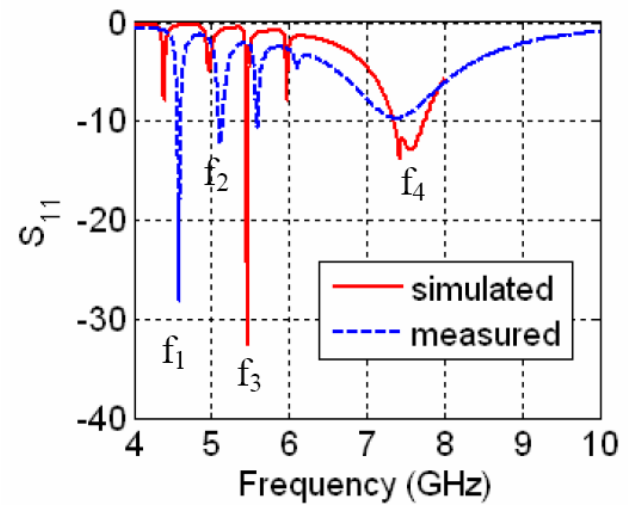

Figure 2.20: Simulated and measured magnitude of the reflection coefficient of the patch antenna filled with a meta-solenoid. The results are in a good agreement [23].

2.2.4.4 Bilotti et al. [24] miniaturization approach

Numerical results obtained by modeling a μ-negative (MNG) metamaterial as an ideal homogeneous and isotropic metamaterial block [25] show that a relevant role in the good radiation properties is played by the geometry of the antenna which is loaded by the MNG metamaterial. For microstrip patch antennas the circular geometry allows to select the desired resonant mode, providing the possibility of obtaining efficient radiation for whatever antenna size. On the contrary, sub-wavelength rectangular patches are not capable to radiate efficiently, even if the resonant mode is used.

For that reason a circular microstrip patch antenna is investigated performing full-wave numerical simulations with the commercial software CST Microwave Studio [26].

A first antenna approach uses a single ring of magnetic inclusions located in the region of the patch where the amplitude of the magnetic field is maximum. The sketch of the proposed metal inclusions geometry can be observed in Fig. 2.21(a).

The antenna substrate has a thickness of $5\,mm$ and a permittivity of $\varepsilon_r = 2.33$. The dielectric thickness of $5\,mm$ is equivalent to $\lambda/80$ at the considered material λ. This constitutes an important drawback in the use of SRRs (Split Ring Resonators) as metal inclusions: the regular SRRs inclusions described in literature have an electrical size of $\lambda/20$. In [27] the multiple split ring resonators (MSRRs) and the spiral resonators (SRs) are studied and compared (their geometry is depicted in Fig. 2.21(b) and (c), respectively). MSRRs are capable of reducing the dimension of the magnetic inclusion to the order of $\lambda/40$, while SRs can reduce it to the order of $\lambda/100$. SRs are the ones finally used in the antenna studied by Bilotti et al.

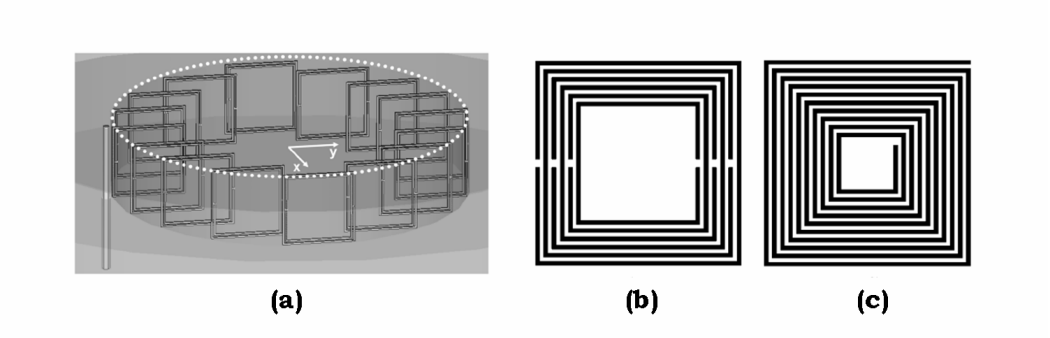

Figure 2.21: (a) Conceptual implementation of a single ring of magnetic resonant inclusions underneath the patch to obtain the required MNG behaviour at the desired frequency. (b) Geometry of an MSRR with six split-rings. (c) Geometry of an SR with ten turns [24].

After some field and density distributions study, it is inferred that the optimal distribution of the metal inclusions under the circular patch should be the more uniform possible. The geometrical sketch of the final design is depicted in Fig. 2.22.

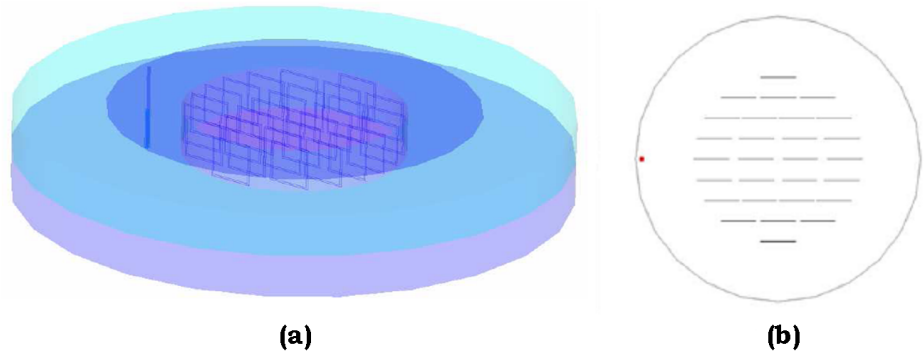

Figure 2.22: (a) Geometrical sketch of the final design of the metamaterial patch antenna, showing the uniform distribution of the SR inclusions inside the cylindrical core cavity underneath the patch. (b) Top-view of the patch, showing the arrangement of the inclusions. SRs with 5 turns are used with the following geometrical dimensions: strip width $w = 0.1\,mm$, separation between two adjacent strips $s = 0.1\,mm$, length of the external side of the SR $l = 4.8\,mm$. The total number of inclusions is 28 in this antenna realization. The distance between neighbouring rows of inclusions is 2.9mm [24].

Figs. 2.23 and 2.24 show, respectively, the return losses and the gain radiation patterns of the antenna. There are two resonant frequencies: a low frequency (where the *MNG* material resonates), 0.47 GHz, and a higher frequency, 2.44 GHz, determined by the electrical size of the patch. At frequencies higher than 0.47 GHz the *MNG* medium behaves as a regular dielectric.

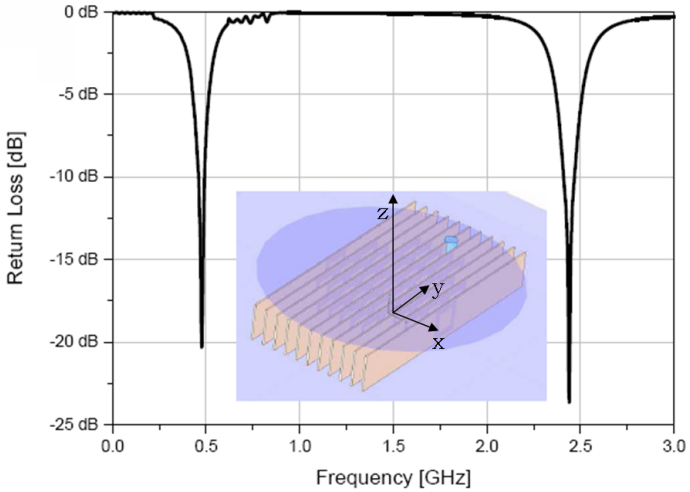

Figure 2.23: Matching features of the antenna. Figure from [24].

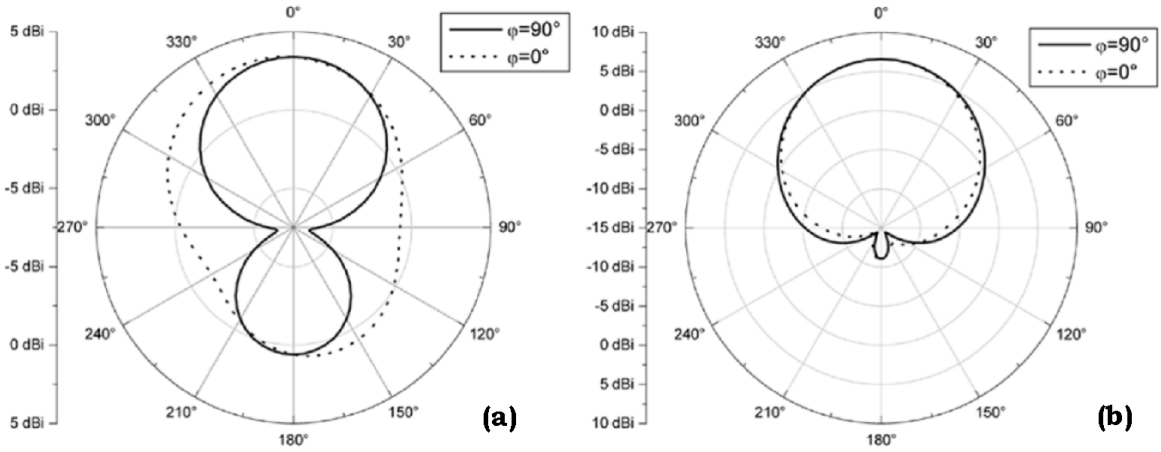

Figure 2.24: Gain radiation patterns of the antenna at 0.47GHz (a) and at 2.44GHz (b) [24].

The radiation efficiency at 0.47 GHz is 0.67, and the gain is 3.4 dBi. At the second resonant frequency of 2.44 GHz the antenna performs a radiation efficiency of 0.92 and its gain is 6.5 dBi.

2.2.4.5 Lee et al. [28] miniaturization approach

Lee et al. used a new design for patch antenna miniaturization with improved impedance bandwidth. The new design replaces the solid metal ground plane with a defected ground plane loaded with complementary split ring resonators (CSRRs). Fig. 2.25 shows the geometry of the CSRR loaded microstrip patch antenna.

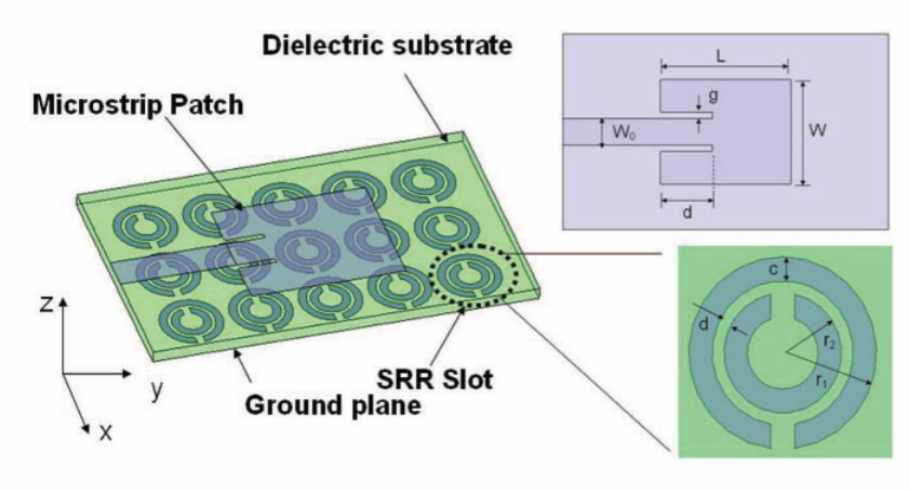

Figure 2.25: Configuration of the CSRR loaded microstrip patch antenna. Figure from [28].

The physical parameters of the CSRR are: $r_1 = 4.0\,mm$, $r_2 = 2.5\,mm$, $c = 1.0\,mm$, $d = 0.5\,mm$. The substrate thickness is $1.6\,mm$ and its dielectric permittivity is $\varepsilon_r = 3$. The antenna measures $30\,mm$ x $50\,mm$.

The physical parameters for the reference patch antenna (with a traditional solid metal ground plane) are: $W = 16\,mm$, $L = 20\,mm$, $g = 1\,mm$, $d = 8\,mm$ and $w = 4.08\,mm$. The physical parameters for the antenna with the metamaterial substrate are the same except: $d = 4\,mm$ and $w = 1.1\,mm$. The parameters d and w are adjusted in order to match the antenna impedance.

Some simulations using the Ansoft HFSS commercial code were carried out, and the resulting return loss parameters indicated that a CSRR loaded antenna using a substrate with $\varepsilon_r = 3$ achieves the same reduction in the antenna resonant frequency than a conventional antenna with a substrate having $\varepsilon_r = 6$. Moreover, the bandwidth at the operating frequency is wider than the original operating frequency.

Four antenna are fabricated and measured. A first pair having $\varepsilon_r = 3$; one printed on a conventional solid ground plane and another printed on a ground plane with CSRR etched on it. The second pair of antennas have a substrate permittivity $\varepsilon_r = 4.7$.

The resulting measurements can be observed in Fig. 2.26.

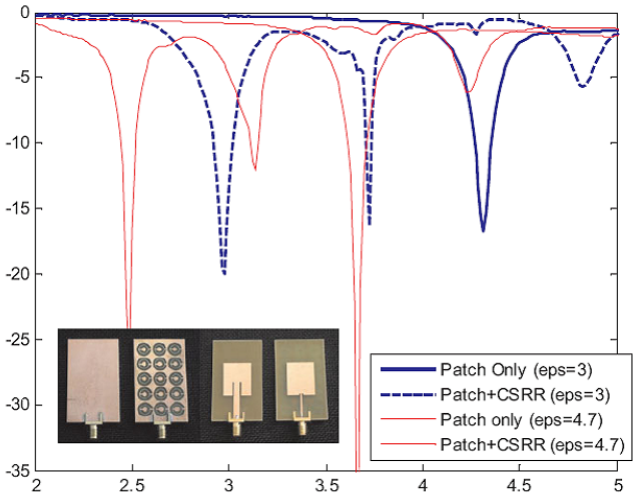

Figure 2.26: Comparison of measured return losses between the conventional antennas and the CSRR loaded ones. Figure from [28].

The resonant frequency of the CSRR loaded antennas were noticeably lower than the ones achieved with the conventional patches. In addition, the impedance bandwidth value was higher. However, the loading effect of the CSRR ground plane is reduced when the ε_r of the substrate employed is increased. Some measurements are gathered in Table 2.3.

Substrate permittivity (ε_r)	Configuration	Resonant Frequency (GHz)	Broadside Gain (dBi)	Fractional Bandwidth (%)	
				S_{11}< -6dB	S_{11}< -10dB
3.0	Conventional	4.31	6.05	3.81	2.01
	Patch with CSRR	2.96	2.06	6.38	3.34
4.7	Conventional	3.66	1.27	4.89	2.74
	Patch with CSRR	2.49	-0.5	5.76	3.21

Table 2.3: Comparison of measured antenna parameters between the conventional and CSRR loaded microstrip patch antenna [28].

The patch antennas loaded with CSRRs present higher backside radiation, which results in reduced broadside gain values. In addition, more ripples are introduced in the radiation pattern shape and the level of the cross polarisation is higher. Fig. 2.27 shows that the CSRR loaded antenna presents omnidirectional patterns. The former effect is due to the reduction of the electrical size of the ground plane, as a consequence of the reduced resonant frequencies obtained with this kind of ground plane.

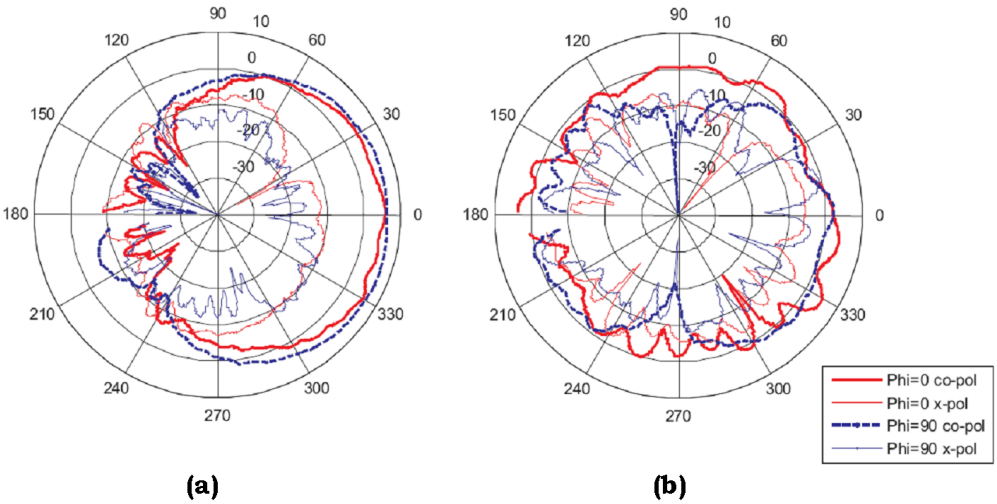

Figure 2.27: Measured radiation patterns: (a) conventional patch antenna (freq. =4.3GHz), (b) CSRR loaded patch antenna (freq. =2.96GHz) [28].

Finally, the authors propose to find an optimized CSRR geometry to improve the performance of the CSRR loaded antennas. Nevertheless, the experimental results confirm that significantly higher antenna miniaturization, of a 69%, can be obtained when compared with conventional antennas among with an improvement of a 67% in the impedance bandwidth.

2.3 Maximum Bandwidth of an antenna under test

As explained in Subsection 2.2.1, there is a limit relating the maximum FBW and the size of an antenna. Two different procedures to compute the maximum FBW are going to be described.

2.3.1 Direct measurement

An antenna can be designed to match to a Z_{ref} or to be resonant at f_0. Whatever the criterion followed to design the antenna, its impedance bandwidth can be computed from the reflection coefficient referred to the reference impedance of the circuitry at which the antenna has to be connected. Fig. 2.28 depicts the situation.

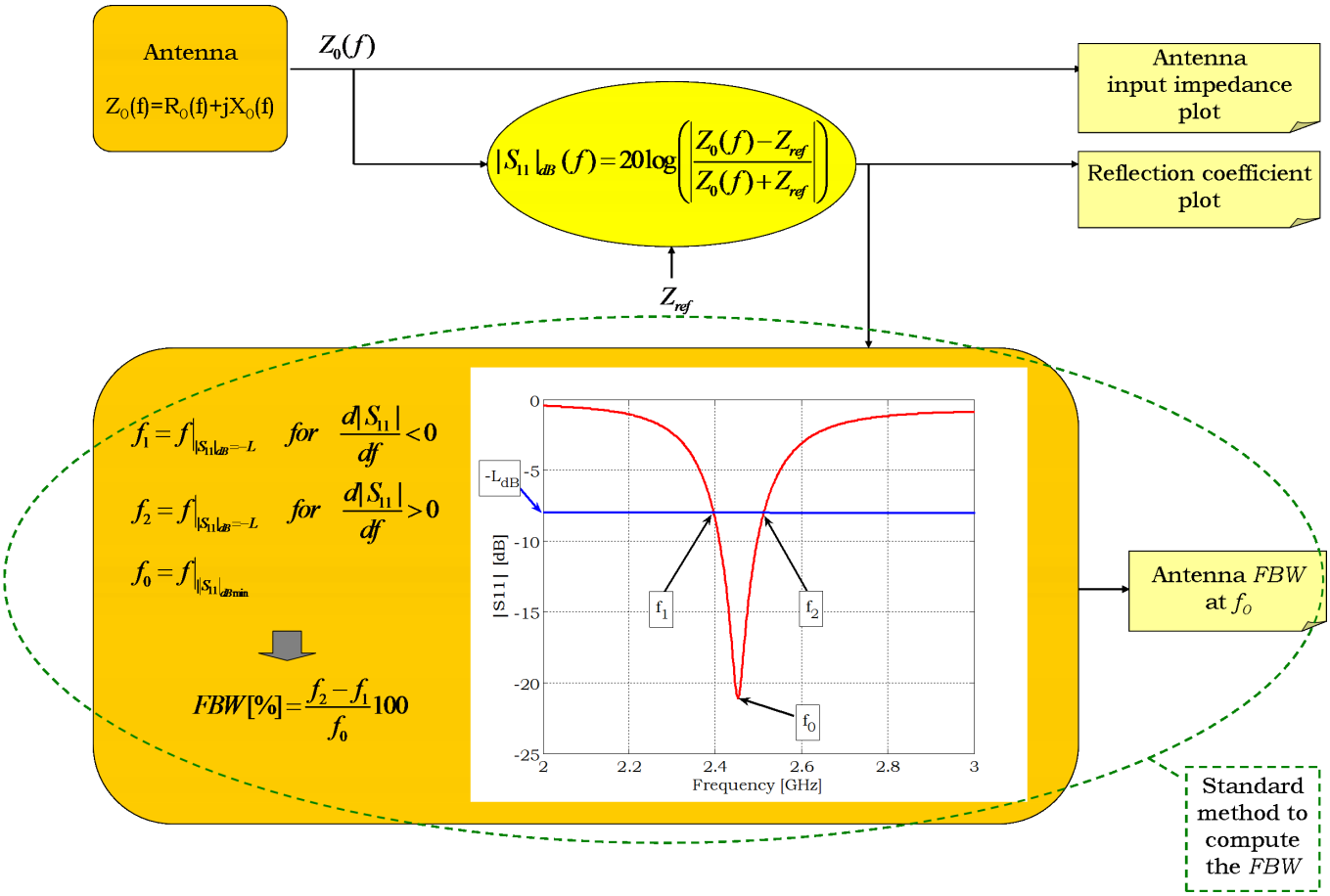

Figure 2.28: Standard method to compute the FBW.

However, the fractional bandwidth obtained in this way is not the maximum that can be achieved. If properly matched, the maximum power would be transferred to the antenna.

2.3.2 Yaghjian's formula

Yaghjian and Best [10] introduced the *matched VSWR bandwidth*, that can be defined at all frequencies (for a small enough fixed reflection coefficient value). That means that exists both in the resonant ($X_0'(\omega_0) > 0$) and in the antiresonant ($X_0'(\omega_0) < 0$) frequency ranges. But, what does this mean?

The radical change in meaning is the following: with the *Yaghjian's VSWR matched fractional bandwidth*[3] (FBW) is possible to obtain a value of the antenna bandwidth even at frequencies where the antenna is not actually properly working. In this way, from an antenna design one can not only know whether that antenna is going to perform a good bandwidth at f_0, but also if it is going to perform a better bandwidth at other frequencies.

[3] Named *matched bandwidth* from now on.

To better understand those implications, it is necessary to know the Yaghjian's proposed formulation:

$$FBW(\omega_0) \approx \frac{4\sqrt{\beta}R_0(\omega_0)}{\omega_0|Z_0'(\omega_0)|}, \quad with\ \sqrt{\beta} = \sqrt{\frac{\alpha}{1-\alpha}} = \frac{S-1}{2\sqrt{S}} \leq 1 \tag{2.12}$$

Where Z_0' is the first derivative (with respect to frequency) of the antenna input impedance after tuning, R_0 is the input resistance of the antenna after tuning, ω_0 the frequency at which the antenna is tuned[4] and S is the desired $VSWR$ value.

This formula is obtained defining the matched $VSWR$ bandwidth as the difference between the two frequencies on either side of ω_0 at which the $VSWR$ equals a given $VSWR$, S. Equivalently, the difference between the two frequencies on either side of ω_0 at which the squared magnitude of the reflection coefficient $|\Gamma_0(\omega)|^2$ equals $\alpha = \frac{(S-1)^2}{(S+1)^2}$. All of this provided that the characteristic impedance of the feed line, Z_{ref}, equals $Z_0(\omega_0) = R_0(\omega_0)$ (the input resistance of the antenna at ω_0). It is considered $\alpha \leq 1/2$ (which means a return loss better than 3dB).

The Eq. 2.12 holds for tuned antennas under the sufficient conditions that $X_0'(\omega)$ and $R_0'(\omega)$ do not change greatly over the bandwidth.

Our aim is to apply this new formulation to the design of microstrip patch antennas loaded with artificial materials.

The sketch of the procedure to be followed in order to compute the maximum matched FBW is depicted in Fig. 2.29. The method computes the maximum FBW from the measured (or simulated) antenna input impedance. The input impedance of the antenna as a function of frequency is required to compute the FBW at each and every frequency.

[4]Note that to tune means to make the reactance zero ($X_0(\omega_0)$=0, by means of using an external series inductance or capacitance), which is not exactly the same as to make the antenna resonant (adjust $X_0(\omega_0)$=0 in the antiresonant -for microstrip antennas- region where $X'_0(\omega_0) < 0$).

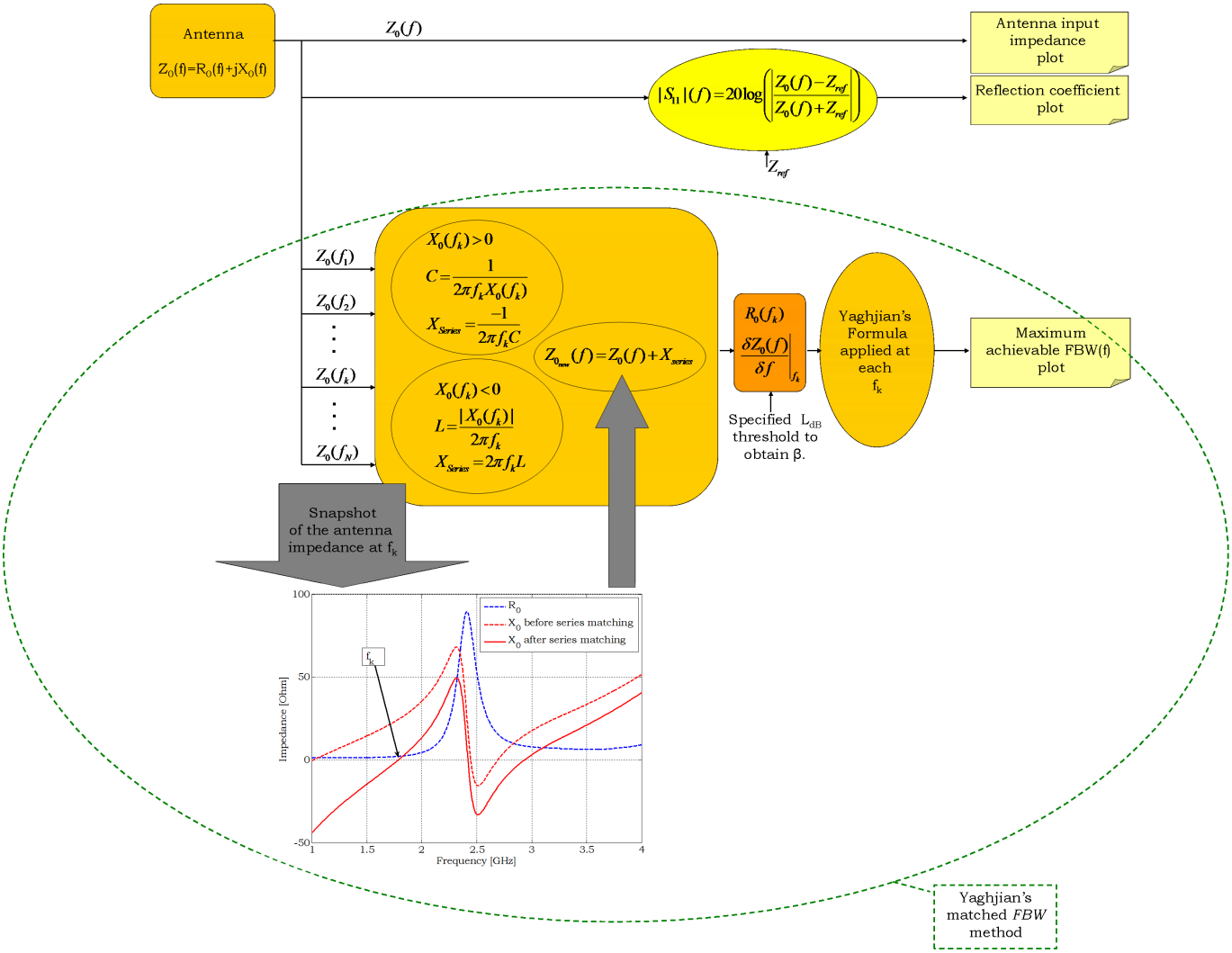

Figure 2.29: Yaghjian's matched FBW: sketch of the procedure.

Chapter 3

Size and Bandwidth Study of Microstrip Patch Antennas Filled with Homogeneous Substrates

The impact that the ε_r and μ_r values of the substrate of a patch antenna have in the $FBW$are studied for positive values (ε_r,μ_r>0).

Our main objective is to study the FBW behaviour when miniaturizing the antenna, in order to determine if a material with given properties allows to shrink the antenna without decreasing its FBW. It will be numerically demonstrated that this can be done by means of loading the patch antenna with a material that presents a high μ_r or a low (near zero) ε_r. Metamaterials are suitable to accomplish this objective. However, a practical substrate would have a dispersive ε_r - μ_r behaviour, anisotropy and losses. Dispersion will be considered in Chapter 4, whilst losses are considered in the present one.

First of all, the direct calculation of the FBW and the obtained by means of the Yaghjian's formula are compared. From this comparison, the method to extract the FBW values subsequently is decided. The effect that the variation of the substrate permittivity and permeability has on the antenna FBW and size is studied for the lossless and homogeneous case. Once firts observations are derived from this cases of study, lossess are introduced to determine their influence in the antenna FBW.

Different antenna design methods are applied to determine whether the design criterion can affect the obtained FBW results, which design method is more practical, etc.

A discussion on the obtained results is carried out, analysing the FBW values the miniaturization factors reached in every of the variations and with every of the design methods studied. An exhaustive explanation of how the Yaghjian's method works and which implies is presented in order to make clear why the obtained results are different from the ones obtained by other authors.

3.1 Substrate Properties Variation

The reference antenna with air filling is depicted in Fig. 3.1, having the parameters listed in Table 3.1. The patch antenna has a patch sized substrate, and the choosen ground plane length, L_{gp}, is a free space wavelength (λ_0) at the operational antenna frequency $f_0 = 2.45\,GHz$ (this value is considered suffieciently large to avoid possible resonant effects that may appear when having a finite ground plane). Both the patch and the ground plane are squared ($L = W$ and $L_{gp} = W_{gp}$).

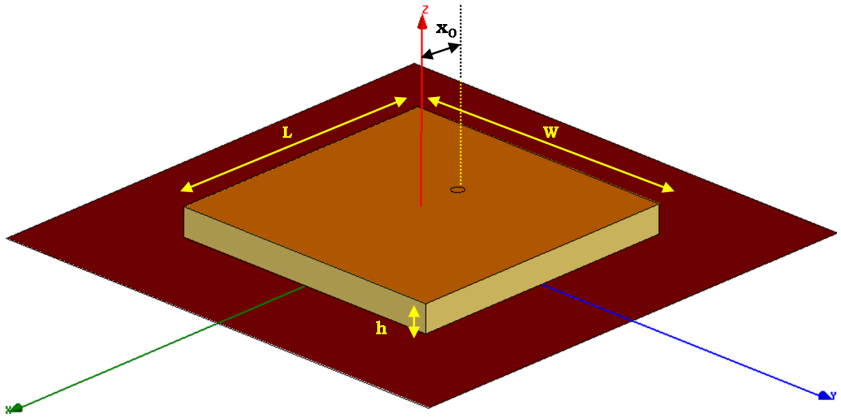

Figure 3.1: Reference patch antenna.

ε_r, μ_r	L (= W) [mm]	x_0 [mm]	λ_m [mm]
1, 1 (air)	53.7138 (λ_m/2.279)	10.1500 (λ_m/12.0639)	122.448

Table 3.1: Reference patch antenna characteristics. Since the reference antenna is filled with air, the wavelentgth in the material is equal to the free space wavelength ($\lambda_m = \lambda_0$).

When working with patch antennas two frequencies are of interest: the antiresonance frequency (the input reactance of the antenna crosses 0Ω with negative slope) and the matching frequency (the input impedance of the antenna matches the reference impedance). These parameters are controlled by different physical properties of the structure. Since the input impedance is affected by the size of the patch and also the feed position inside the patch, both the reactance and the impedance change with the variation of these parameters. However, that happens provided that other characteristics of the antenna are not changed (i.e.: the high, length and/or width of the substrate).

The typically used frequency to design an antenna is its matching frequency (f_0). That is the method that will be followed: the matching of the antenna at 2.45GHz. The objective would be twofold: to have the antenna matched at a frequency the nearest possible to f_0 and at the same time to set the matching level at approximately -20dB. One of the advantages when following this criterion is that one can rapidly compare the results by having a quick look at the $|S_{11}|_{dB}$ parameter (or equivalently the return losses) of the different designs.

Ansoft HFSS v11 **[29]**, a Finite Element Method (FEM) software has been used to perform these simulations.

3.1.1 FBW direct measurement vs. Yaghjian's formula

Before analysing variations in the substrate properties, the direct measurement for computing the maximum FBW and the method proposed by Yaghjian (Subsection 2.3.2) are compared. The results can be observed in Fig. 3.2.

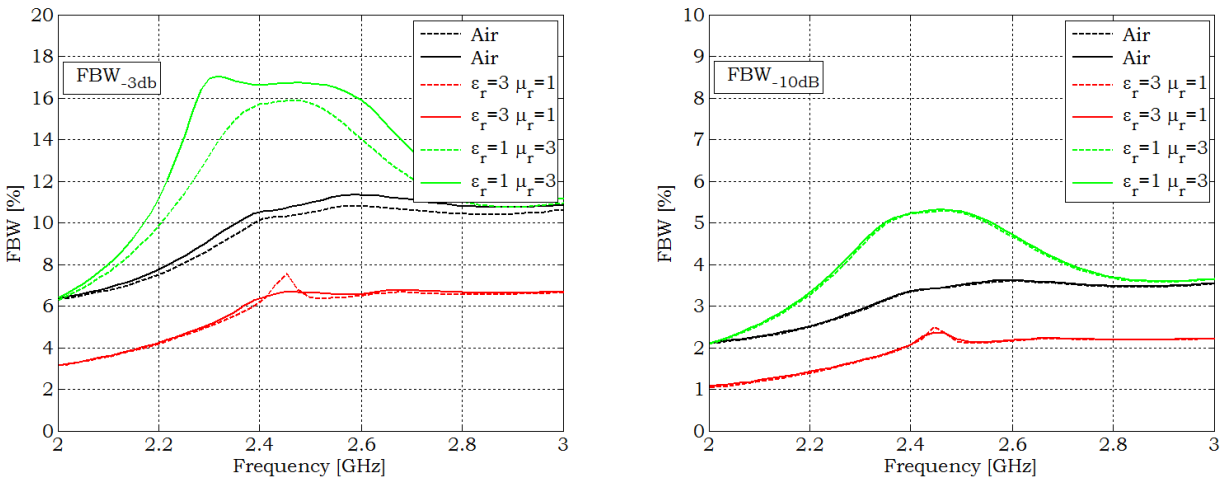

Figure 3.2: Computed FBW_{-3dB} (a) and computed FBW_{-10dB} (b). Comparison between the Yaghjian's formula (dashed lines) and the direct measurement (solid lines).

The values chosen to carry out the comparison are: the reference air case, $\varepsilon_r = 3$ and $\mu_r = 3$. As it is expected from Hansen's BW formula (Subsection 2.2.3), the $\varepsilon_r > 1$ case has lower FBW values than the air, while the $\mu_r > 1$ case has higher FBW than the reference case. Fig. 3.2 (a) shows the FBW_{-3dB}, while Fig. 3.2 (b) the FBW_{-10dB}. As it can be observed, for a threshold L=3dB the difference between the two compared methods is more noticeable than in the L=10dB case. Nevertheless, the matched bandwidth results are more conservative for almost all the frequency range than the ones obtained through the direct measurement. Therefore, the matched bandwidth is the method that will be used hereinafter to compute the maximum achievable FBW.

3.1.2 Permittivity (ε_r) value variation

In the nature materials like glass or porcelain have high ε_r and another substances like water can reach very high values.

Material	ε_r	tan δ_e
Air	1.0006	-
Glass	4 -7	$1x10^{-3}$
Paper	3	$8x10^{-3}$
Porcelain	6	$14x10^{-3}$
Teflon	2.1	$3x10^{-4}$
Titanium dioxide	100	$14x10^{-4}$
Water (distilled)	80	$4x10^{-2}$
Water (sea)	81	4.64
Wood (dry)	1.5-4	$1x10^{-2}$

Table 3.2: Dielectric constants of typical dielectric materials.

In our case, we are interested in high frequency laminates which can resist and present a good performance, having low dissipation factor ($\tan\delta_e$) or temperature stability, for example. Some dielectric materials specially designed for applications like the one described in this Chapter have ε_r values ranging from 3 to 10.2 (Rogers RO3000 and RO4000 families).

On the contrary, it is difficult to obtain a material which naturally presents a nearzero response of its ε_r at the microwave frequencies. There exists, for example, an artificial medium called *wire medium* having $\varepsilon_r < 1$ [30]. However it suffers from frequency dispersion.

We firstly analyse the effect of increasing the ε_r of the substrate having as a reference the case filled with air. Permeability, μ_r, is considered to be one in all the cases. Not only the values greater than one will be considered, but the ones having $0 < \varepsilon_r < 1$ will be also studied (which are referred to as near-zero). So we have $0 < \varepsilon_r < 10$, $\mu_r = 1$.

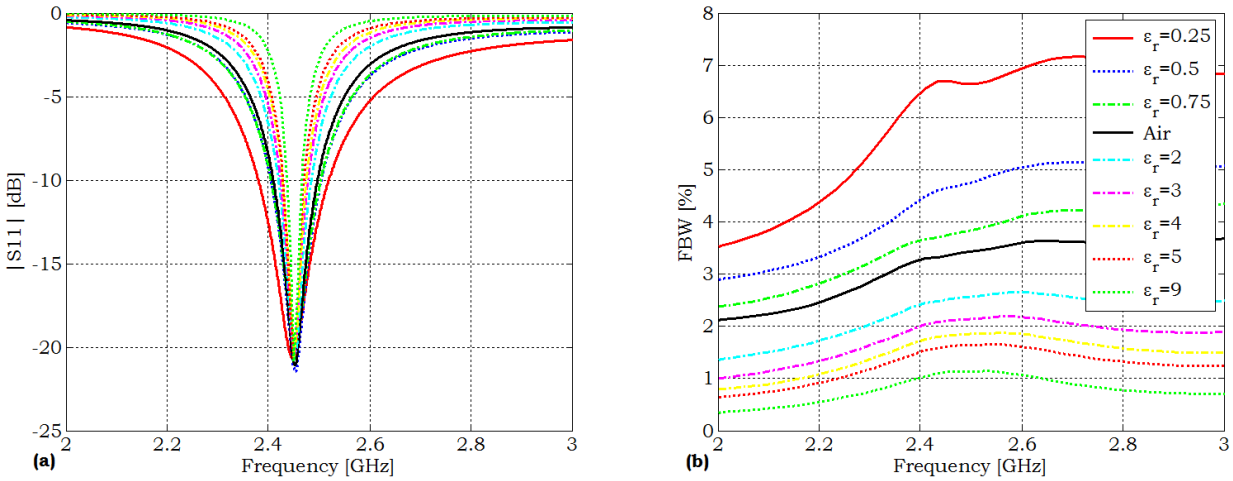

Figure 3.3: (a) Magnitude of the simulated reflection coefficient and (b) computed FBW_{-10dB} when $0 < \varepsilon_r < 10$.

As expected (Eq. 2.11) an increase in the ε_r value (with $1 < \varepsilon_r < 10$) produces a decrease in the bandwidth, always worst than the air filled bandwidth value. In addition, the antenna size shrinks, thus obtaining an interesting effect of antenna miniaturisation. Better FBW results appear when the ε_r value is between 0 and 1. Nonetheless, for these cases the antenna increases in size.

Some antenna parameters considered in the results of Fig. 3.3 can be observed in Table 3.3. To be resonant the antenna size is not necessarily $\frac{\lambda}{2}$, hence differing the results obtained from the predicted ones through Eq. 2.8. In addition, the values of x_0 change in a non-easy predictable way from one ε_r to another.

ε_r (μ_r=1)	FBW_{-10dB} (f_0) [%]	λ_m [mm]	L [mm]	x_O [mm]
0.25	6.7	244.8	80.85 (λ_m/3.0)	19.5 (λ_m /12.5)
0.5	4.6	173.1	67.53 (λ_m/2.5)	13.1 (λ_m /13.2)
0.75	3.7	141.3	59.37 (λ_m/2.3)	12.355 (λ_m /11.4)
1 (air)	3.3	122.4	53.7138 (λ_m/2.2)	10.1500 (λ_m /12.0)
2	2.5	86.5	41.75 (λ_m/2.0)	6.65 (λ_m /13.0)
3	2.0	70.6	35.4 (λ_m/1.9)	5.05 (λ_m /13.9)
4	1.8	61.2	31.32 (λ_m/1.9)	4.05 (λ_m /15.1)
5	1.6	54.7	28.5 (λ_m/1.9)	3.41 (λ_m /16.0)
9	1.1	40.8	22.08 (λ_m/1.8)	2.1 (λ_m /19.4)

Table 3.3: Antenna FBW_{-10dB} at $f_0 = 2.45\,GHz$ and physical parameters variation when ε_r is changed from 0.25 to 9. In the table $\lambda_m = \frac{\lambda_0}{n}$, being $\lambda_0 = \frac{c}{f_0}$ the wavelength at f_0 (2.45GHz in our case) and n=$\sqrt{\varepsilon_r \mu_r}$.

3.1.3 Permeability (μ_r) value variation

Although materials having a μ_r value different to one at microwave frequencies are difficult to be found, the study of the FBW of an antenna loaded with high-μ_r materials is interesting. With the recent advances in metamaterial structures engineering it is not impossible that a forthcoming discovery could lead to the existence of really high-μ_r materials. Natural materials such as some metals (nickel) with values of μ_r hundreds of times greater than a normal material exist, nonetheless their conductance is very poor and they are not used due to their losses. Another option would be the use of ferrites, but their high μ_r values are valid only when working at MHz at the most.

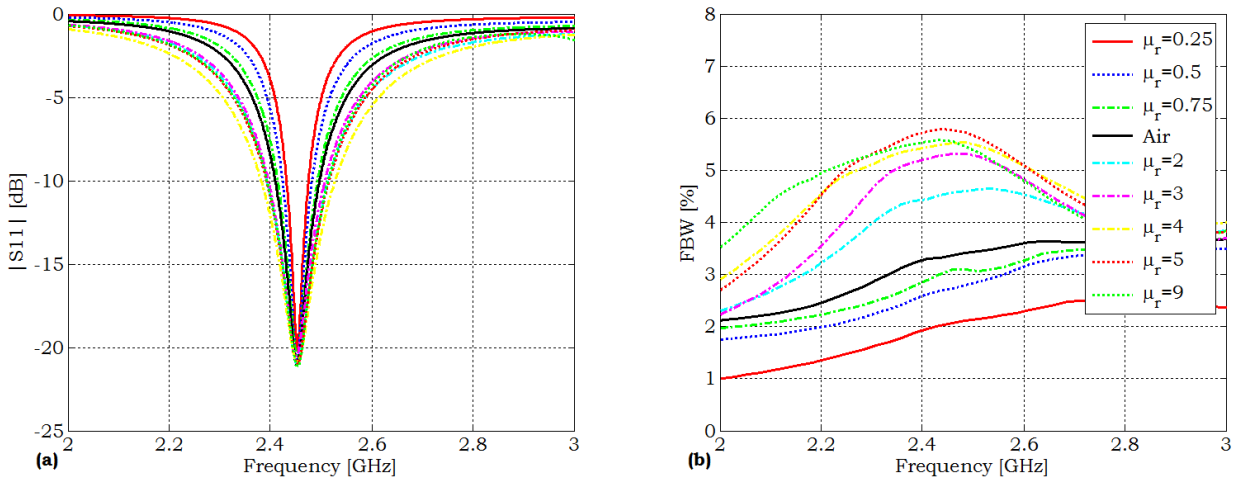

Figure 3.4: (a) Magnitude of the simulated reflection coefficient and (b) FBW_{-10dB} when $0 < \mu_r < 10$.

As it can be observed in Fig. 3.4, when μ_r is smaller than unity a low-FBW performance can be observed. However, it has to be pointed out that those low values in the FBW performance are not as low as the high-ε_r cases noticed in section 3.1.2. For instance, the ε_r= 3 case, which is a typical ε_r value, is comparable to the one having μ_r= 0.25, the worst of the near-zero μ_r cases studied. Thus, even the worst results with permeability substrates are better in terms of FBW than the ones considering only permittivity.

For high-μ_r values, the maximum achievable FBW is higher than the obtained in the air case. Hence, better FBW values than in the high-ε_r cases are obtained. However, there exists a limit in the maximum FBW enhancement. With $\mu_r = 2$ and $\mu_r = 3$ the obtained maximum FBW improves noticeably with respect to the air case. Higher permeability values ($\mu_r > 3$) lead to a slight maximum FBW improvement comparing with the previous results.

The variation in size of the patch antenna and its feeding position are shown in table 3.4.

μ_r (ε_r=1)	FBW_{-10dB} (f_0)[%]	λ_m [mm]	L [mm]	x_0 [mm]
0.25	2.0	244.8	108.7 (λ_m /1.2)	25.9 (λ_m /4.7)
0.5	2.7	173.1	74.43 (λ_m /2.3)	14.2 (λ_m /12.1)
0.75	3.0	141.3	60.8 (λ_m /2.3)	12.25 (λ_m /11.5)
1 (air)	3.3	122.4	53.7138 (λ_m /2.2)	10.1500 (λ_m/12.0)
2	4.5	86.5	41.25 (λ_m /2.0)	7.9 (λ_m /10.9)
3	5.3	70.6	35.92 (λ_m /1.9)	6.25 (λ_m /11.3)
4	5.5	61.2	34.05 (λ_m /1.7)	8.35 (λ_m /7.3)
5	5.5	54.7	31.7 (λ_m /1.7)	7.2 (λ_m /7.6)
9	5.7	40.8	28.65 (λ_m /1.4)	9.25 (λ_m /4.4)

Table 3.4: Antenna FBW_{-10dB} at $f_0 = 2.45\,GHz$ and physical parameters variation when μ_r is varied from 0.25 to 9. In the table $\lambda_m = \frac{\lambda_0}{n}$, being $\lambda_0 = \frac{c}{f_0}$ the wavelength at f_0 (2.45GHz in our case) and n=$\sqrt{\varepsilon_r \mu_r}$.

3.1.4 $\varepsilon_r \cdot \mu_r$ product variation

In most cases it would not be possible to design an artificial material with μ_r>1 and ε_r=1, but this material would have a permittivity $\varepsilon_r > 1$. For that reason it is obliged to check in what sense this situation is going to affect the antenna bandwidth.

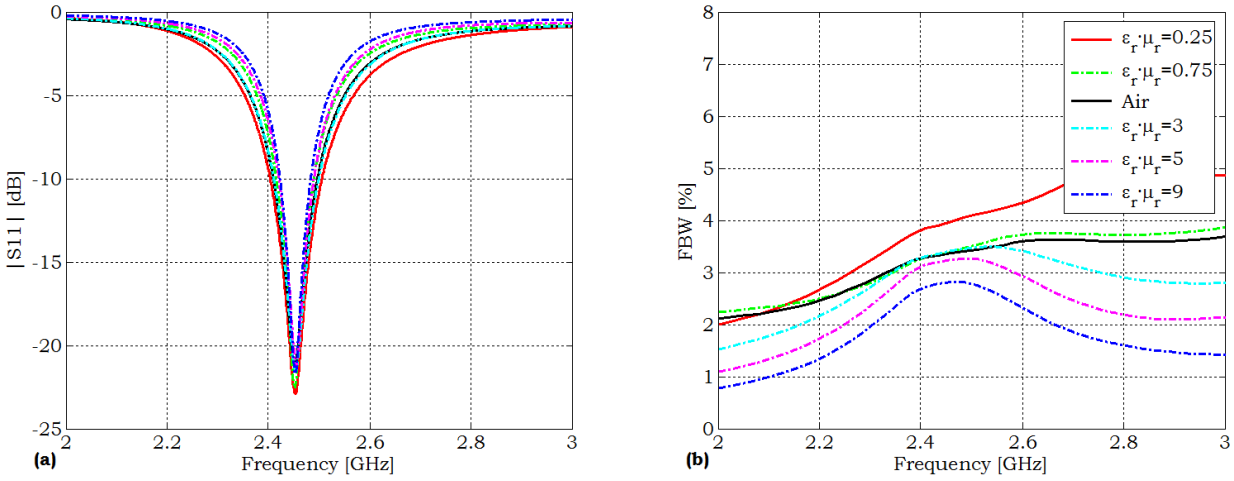

Figure 3.5: (a) Magnitude of the simulated reflection coefficient and (b) FBW_{-10dB} when increasing both the substrate ε_r and μ_r values, with ε_r=μ_r.

From Fig. 3.5 it can be extracted that if the substrate possesses a similar value of ε_r and μ_r a miniaturisation of the antenna while retaining the same bandwidth is possible. This idea has recently been exposed by Petrov et al. [31], who had the objective of achieving a high and equal μ_r and ε_r in order to obtain a certain miniaturisation of the antenna while retaining the matching to free-space. With that effect, no reflections between the antenna substrate and the air surrounding medium are expected to occur. Therefore the energy trapped in the substrate should be reduced compared with the non air-like impedance situations, achieving a higher bandwidth by means of lowering the Q. The problem in this study relies in the use of the ferrite-ferroelectric composites as a substrate; the size reduction is fulfilled at *MHz* frequencies, but in the *GHz* present high losses and scarcely miniaturises the antenna.

$n^2=\varepsilon_r \cdot \mu_r$	FBW_{-10dB} (f_0) [%]	λ_m [mm]	L [mm]	x_0 [mm]
0.25	3.9	244.8	98.7 (λ_m /1.7)	30.98 (λ_m /5.5)
0.75	3.3	141.3	60.6 (λ_m /2.3)	10.29 (λ_m /13.7)
1 (air)	3.3	122.4	53.7138 (λ_m /2.2)	10.1500 (λ_m /12.0)
3	3.3	70.6	35.62 (λ_m /1.9)	5.64 (λ_m /12.5)
5	3.2	54.7	29.4 (λ_m /1.8)	3.5 (λ_m /15.6)
9	2.8	40.8	24 (λ_m /1.7)	2.525 (λ_m /16.1)

Table 3.5: Antenna FBW_{-10dB} at $f_0 = 2.45\,GHz$ and physical parameters when the product $\varepsilon_r \cdot \mu_r$ is varied from 0.25 to 9, being $\varepsilon_r = \mu_r$. In the table $\lambda_m = \frac{\lambda_0}{n}$, being $\lambda_0 = \frac{c}{f_0}$ the wavelength at f_0 (2.45GHz in our case) and n=$\sqrt{\varepsilon_r \mu_r}$.

3.2 Losses in the Substrate

To approach a step to reality, the losses in the substrate are now considered. The objective is to know how losses affect to the FBW. Permittivity and permeability are not real values. The following equations consider the lossy nature of a material:

$$\varepsilon_r = \varepsilon' + j\varepsilon'' = \varepsilon'(1 + j\frac{\varepsilon''}{\varepsilon'}) = \varepsilon'(1 + j\,tan\delta_e) \tag{3.1}$$

$$\mu_r = \mu' + j\mu'' = \mu'(1 + j\frac{\mu''}{\mu'}) = \mu'(1 + j\,tan\delta_m) \tag{3.2}$$

Where tanδ_e is the dielectric loss tangent and tanδ_m is the magnetic loss tangent. These parameters model the losses in the patch substrate. When the substrate is lossless, $\varepsilon_r = \varepsilon'$ and $\mu_r = \mu'$.

The reference considered cases are ε'=2 and μ'=2 separately, following the matching method seen in sections 3.1.2, 3.1.3 and 3.1.4. The dielectric and magnetic tangent losses are increased progressively.

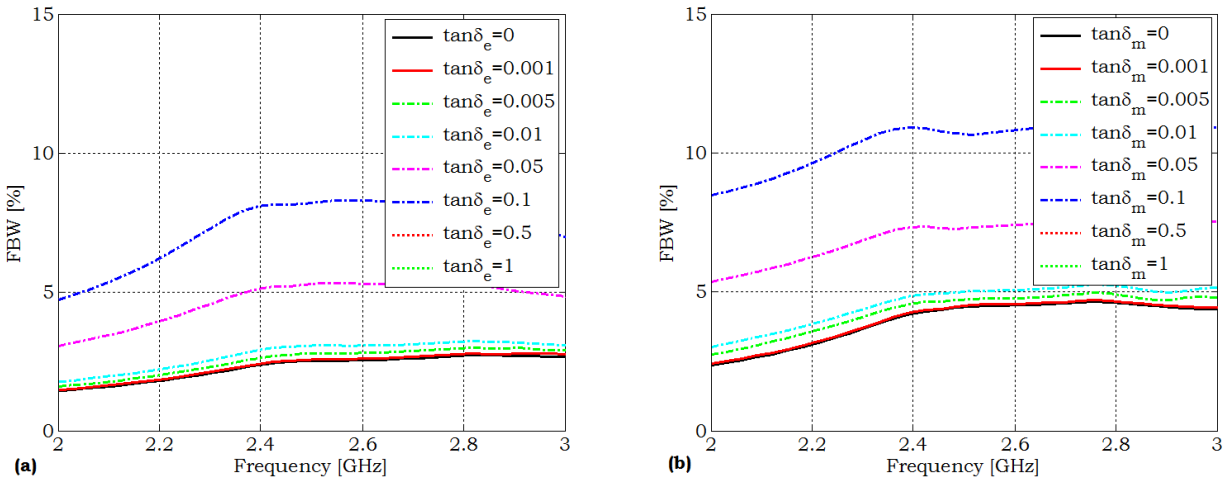

Figure 3.6: Computed FBW_{-10dB} when increasing the (a) dielectric loss tangent and (b) the magnetic loss tangent. The reference lossless cases are ε_r=2 and μ_r=2.

The results in Fig. 3.6 clearly show that the losses in the dielectric increase the FBW. However this is a common effect in all kind of antennas and not only in microstrip patches. The achieved FBW for loss tangents with values 0.5 and 1 are higher than 15% and are not shown in the figures. In those cases the antenna is not naturally resonant (the reactance is always higher than zero). The problem is that the efficiency decreases, as shown in Table 3.6. It has also been assessed that the same conclusions apply to lossy magnetic substrates.

tan δe	R_{in} [Ω]	η_{HFSS}	$\eta_{Rin\ definition}$	*tan δm*	R_{in} [Ω]	η_{HFSS}	$\eta_{Rin\ definition}$
0	155.9	1.01	1	0	168.4	1.01	1
0.001	152.6	0.99	0.97	0.001	166.6	0.99	0.98
0.005	141.8	0.91	0.90	0.005	159.5	0.94	0.94
0.01	127.3	0.83	0.81	0.01	152	0.89	0.90
0.05	75.31	0.49	0.48	0.05	109.3	0.62	0.64
0.1	51.12	0.32	0.32	0.1	82.74	0.44	0.49
0.5	16.45	0.09	0.10	0.5	56.82	0.11	0.33
1	11.67	0.04	0.07	1	47.88	0.05	0.28

Table 3.6: Computed antenna input resistance and radiation efficiency when the electric and the magnetic losses in the substate increase.

The HFSS-computed radiation efficiency seems to have a little error, as it can be extracted from the fact that the radiation efficiency is greater than 1 in the lossless cases. It can be due to the different round-offs of decimal numbers obtained during the computation, which can lead to obtain a final value a little over the exact one [32]. Another cause could be the air box dimensions; normally the air box boundaries are drawn a quarter-wavelength from the nearest radiating edge of the structure (the edge of the substrate). It is considered to be a sufficient distance but a larger one can lead to more accurate results.

The HFSS-computed radiation efficiency values are compared with the efficiencies computed using the definition of radiation efficiency in Eq. 3.3:

$$\eta = \frac{R_{in}(lossless\,substrate)}{R_{in}(lossy\,substrate)} \tag{3.3}$$

As it can be seen in the table the efficiency values are very similar.

If the reflection coefficients are observed (Fig. 3.7) it is clear that a 50Ω match is improved for some cases. This is due to the fact that the quality of the matching to 50Ω in the reference cases ($\varepsilon_r = 2, \mu_r = 2$) was tuned moving the fed position inside the structure, therefore if its impedance is modified in any sense the matching will result affected.

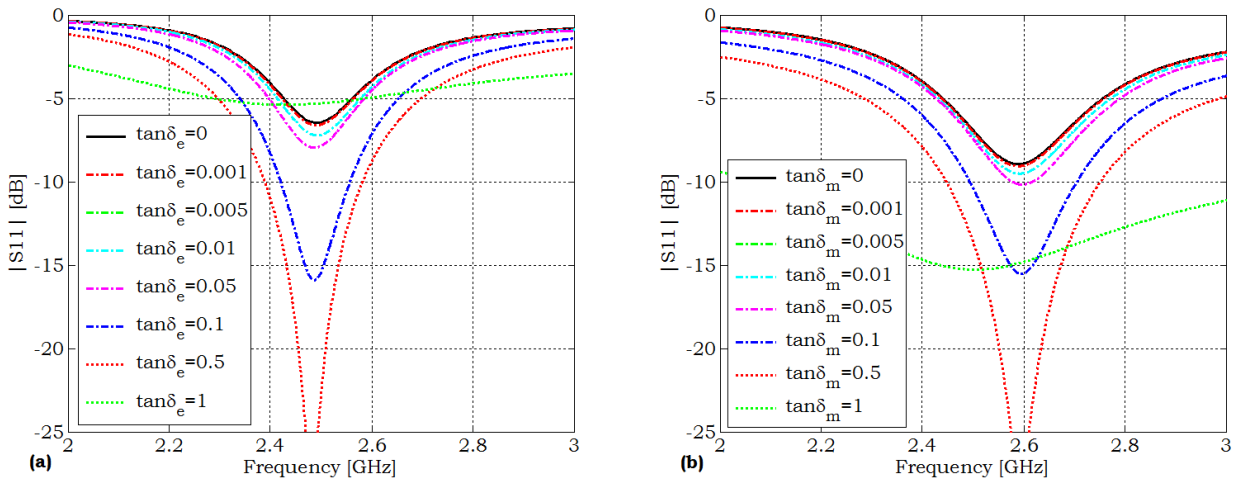

Figure 3.7: Magnitude of the simulated reflection coefficient (a) when increasing the electric loss tangent and (b) when the magnetic loss tangent is increased.

3.3 Antenna design methods

There is not a unique manner to design the patch antenna. It depends on whether the antenna has to resonate or to be matched at f_0. In the following subsections the advantages and disadvantages of

three different methods are analysed, taking into account the pragmatism of each method in order to obtain a maximum matched *FBW* estimation. An outline of each of them and their implications can be seen in Fig. 3.8.

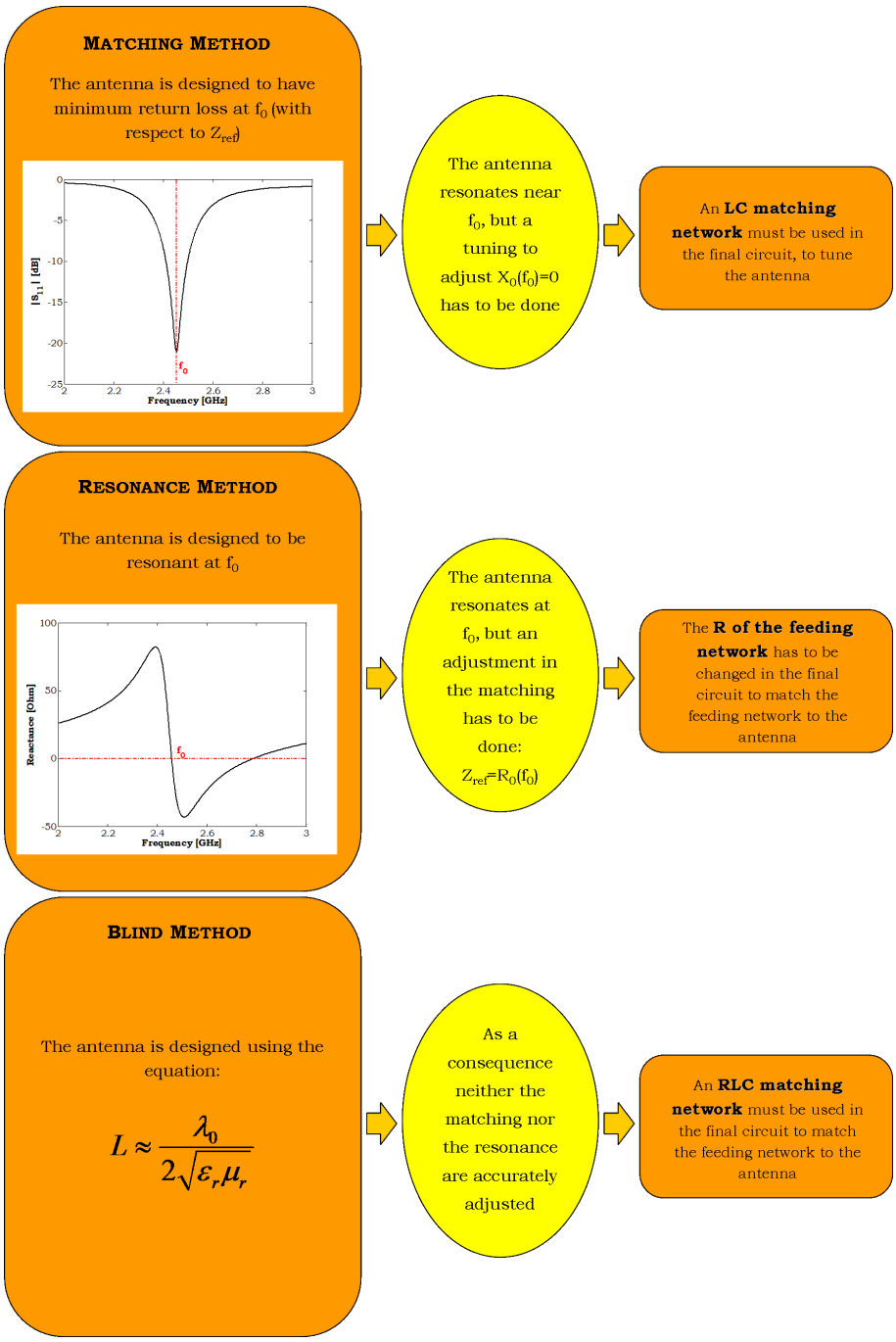

Figure 3.8: Block diagram of the antenna method design possibilities having as an objective to fulfill the maximum *FBW* possible. (a) *matching method*, (b) *resonance method* and (c) *blind method*.

3.3.1 Minimum S_{11} at f_0 or matching method

The method applied since the moment consisted on matching the antenna at 2.45GHz to a 50Ω reference impedance. The objective was to have the antenna matched at f_0 and at the same time to set the matching level at approximately -20dB.

To obtain the desired results both the length of the patch and the fed position had to be varied, in an iterative process to find the adequate reflection coefficient tuning and matching. This is not a rapid process, especially for high-μ_r values[1].

The computed maximum FBW based on the Yaghjian's formula considers the antenna to be tuned and matched at every frequency where the formula is applied. In addition, the maximum value of the curve representing the maximum FBW does not have to coincide with the frequency at which the antenna has the better matching level to 50Ω.

In conclusion, applying the Yaghjian's method the best FBW will probably appear at a frequency where the resistance of the antenna is not 50Ω. In the cases studied in the last subsections (where the method used is the *matching method*) it is not strange that the maximum value of the maximum FBW figure had appeared near f_0. The reason is very clear: the matching of the antenna was accurately adjusted for a 50Ω reference impedance at f_0. This can be checked looking at Table 3.7, where the magnitude of the antenna input impedance, $|Z_0|$, is clearly around 50Ω. However, the circuit where the antenna will be connected will not always have Z_{ref}=50Ω. For this reasons the *matching method* used since the moment is not the best one.

Parameter value	Varied parameter: ε_r (μ_r =1)			Varied parameter : μ_r (ε_r =1)			Varied parameter : ε_r μ_r		
	$R_0(f_0)$ [Ω]	$X_0(f_0)$ [Ω]	$\|Z_0(f_0)\|$ [Ω]	$R_0(f_0)$ [Ω]	$X_0(f_0)$ [Ω]	$\|Z_0(f_0)\|$ [Ω]	$R_0(f_0)$ [Ω]	$X_0(f_0)$ [Ω]	$\|Z_0(f_0)\|$ [Ω]
0.25	43.7	6.1	44.1	41.7	6.0	42.1	57.7	-2.01	57.7
0.5	45.6	7.0	46.1	43.1	5.4	43.4	-	-	-
0.75	58.6	-6.6	58.9	59.8	-4.0	59.9	45.2	5.5	45.5
1 (air)	58.0	-5.5	58.2	58.0	-5.5	58.2	58.0	-5.5	58.2
2	58.3	-5.4	58.5	52.1	-8.9	52.8	-	-	-
3	58.7	-5.5	58.9	52.1	9.4	52.9	56.2	-7.1	56.6
4	59.3	-4.2	59.4	42.6	-7.6	46.2	-	-	-
5	57.0	-6.7	57.3	57.8	5.8	58.0	51.2	9.9	52.1
9	59.9	-1.0	59.9	59.5	1.8	59.5	53.3	8.5	53.9

Table 3.7: Antenna input impedance values at 2.45GHz for the different substrate parameter variation. *Matching method* applied to design the antenna.

[1] For high-μ_r values the antena input impedance in a certain point of the patch surface increases rapidly (as it will be demonstrated in the next subsections), thus making more difficult the antenna matching.

3.3.2 Antenna made resonant at f_0 or resonance method

Another antenna design method consists in making the antenna resonant at f_0. Then, the maximum matched FBW computed will be obtained simply matching the circuit which is going to be connected to the antenna to $R_0(f_0)$, the antenna input resistance at f_0. The objective is to check if this method is better than the applied since the moment.

In Figs. 3.9, 3.10 and 3.11 the results obtained applying the new designing criterion are shown, and the main antenna parameters are summarised in Table 3.8. Note that the probe position, x_0, is not indicated because it is fixed to $\frac{\lambda}{8}$.

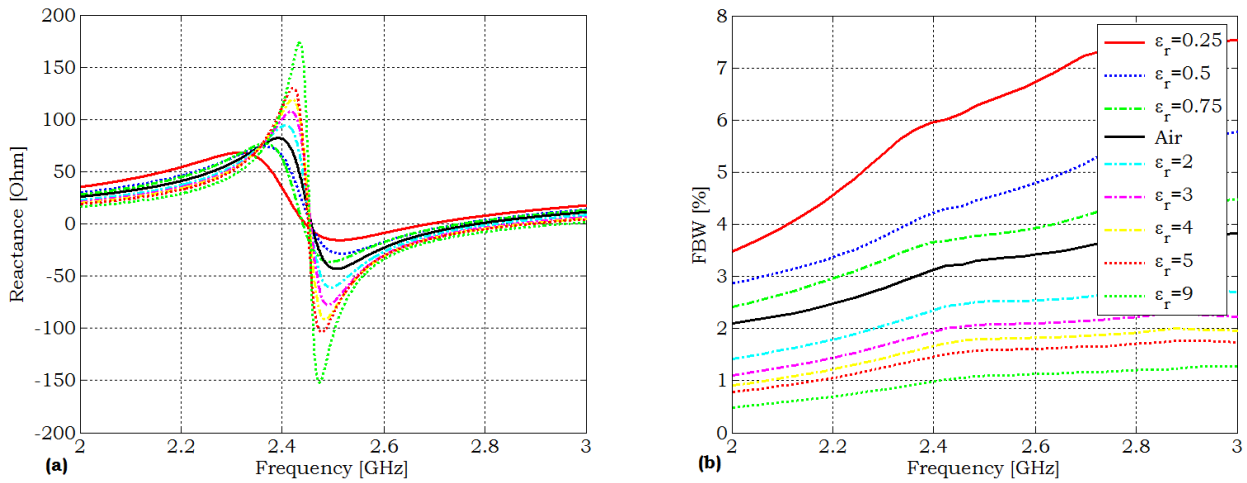

Figure 3.9: Antenna (a) input reactance and (b) computed FBW_{-10dB} when incresing the substrate ε_r. The antenna design method applied is the *resonance method*.

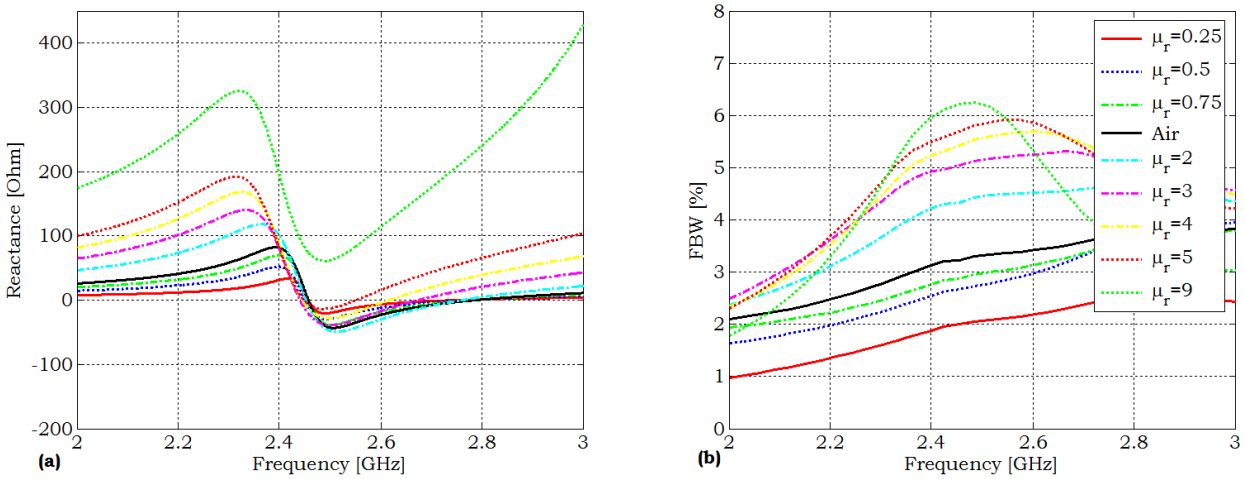

Figure 3.10: Antenna (a) input reactance and (b) computed FBW_{-10dB} when increasing μ_r. The antenna design method applied is the *resonance method*.

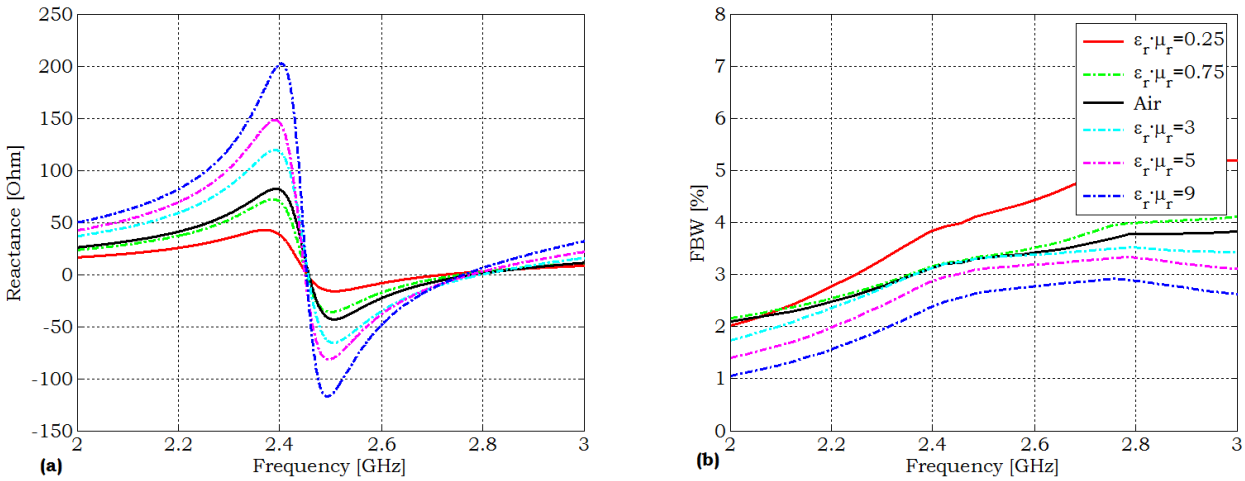

Figure 3.11: Antenna (a) input reactance and (b) computed FBW_{-10dB} when the product $\varepsilon_r \cdot \mu_r$ is increased with $\varepsilon_r = \mu_r$. The antenna design method applied is the *resonance method*.

Parameter value	λ_m [mm]	Varied parameter: ε_r (μ_r =1)		Varied parameter: μ_r (ε_r =1)		Varied parameter: $\varepsilon_r \mu_r$	
		FBW_{-10dB} (f_0)[%]	L [mm]	FBW_{-10dB} (f_0)[%]	L [mm]	FBW_{-10dB} (f_0)[%]	L [mm]
0.25	244.8	6.1	84 (λ_m /2.9)	1.9	109 (λ_m /2.2)	3.9	98 (λ_m /2.4)
0.5	173.1	4.3	68 (λ_m /2.5)	2.6	75 (λ_m /2.3)	-	-
0.75	141.3	3.7	60 (λ_m /2.3)	2.8	61.8 (λ_m /2.2)	3.2	61.5 (λ_m /2.2)
1 (air)	122.4	3.2	54 (λ_m /2.2)	3.2	54 (λ_m /2.2)	3.2	54 (λ_m /2.2)
2	86.5	2.4	41.35 (λ_m /2.0)	4.3	40 (λ_m /2.1)	-	-
3	70.6	2.0	34.8 (λ_m /2.0)	5.0	35 (λ_m /2.0)	3.2	34.75 (λ_m /2.0)
4	61.2	1.7	30.80 (λ_m /1.9)	5.4	32 (λ_m /1.9)	-	-
5	54.7	1.5	28.05 (λ_m /1.9)	5.6	30.2 (λ_m /1.8)	3.0	28.8 (λ_m /1.9)
9	40.8	1.0	21.65 (λ_m /1.8)	6.2	26 (λ_m /1.5)	2.5	23.35 (λ_m /1.7)

Table 3.8: Antenna physical parameters when varying the substrate parameters. *Resonance method* applied to design the antenna.

Now return losses are not referred to 50Ω at f_0 for different ε_r and μ_r values, because what is tuned is the resonance of the antenna at 2.45GHz. Accurate input impedance values at 2.45GHz are in Table 3.9. These values are different to 50Ω:

Parameter value	Varied parameter: ε_r (μ_r =1)			Varied parameter : μ_r (ε_r =1)			Varied parameter : $\varepsilon_r \mu_r$		
	$R_0(f_0)$ [Ω]	$X_0(f_0)$ [Ω]	$\lvert Z_0(f_0)\rvert$ [Ω]	$R_0(f_0)$ [Ω]	$X_0(f_0)$ [Ω]	$\lvert Z_0(f_0)\rvert$ [Ω]	$R_0(f_0)$ [Ω]	$X_0(f_0)$ [Ω]	$\lvert Z_0(f_0)\rvert$ [Ω]
0.25	78.1	-2.3	78.1	54.3	11.2	55.4	58.5	2.5	58.5
0.5	104.5	7.7	104.7	81.3	0.67	81.3	-	-	-
0.75	105.2	-13.2	106.0	109.8	14.9	110.8	108.8	4.0	108.8
1 (air)	127.7	15.3	128.6	127.7	15.3	128.6	127.7	15.3	128.6
2	156.7	18.1	157.7	169.9	5.6	166.9	-	-	-
3	184.9	30.7	187.4	161.4	-12.9	161.9	188.2	17.6	189.0
4	210.6	25.5	212.1	173.3	-5.7	173.3	-	-	-
5	234.3	5.4	234.3	170.3	-0.55	170.3	228	-1.2	228.0
9	316	66.1	322.8	252.4	82.2	265.4	322.2	20.4	322.8

Table 3.9: Antenna input impedance values at 2.45GHz. *Resonance method* applied to design the antenna.

By changing the design method we have found that maximum FBW are similar both in the matching criteria and in the resonance criteria. But this does not mean that there is no advantage in changing the method. On the contrary: having approximately the same response the design process can be made simpler and quicker. One can design a resonant antenna by only tuning the patch length. Then the reference input impedance should be R_0, the input resistance of the patch antenna at resonance.

The number of steps done to adjust the reactance near zero at the desired frequency is much less than the ones done to adjust the 50Ω-matching value in the former method of design considered. In addition, only one parameter is changed with the *resonance method*, which is the patch size, whereas in the *matching method* both the patch size and the pin probe position were adjusted to obtain the desired results.

In most of the situations the resistance increases and the reactance slope is higher when the product $\varepsilon_r \cdot \mu_r$ value is growth. The only case in which the tuning had not being possible is for μ_r=9, where apart from decreasing the patch size a modification on the pin probe position should have been done in order to make the antenna resonant.

There is not a simple law which relates the antenna input impedance with the feed position. Apart from theoretical explanations on how the input impedance varies with the frequncy [12], some investigations have been carried out [33] where the input impedance results are obtained at resonance. However, a fixed value of ε_r is considered and the results of the study may not be suitable for all the situations investigated through the present work.

3.3.3 Blind method (or academic method)

The third method arises in order to state whether the results change substantially or not when the antenna is designed applying Eq. 2.8 without making any other adjustment. In that case, hence, neither the patch size (L) nor the probe position (x_0) are varied from their initial values. The obtained results are shown in Figs. 3.12, 3.13 and 3.14.

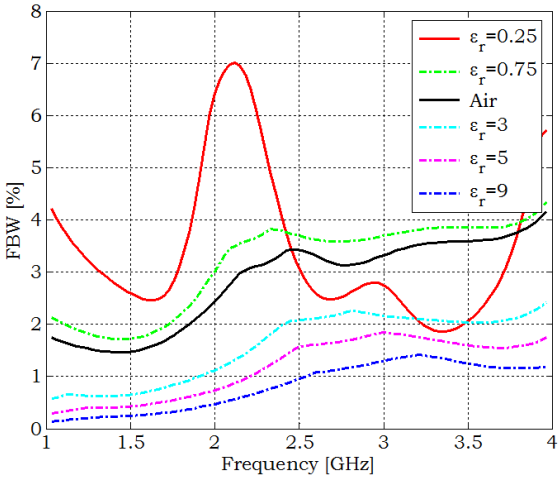

Figure 3.12: Computed FBW_{-10dB} for $0 < \varepsilon_r < 10$. The antenna design method applied is the *blind method*.

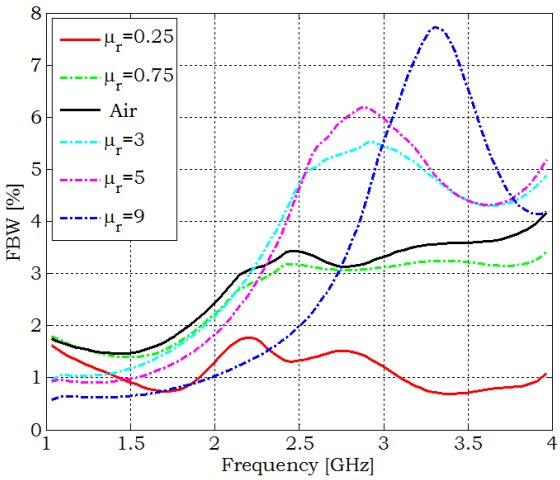

Figure 3.13: Computed FBW_{-10dB} for $0 < \mu_r < 10$. The antenna design method applied is the *blind method*.

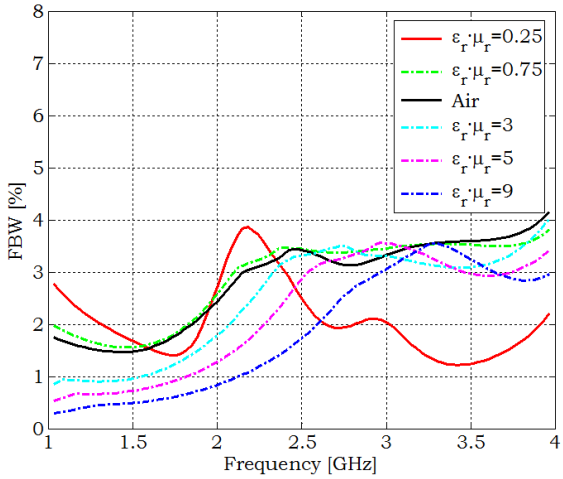

Figure 3.14: Computed FBW_{-10dB} for $0 < \varepsilon_r \mu_r < 10$. The antenna design method applied is the *blind method*.

In that case, neither the matching nor the resonance are adjusted. To better observe the curves, plots show a frequency range from 1 to 4 GHz instead of a range from 2 to 3 GHz because a detailed view around 2.45 GHz is not required.

The input impedance values at 2.45GHz on each case are gathered in Table 3.10.

Parameter value	Varied parameter: ε_r (μ_r =1)			Varied parameter : μ_r (ε_r =1)			Varied parameter : $\varepsilon_r \mu_r$		
	$R_0(f_0)$ [Ω]	$X_0(f_0)$ [Ω]	$\lvert Z_0(f_0)\rvert$ [Ω]	$R_0(f_0)$ [Ω]	$X_0(f_0)$ [Ω]	$\lvert Z_0(f_0)\rvert$ [Ω]	$R_0(f_0)$ [Ω]	$X_0(f_0)$ [Ω]	$\lvert Z_0(f_0)\rvert$ [Ω]
0.25	3.248	16.6	16.91	1.21	-2.207	2.516	2.765	1.537	3.163
0.75	3.968	8.79	9.644	3.364	2.794	4.372	3.712	5.36	6.519
1 (air)	5.199	1.718	5.495	5.199	1.781	5.495	5.199	1.781	5.495
3	117.7	-71.78	137.8	69	147.4	162.7	126.6	-55.59	138.2
5	44.1	107.2	115.9	60.35	190.6	199.9	45.44	127.6	135.4
9	6.338	56.57	56.92	12.27	194.1	194.4	7.835	86.36	86.71

Table 3.10: Antenna input impedance values at 2.45GHz. *Blind method* applied to design the antenna.

It is very clear that the $R_0(f_0)$ value is more different to 50Ω, for the same L and x_0=$\frac{\lambda}{8}$ value, in the high-μ_r cases than in the high-ε_r ones.

Although the FBW also increases when increasing μ_r and decreases when decreasing ε_r, the maximum FBW_{-10dB} changes in value at the desired frequency of $2.45\,GHz$ compared with the methods of

matching and tuning the antenna. In Table 3.11 the values of FBW_{-10dB} at $2.45\,GHz$ are gathered among with the maximum values of the FBW_{-10dB} in the frequency bandwidth from 2 to 3 GHz.

Parameter value	Varied parameter: ε_r (μ_r=1)		Varied parameter: μ_r (ε_r=1)		Varied parameter: $\varepsilon_r\,\mu_r$	
	FBW_{-10dB} (f_0)[%]	FBW_{-10dB} [%] maximum between 2GHz - 3GHz	FBW_{-10dB} (f_0)[%]	FBW_{-10dB} [%] maximum between 2GHz - 3GHz	FBW_{-10dB} (f_0)[%]	FBW_{-10dB} [%] maximum between 2GHz - 3GHz
0.25	3.975	7.014	1.361	1.770	2.743	3.866
0.75	3.743	3.818	3.174	3.173	3.459	3.470
1 (air)	3.436	3.436	3.436	3.436	3.436	3.436
3	2.058	2.256	4.391	5.535	3.285	3.520
5	1.468	1.845	4.192	6.196	2.649	3.565
9	0.8446	1.292	1.846	5.499	1.600	3.048

Table 3.11: Matched FBW at 2.45GHz and maximum matched FBW in the range of 2 to 3 GHz when $0 < \varepsilon_r < 10$.

Comparing maximum FBWs obtained with the three different methods explored we found that approximately the same level of maximum FBW_{-10dB} is obtained, but shifted in frequency. Hence, it is not necessary to take care neither fixing the antenna resonance nor matching the antenna if the objective is only knowing the maximum FBW. Once known, the antenna can be designed following one method or another depending on the requirements to be accomplished.

3.3.4 Substrate size comparison

The substrates of the patches considered until this section have the same size than the patch. However, it is important to know what would imply the variation of the substrate size under the patch antenna. Fig. 3.15 (a) gathers the computed FBW_{-10dB} values when the substrate has the same size than the ground plane (λ_0 x λ_0), while in Fig. 3.15 (b) the same results are plotted with a patch-sized substrate.

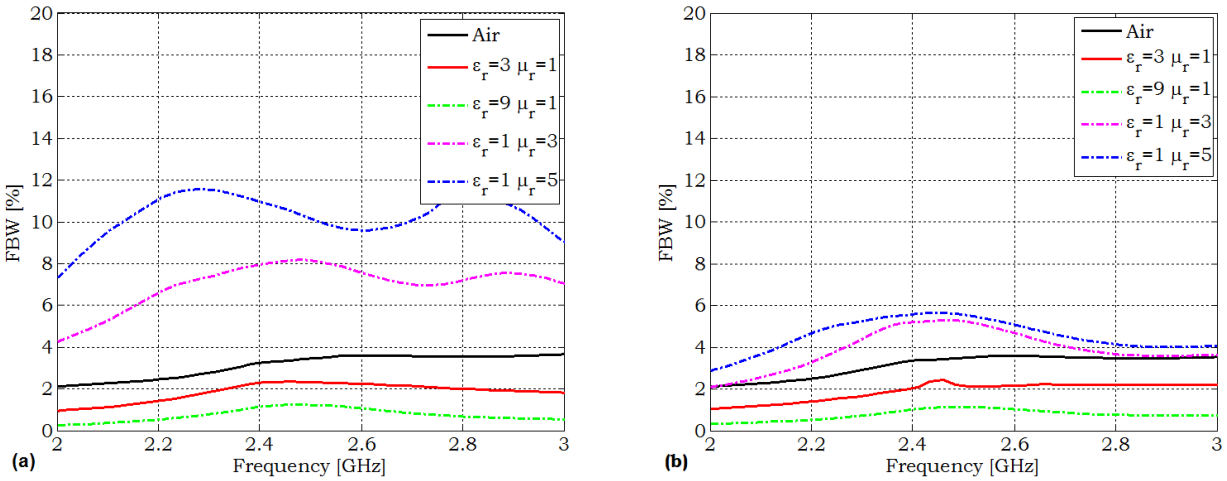

Figure 3.15: Computed FBW_{-10dB} for a substrate with the size of the ground plane (a) and for a substrate with the size of the antenna patch (b).

The design method followed is similar to the *matching method*. The difference is that the return loss level is not fixed to a specified value provided this is better than -10dB (again, this is obtained by changing the patch size and the feed position).

Comparing both substrate sizes, there is a noticeable variation in the matched FBW curve for the high-μ_r cases. In the high-ε_r cases the FBW values reached are approximately the same having a substrate with the size of the patch or with the size of the ground plane. On the contrary, the FBW improvement when μ_r increases is higher with a substrate having the same size than the ground plane.

3.3.5 Why high FBW with high μ_r but not with high ε_r

A reference patch antenna filled with air has a FBW_{-10dB} of 3.2-3.4%. To miniaturise the antenna an increase in the ε_r or in the μ_r values are possible. With high-μ_r values a higher maximum matched FBW can be obtained (FBW_{-10dB} around 5-6%). On the contrary, high-ε_r values lead to low matched FBW values (FBW_{-10dB} around 1-2%). But, what is the physical insight of the results obtained?

If we focus on the results obtained when the *blind method* is applied (no need of patch length and pin position adjustments):

ε_r (μ_r=1)	$\|Z_0\|$ [Ω]	μ_r (ε_r=1)	$\|Z_0\|$ [Ω]
3	132.7	3	162.7
5	114.9	5	199.9
9	56.8	9	194.4

Table 3.12: Comparison between the antenna input impedance when the parameter increased is ε_r or μ_r. These are the impedance values required to carry out the adjustments that will lead to the maximum achievable predicted FBW.

The former values are extracted from simulations where the antenna physical parameters are exactly the same from an ε_r case to the μ_r case having the same value (i.e., $\varepsilon_r = 3$ and $\mu_r = 3$ have the same antenna physical parameters, and also $\varepsilon_r = 5$ and $\mu_r = 5$ or $\varepsilon_r = 9$ and $\mu_r = 9$ between them). So for the same patch size and the same patch point where the input impedance is extracted, the antenna input impedance is higher in the high-μ_r cases compared with the same high-ε_r values.

The results obtained coincide with the conclusions of Ikonen et al in a recently published work [34]. They conclude that the use of magnetic materials leads to smaller amplitude of the current induced to the antenna, when compared with the use of dielectric materials (this is equivalent to affirm that the antenna input impedance is bigger when using magnetic materials when compared with the use of dielectric materials). In this way, the energy stored in the antenna volume is smaller leading to a decreased quality factor (hence, the FBW improves).

However, the advantages of using magnetic materials are only theoretical since high-μ_r materials are not present in nature.

3.4 Discussion

Once the different homogeneous and non dispersive antenna fillings have been analysed in terms of maximum achievable bandwidth, it is time to summarise the most important information and extract some conclusions. The objective is finding a method to design patch antennas with the maximum bandwidth possible.

3.4.1 Best bandwidth results

Before reaching any conclusion, it would be interesting to compare some of the results obtained in the previous sections to obtain a general perspective of the antenna performance when the substrate has different values of $\varepsilon_r \cdot \mu_r$. The results obtained applying the *matching method* are the ones used to make the plots in Fig. 3.16.

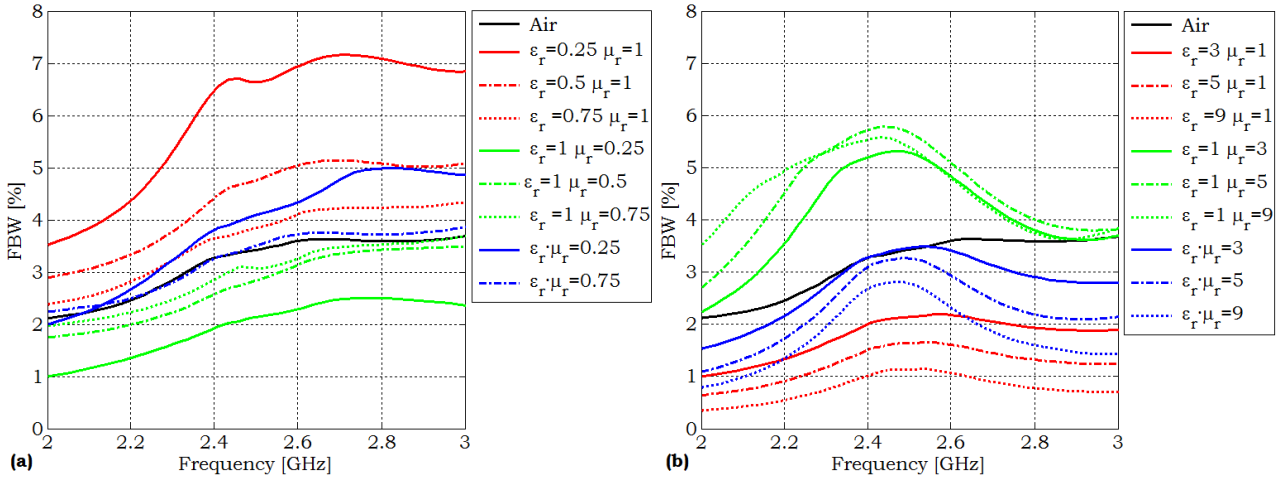

Figure 3.16: FBW versus frequency summary: (a) $0 < \varepsilon_r\mu_r < 1$ and (b) $1 < \varepsilon_r\mu_r < 10$. The antenna design method applied is the *matching method*.

It is obvious that:

1. The greater ε_r, the worse the FBW_{max} we obtain. However, introducing a similar value of μ_r ($\varepsilon_r = \mu_r$) an air-like FBW value can be obtained at the desired frequency and miniaturizing the antenna in addition.

2. Very high FBW values are observed in the cases where ε_r is near-zero or for high-μ_r. However, whilst in the former situation an antenna miniaturisation is achieved, in the near-zero ε_r situation the antenna would be bigger than in the air case. In that sense, another improvement in the antenna performance should exist to compensate that antenna enlargement; i.e.: a better directivity, for instance.

3. There seems to exist a limit on the enhancement in FBW with the increase of μ_r . It is inferred from Fig. 3.16 that for μ_r=5 a higher FBW is obtained compared with the one for μ_r=9. In addition, those values are not much better than those obtained with μ_r=3. Since it has been found that no μ_r value much greater than 2 (without having a narrowband response) can be artificially obtained for the moment[2], knowing that with μ_r>2 the FBW wouldn't suffer a dramatic improvement is an advantage.

The computed FBW_{-10dB} at 2.45 GHz values versus the product $\varepsilon_r{\cdot}\mu_r$ variation are plotted in Fig. 3.17. This figure contains information about the matched bandwidth variation compared with the

[2]In Chapter 4 this statement will be demonstrated.

Hansen and Burke predicted on [19]. As it will be explained in the next subsection (3.4.2) these two methods can not be directly compared, and thus it is not expected that the curves exactly coincide. The comparison has been done considering that the Hansen and Burke formula has the premise of VSWR=2. Hence, the matching considered to obtain the matched bandwidth to compare them is approximately -10dB.

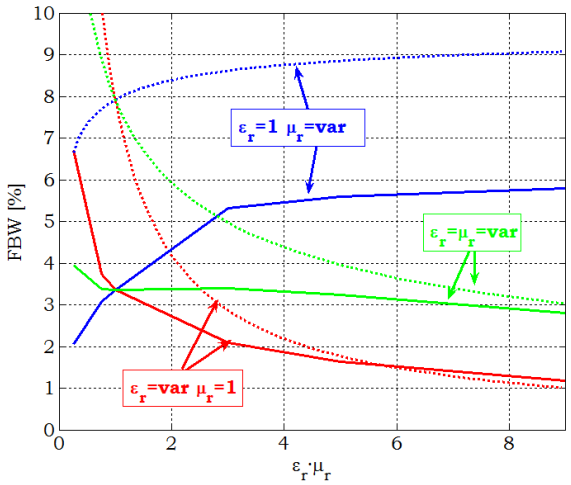

Figure 3.17: Computed FBW_{-10dB} at 2.45GHz versus $\varepsilon_r \cdot \mu_r$. Comparison between Hansen's predicted FBW (dotted lines) and computed matched FBW (solid lines). The antenna design method applied is the *matching method*.

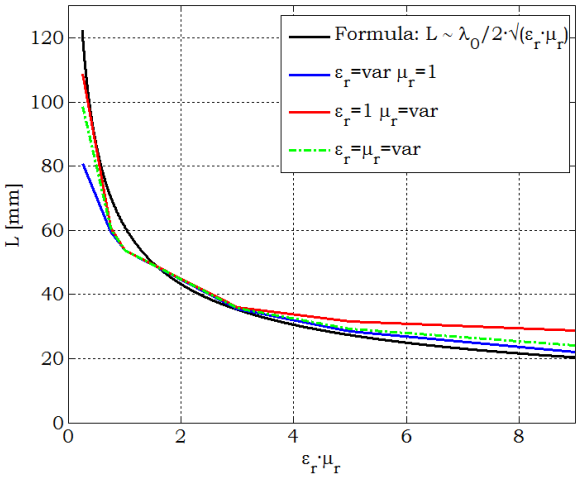

Figure 3.18: Patch length L versus $\varepsilon_r \cdot \mu_r$. The antenna design method applied is the *matching method*.

The antenna miniaturisation when ε_r, μ_r or $\varepsilon_r\mu_r$ are increased is depicted in the former figure, Fig. 3.18. Remember that L is not the only parameter tuned in order to obtain the same matching at f_0 for all the ε_r and μ_r values, but also the coaxial pin position.

For the *ENZ* (Epsilon Near Zero) cases the obtained patch length is closely adjusted to the theory, whereas for high-ε_r values it differs a bit. On the contrary, for high-μ_r values the results are more similar to the predicted ones than for the *MNZ* (Mu Near Zero) case.

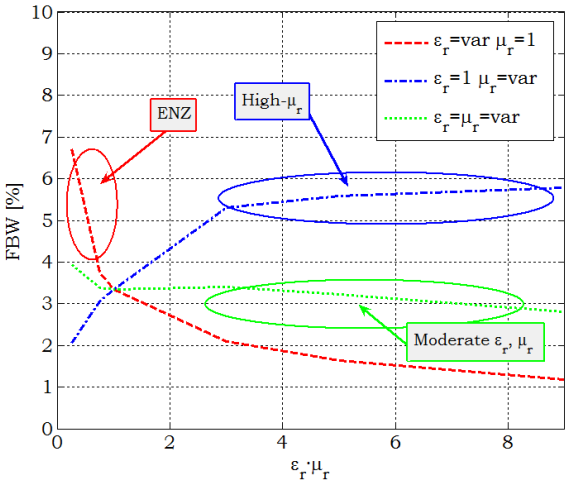

Figure 3.19: Computed FBW_{-10dB} at 2.45GHz versus $\varepsilon_r{\cdot}\mu_r$. Three main regions of interest for antenna applications.

Forgetting the comparison for a moment and focusing on the computed matched FBW obtained (Fig. 3.19), three main areas of interest can be identified:

1. The *ENZ* area: with high FBW values, but bigger antennas.
2. The high-μ_r area, with high FBW and miniaturized antennas.
3. A moderate and equal ε_r and μ_r zone ($1<\varepsilon_r\mu_r<4$), where the air FBW is retained and the antenna results miniaturised.

The problem is that the last situations are not feasible having real artificial dispersive μ_r and ε_r materials. The dispersion in the substrate parameters will be treated in Chapter 4.

The former observations have been done plotting the results obtained in the *matching method*. However, if the same process is repeated using the FBW and L values obtained when the *resonant method* is

applied, only a small difference is noticed. Fig. 3.20 gathers the $L(\varepsilon_r\mu_r)$ values of that second method plotted in a logarithmic scale, in order to graphycally predict how the antenna length varies with ε_r, μ_r and λ_0. The L curve almost follows a linear relation with the product $\varepsilon_r \cdot \mu_r$.

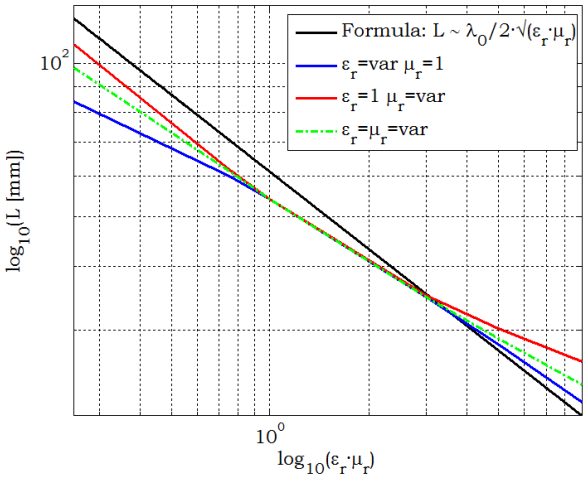

Figure 3.20: Empirical patch length as a function of $\varepsilon_r\mu_r$. Both plots are logarithmic. The antenna design method applied is the *resonance method*.

3.4.2 Impedance explanation

At this point, it is important to note that the enhancement in FBW observed in the figures seen since the moment is better than the bandwidth values we can extract directly from the $|S11|_{dB}$ figures. To explain why does this happens we will analyse how one should act when designing the antenna in order to obtain the maximum FBW possible at f_0 starting from the results obtained when applying the *resonance method* (where $R_0 \neq 50\Omega$).

If we focus in the reflection coefficient Fig. 3.3 and take the ε_r values of 0.5 and 0.75, it seems that these two cases have the same bandwidth. So why in the FBW figure there is a huge difference in value between the ε_r cases we are focusing on in this example? The answer is not obvious, and stems from the Yaghjian's FBW formulation. As it has been said in Chapter **2** when explaining the matched bandwidth, the antenna has to be tuned and matched to the input impedance at each frequency where the FBW is computed through this method. As the figures of the FBW versus frequency have been obtained for different values of frequency, that means that a tuning and a matching to the input antenna resistance have to be done at each frequency of the plotted range.

A graphical explanation of what is happening for the specific case of increasing μ_r value is exposed. First of all, suppose those cases where the μ_r value is 3 and 5 and observe the input impedance (Fig.

3.21). Knowing the value that the antenna input impedance has, the necessary adjustments to compute the FBW in the same conditions as in the matched bandwidth are done. The first step is to tune the antenna to the desired frequency: $f_0 = 2.45\,GHz$. As the antenna has been designed to be naturally tuned, the kind of adjustment done in 3.22(a) is a fine tuning. The remaining adjustment to do is to match the antenna to R_0. That is what has been done to obtain the $|S11|_{dB}$ plot in Fig. 3.22(a), whilst to obtain the result plotted on Fig. 3.22(c) no tuning has been forced to 2.45GHz and the antenna has been matched to 50Ω. In 3.22 (b) an intermediate situation has been considered where the fine tuning has not been forced and the Z_{ref} has been adjusted to the antenna input impedance value, $R_0(f_0)$.

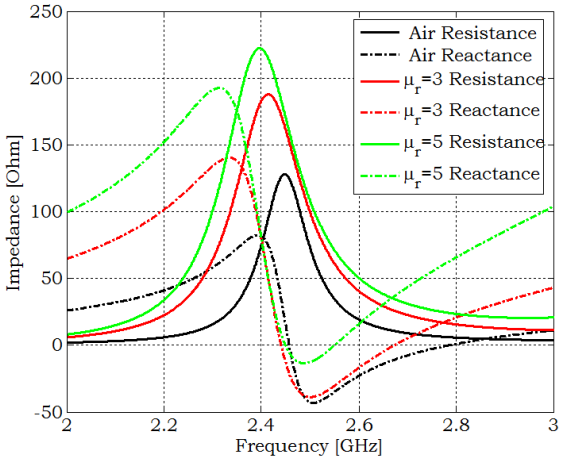

Figure 3.21: Input impedance of the antenna with different fillings. Air: R_0(2.45GHz)=127.7Ω, X_0(2.45GHz)=15.32Ω; μ_r=3: R_0(2.45GHz)=161.4Ω, X_0(2.45GHz)=-12.99Ω; μ_r=5: R_0(2.45GHz)=170.3Ω, X_0(2.45GHz)=-0.5551Ω.

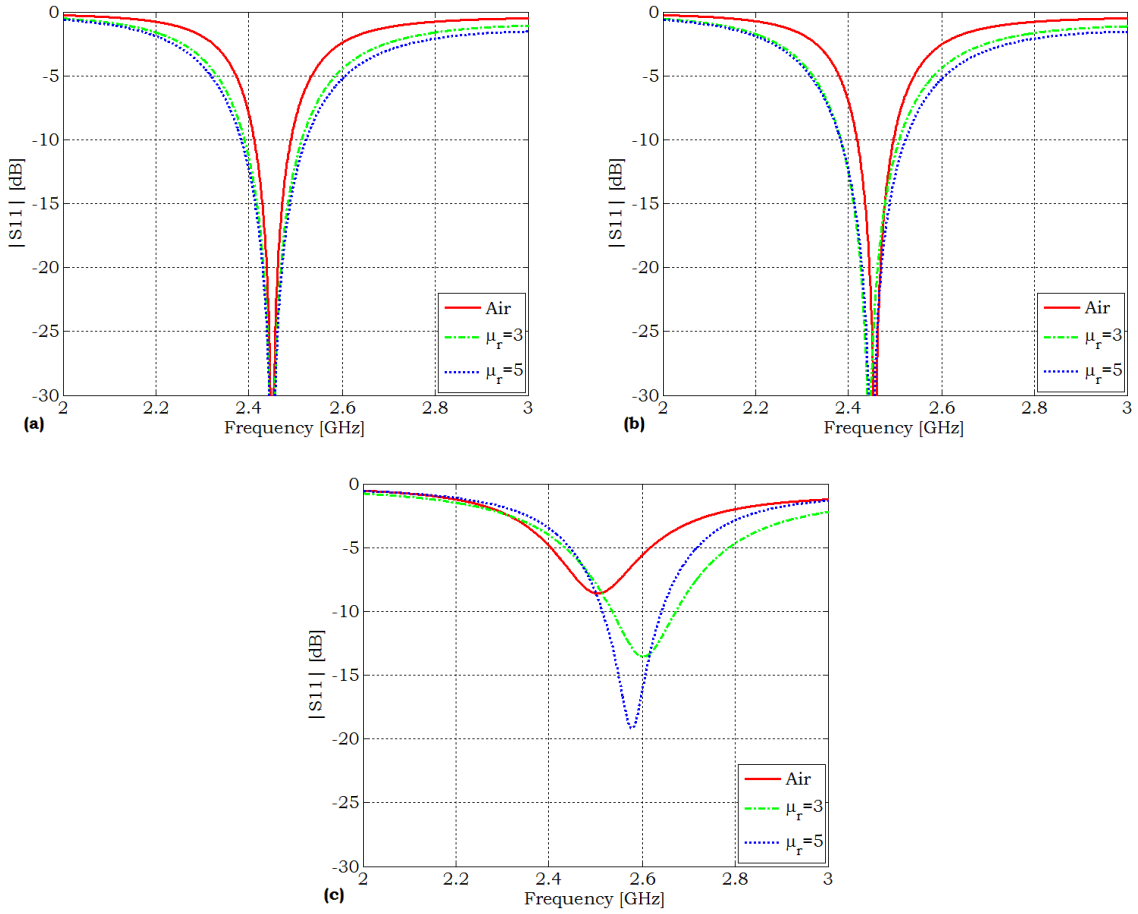

Figure 3.22: Magnitude of the simulated reflection coefficients when: (a) Z_{ref} =R₀ and fine tuning of the antenna at 2.45GHz, (b) Z_{ref} =50Ω with the antenna naturally resonant at ∼2.45GHz (c) Z_{ref} =50Ω with the antenna naturally resonant at ∽2.45GHz.

Because the antenna has been designed to be resonant at approximately 2.45 GHz, there is little difference between Fig. 3.22 (a) and (b). In (a) the antenna input impedance reactive part has been totally compensated using a capacitor or an inductor and R_{ref}=R₀. When the matching to the input impedance is forced the $|S11|_{dB}$ plot shows a good matching at 2.45 GHz, compared with the matching when $R_{ref} = 50\Omega$ like in Fig. 3.22 (c). That happens because the best impedance to match the antenna is not always 50Ω.

The obtained values when computing the *FBW* from Fig. 3.22 (a) are gathered in Table 3.13.

Material	FBW [%] Direct measurement	FBW [%] Yaghjian method
Air	3.1	3.2
μ_r=3	4.9	5.0
μ_r=5	5.6	5.6

Table 3.13: Comparison between the FBW_{-10dB}: direct measurement from the magnitude of the simulated reflection coefficient versus computed FBW from the Yaghjian's method.

It is clear that the approximation is good enough to consider the matched bandwidth formula the manner to compute the maximum FBW achievable.

The method applied to compute the FBW from the magnitude in dB of the reflection coefficient, $|S11|_{dB}$, has been the direct measurement (remember Subsection 2.3.1).

There is no doubt in how high-μ_r substrates offer a better FBW than air.

Operating in the same way for the cases ε_r=3 and ε_r=5, we obtain that the input impedance is the one shown in Fig. 3.23. Fig. 3.24 has the magnitude of the reflection coefficient values when: (a) both the tuning and the matching to the input resistance of the antenna are applied, (b) only the matching to the input impedance of the antenna is done and (c) the matching has been done referred to 50Ω.

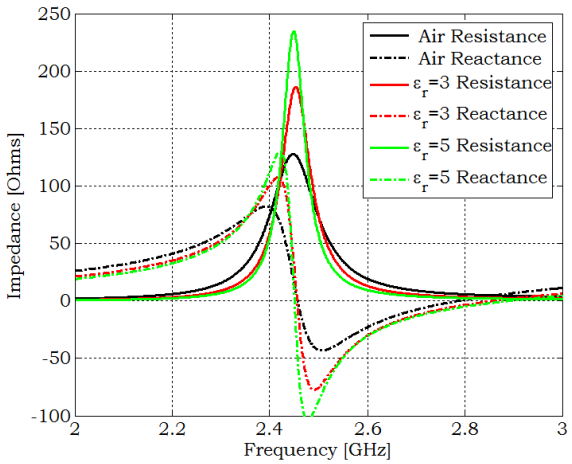

Figure 3.23: Input impedance of the antenna with different fillings. Air: R_0(2.45GHz)=127.7Ω, X_0(2.45GHz)=15.32Ω; ε_r=3: R_0(2.45GHz)=184.9Ω, X_0(2.45GHz)=30.74Ω; ε_r=5: R_0(2.45GHz)=234.3Ω, X_0(2.45GHz)=5.449Ω.

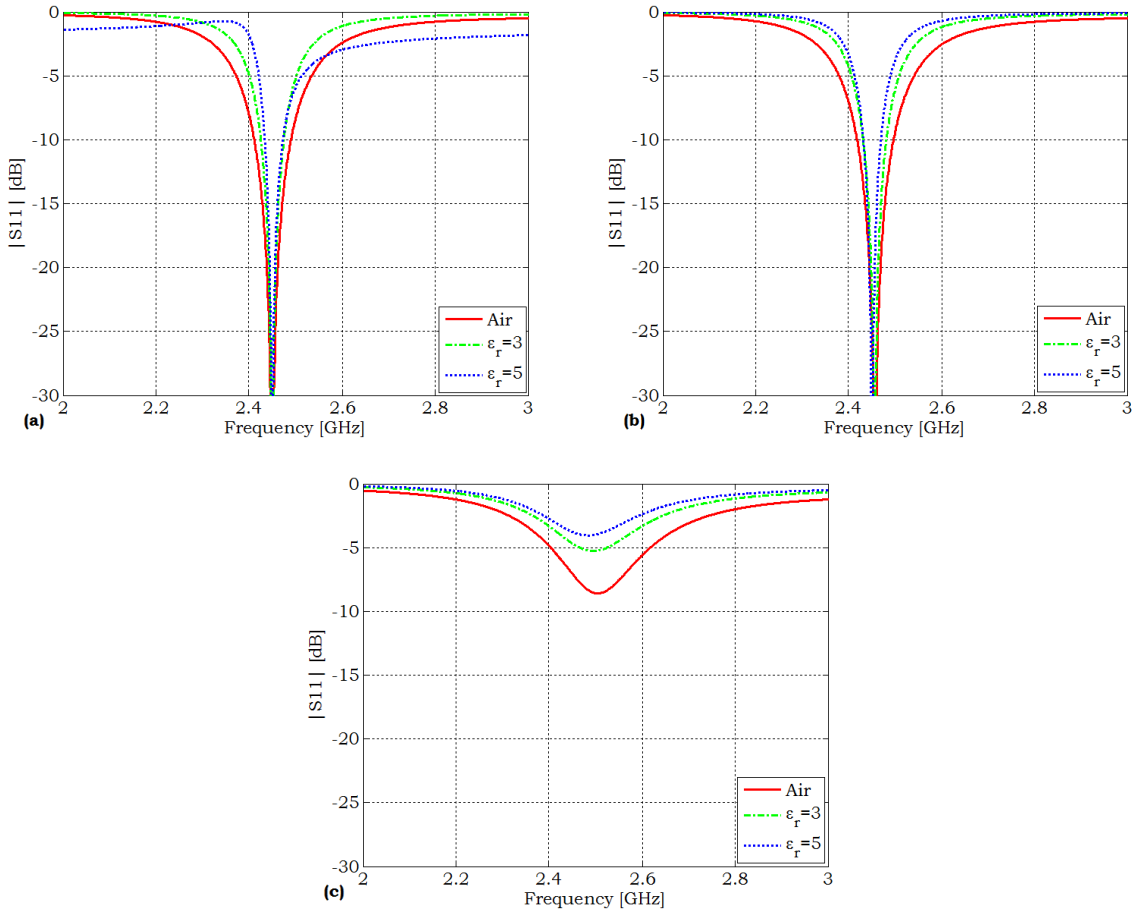

Figure 3.24: Magnitude of the simulated reflection coefficients when: (a) Z_{ref} =R₀ and fine tuning of the antenna at 2.45GHz, (b) Z_{ref} =50Ω with the antenna naturally resonant at ∼2.45GHz (c) Z_{ref} =50Ω with the antenna naturally resonant at ∽2.45GHz.

The obtained values when computing the FBW from Fig. 3.24 (a) are gathered in Table 3.14.

Material	FBW [%] Direct measurement	FBW [%] Yaghjian method
Air	3.1	3.2
ε_r=3	2.0	2.0
ε_r=5	1.6	1.5

Table 3.14: Comparison between the FBW_{-10dB}: direct measurement from the magnitude of the simulated reflection coefficient versus computed FBW from the Yaghjian's method.

In that case, in Fig. 3.24 (c) the magnitude of the reflection coefficients are not much different between

them as in Fig. 3.22 (c). This happens because the antenna input impedance varies much more between different μ_r values than between different ε_r values.

From previous results it is now understandable why the Hansen and Burke FBW values do not coincide with the obtained applying the Yaghjian's method (remember Fig. 3.17(b)). Hansen's and Burke do not consider the antenna matched at every single frequency.

To conclude, the best method is the one that tunes the resonance frequency because the only adjustment to make is matching the input resistance of the feeding network with the antenna input impedance.

3.4.3 Conclusions

The statement that in terms of bandwidth is better to have an antenna loaded with a high-μ_r material than with a common dielectric ($\varepsilon_r > 1$) only (Hansen and Burke, [19]) has been numerically assessed. We have also concluded that a substrate with relatively high μ_r (values of 2 - 3) improves dramatically the bandwidth, almost doubling it. It is not necessary a high relative permeability μ_r to improve both the air FBW and antenna miniaturization. The improvement obtained with $\mu_r > 3$ is much less relevant compared to the obtained with $\mu_r = 2$ or $\mu_r = 3$ compraed to the air case.

One of the advantages of tuning the matching of the antenna to 50Ω is that one can compare rapidly the results by having a quick look at the $|S_{11}|_{dB}$ parameter of the different designs. Nevertheless, this is shown not to be an appropriate criterion in order to ascertain whether a given material can improve or not the FBW response of the microstrip antenna. One can not compare directly the return losses in terms of maximum achievable impedance bandwidth; the maximum value of bandwidth that can be obtained with a specific material has to be studied applying certain conditions. Here is where the compute of the FBW through Yaghjian's formula can help us. This formulation assumes the antenna tuned ($X_0(f_0) = 0$, being X_0 the antenna reactance) and matched ($Z_{ref} = R_0(f_0)$ and not $Z_{ref} = 50\Omega$, being Z_{ref} the reference impedance of the circuit which is connected to the antenna $Z_{ref} = R_{ref}$, $X_{ref} = 0$) and $R_0(f_0)$ the antenna impedance at the frequency of interest afer tuning). So the differences between our results and the ones obtained by other authors are due to the matched bandwidth formulation.

The effect of miniaturisation while keeping the air case FBW obtained when increasing the ε_r and μ_r values at the same time and being $\varepsilon_r = \mu_r$ coincides with the recently presented work of Petrov et al. [31].

We also have assessed that magnetic materials lead to higher antenna input impedances, comparing the same antenna (without modifying its physical parameters, applying the *blind method* as explained in Subsection3.3.3) filled with high-ε_r materials and with high-μ_r materials. This is the conclusion reached in Ikonen et al. recent work [34], where they conclude that using magnetic materials smaller

amplitude of the current induced to the antenna is obtained, when compared with the use of dielectric materials (this is equivalent to affirm that the antenna input impedance is bigger when using magnetic materials when compared with the use of dielectric materials). In this way, the energy stored in the antenna volume is smaller leading to a decreased quality factor (and hence, better FBW).

ENZ and *MNZ* substrates have also been studied and better FBW than the air case has been found for *ENZ* materials. However, *ENZ* substrate properties lead to a increase in antenna size.

Three different methods to design a patch antenna are studied and we conclude that the best of them in order to obtain the maximum achievable FBW at the desired frequency is the *resonance method*. That method consists of design the antenna resonant at f_0. However, an adjustment in the matching has to be done: $Z_{ref} = R_0(f_0)$. The R_{ref} of the feeding network has to be changed in the final circuit to match the feeding network to the antenna. Nevertheless, when the objective is only to know the maximum value of the FBW that a certain patch antenna can perform the *blind method* is the quicker one to apply. This method uses equation (referència capitol 2) to obtain the antenna size and any adjustment is done to match or to make resonant the antenna.

Chapter 4

Size and BW Study of Microstrip Patch Antennas Filled With Dispersive Substrates

In this Chapter it is studied the miniaturization effect due to the use of metasubstrates in the realization of microstrip antennas. Other important features like the achieved bandwidth, the antenna efficiency and the radiation pattern are analyzed in order to state whether the use of metamaterials is feasible in the fabrication of this type of antennas.

Like in Chapter 3, the FBW behaviour when miniaturizing the antenna is studied and its calculation from fixing a matching level is compared with the computed through the Yaghjian formulation.

First of all the material that fills the antenna is selected. It is characterized in terms of its frequency of resonance and its effective relative parameters (permittivity and permeability) are extracted using a well-known effective parameter extraction method [37]. We are interested in materials which make the antenna work at approximately 2.45GHz.

After two different metasubstrate are selected, the antenna behaviour is simulated.

Finally the antenna is fabricated in order to compare its measured parameters with the simulated ones. The achieved antenna miniaturization factor, the FBW and the efficiency are discussed.

4.1 Physical Miniaturization and Electrical Miniaturization

The concept of miniaturization can be understood from two different perspectives. As in this work we will refer to both of them, it is necessary to make clear what each of them mean. As this work is centered in the study of patch antennas, the examples used will refer to them.

Having a patch antenna like the one shown in Fig. 4.1, this antenna is matched at a frequency f_0. The matching frequency is related with the physical size of the antenna, L, through the Eq. 2.8.

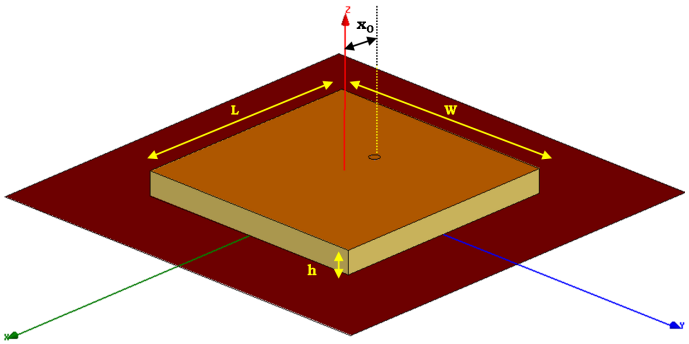

Figure 4.1: Reference patch antenna.

The frequency at which the antenna is matched can be shifted by means of changing its substrate. As it has been observed in Chapter 3, when the ε_r and/or the μ_r of the material are increased, the f_0 decreases. If the new substrate has higher $\varepsilon_r\mu_r$ value (remember that $n = \sqrt{\varepsilon_r\mu_r}$) than the original one, the matching frequency will be shifted to lower values.

Here is where the distinction of the physical miniaturization and the electrical miniaturization can be done.

- If the antenna at the new matching frequency, f_0', is properly matched and the physical dimensions of the antenna are not modified, the antenna has been electrically miniaturized. The patch length expressed in terms of the free-space wavelength, λ_0, is lower than the original one:

  $L = \frac{\lambda_0}{2n} = \frac{c}{2f_0 n}$ and $L' = \frac{\lambda_0}{2n'}$, with $f_0' < f_0$ to have $L' = L$ when $n' > n$

- If the patch antenna length is modified in order to return to the original operational frequency, f_0, and the antenna is finally matched again at this frequency, the antenna has been physically miniaturized:

  $L = \frac{\lambda_0}{2n} = \frac{c}{2f_0 n}$ and $L' = \frac{\lambda_0}{2n'}$, with $L' < L$ to have $f_0 = f_0$ when $n' > n$

4.2 Material characterization

In Chapter 3, high-μ materials have proved to be the ones that both achieve antenna miniaturization and FBW improvement in front of the air as a substrate. In addition, it has been observed that $\mu_r = 2$ and $\mu_r = 3$ are the values which make the difference with respect to the air case for the considered antenna geometry. Higher values do not significantly improve the results.

As it has been explained in Chapter 2 many kinds of materials have been used to miniaturize patch antennas, from the Ikonen's metasolenoid [20] to the SRs used in the MNG circular patch of Bilotti et al. [24].

An existent material is proposed to be used as the loading of the microstrip antenna, since the objective of this work is not to design a material with tailored properties. An SR slab is an AMM (Artificial Magnetic Material) used to act as a magnetic surface leading to low profile and compact antenna systems designed and synthesized by P.J.Ferrer et al. [35] (Fig. 4.2). Its PMC-like reflector around 2.67GHz performance was assessed.

Figure 4.2: Fabricated single layer SR on a Styrofoam board. Fig. from [35].

Thus, the loading will be formed by the metamaterial based on Greek key or square spiral resonators (SRs) printed on Rogers RO4003C. The unit cell, when arranged along the x and y axis (example in Fig. 4.4), will conform the final metamaterial slab.

Through the modification of the SRs physical parameters, the material resonance can be shifted along the frequency range. In the following sections, a couple of variations of the initial design in [35] will be used.

4.2.1 Parameter extraction

As explained in [1], Infinite Boundary Conditions (IBC) have to be used to simulate in HFSS the unit cell acting as an infinite array . Those conditions are based on the Image Theory, and state that the unit cell is embedded in a cube where two faces have the PEC boundary condition and the other two have the PMC boundary condition; the remaining two faces of the unit cell are used as Wave Ports to simulate the electric field incidence, reflection and transmission through the unit cell.

The asymmetric arrangement of the spirals after applying image theory to the unit cell has no influence on the final macroscopic performance (S-parameters) as shown in P.J. Ferrer et al. [36] (Fig. 4.3).

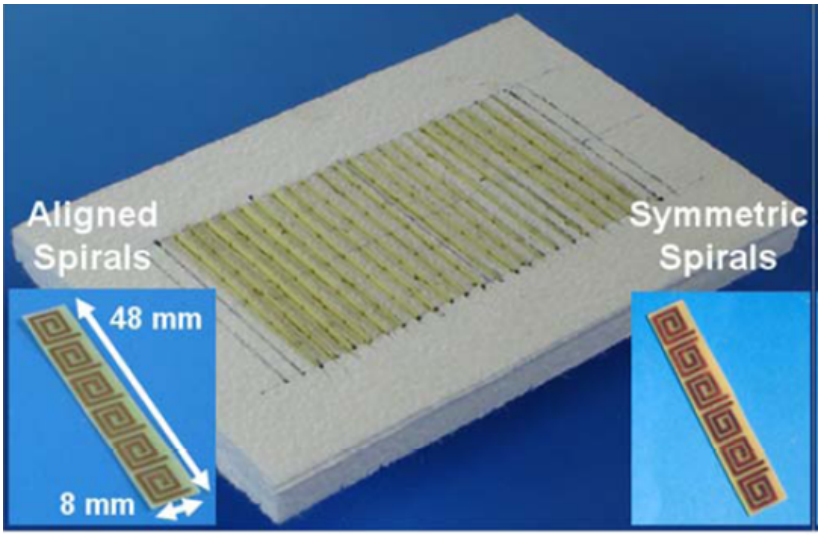

Figure 4.3: SR slab with the two possibilities for the IBC conditions applied to the unit cell. Fig. taken from [36].

Hence, from the simulated transmission and reflection parameters we can extract the effective medium parameters using the method proposed by R.W. Ziolkowski [37] based on NRW (Nicolson-Ross-Weir) approach:

$$\varepsilon_r = \frac{2}{jk_0 d}\frac{1-V_2}{1+V_2} \tag{4.1}$$

$$\mu_r = \frac{2}{jk_0 d}\frac{1-V_1}{1+V_1} \tag{4.2}$$

Where $V_1 = S_{21} + S_{11}$, and $V_1 = S_{21} - S_{11}$.

There are other suggested methods to obtain those parameters, and there is still work to be done since none of the methods has proven to be sufficiently general and accurate. Another of those methods

is proposed by Xudong et al. [38]. They claim that in Ziolkowski's approach the asymmetry of the structure along the propagation hasn't been taken into account and that the choice of the sign in square root equations is not the proper one. However, Ziolkowski's method is widely used in literature and the one that is used in the present work because its ease of application and because it has proven to be enough accurate in most metamaterial applications.

Some considerations to have in mind are:

- Since the method extracts the parameters from S_{11} and S_{21} of the unit cell, the interaction between the consecutive unit cells (along the y axis) which form the slab that conforms the metasubstrate are not taken into account. The medium is anisotropic, which means that the effective parameters μ_{xx}, μ_{yy} and μ_{zz} can be different. However, some studies like the one carried out by Semichaevsky et al [39] state that μ_{xx} and μ_{zz} can be assumed to be close to 1, for a magnetic metamaterial embedded in a grounded slab that is used as an antenna substrate oriented as the one considered in our study.
- The considered unit cell is not symmetrical from the wave ports point of view. Therefore, it is highly probable that $S_{11} \neq S_{22}$ and $S_{21} \neq S_{12}$ stating in this way the improvements to be done in the method.
- It is different to consider the unit cell in free-space than to place it in a non-homogeneous host medium like the grounded substrate medium that constitutes the patch antenna. The effective parameters may be different.
- In addition, the effects of the scattering losses would have to be considered for an accurate parameter extraction. The scattering losses are defined as the portion of the transmission losses due to the scattering within the medium.

In that sense, the work done by Semichaevsky et al [39] has tried to be more accurate in the parameter extraction. It takes into account the interaction between unit cells forming the metasubstrate and the scattering losses considering this metasubstrate placed in the non-homogeneous medium which constitutes the microstrip patch antenna. However, some authors like Alù et al. [40] consider that it is proven that a periodic arrangement of inclusions cancels out the scattering losses from each individual particle.

The initial unit cell in [35] has been modified with the dimensions in Fig. 4.4 in order to have the material resonance sufficiently far from the antenna resonant frequency. Increasing the unit cell thickness (t) and height (h), the adjacent spirals are further between them, and the resonant frequency of the SR becomes higher. The first SR design is composed of a two loop SR facing down and denoted as s2d. Applying the IBC to the considered unit cell (Fig. 4.5) the S11 and S12 parameters, required to extract the effective medium parameters, are simulated (Fig. 4.6).

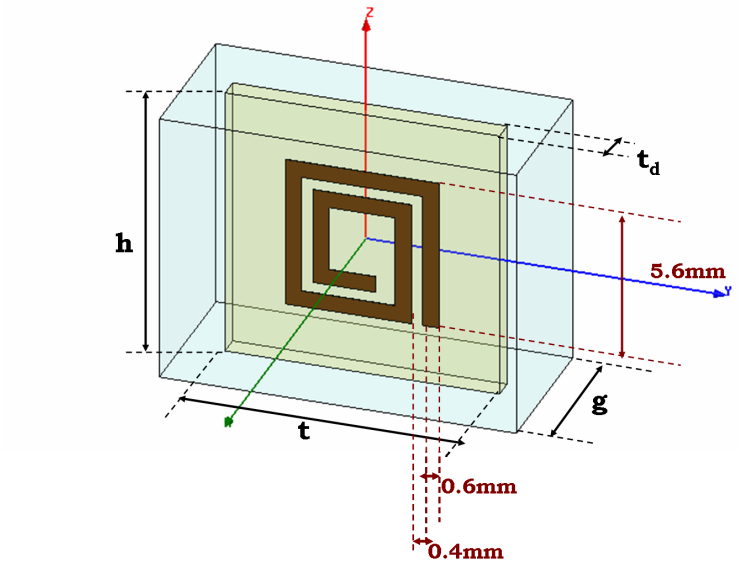

Figure 4.4: Dimensions of the unit cell of the SR. Unitt cell height $h = 10mm$, unit cell thickness $t = 10mm$, gaps between consecutive strips of spirals $g = 6mm$ and dielectric thickness $t_d = 0.8mm$. The dimensions of the spiral resonator are the major side width (5.6mm), the line width (0.6mm) and the line gap (0.4mm).

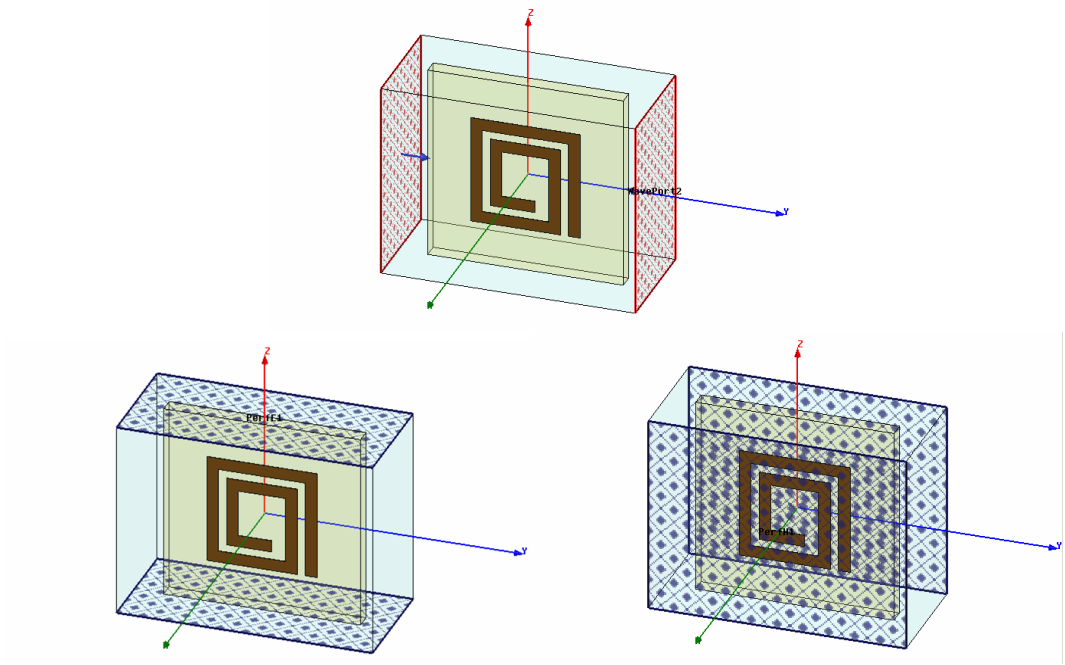

Figure 4.5: Waveports (top), PEC boundary conditions (bottom left) and PMC boundary conditions (bottom right).

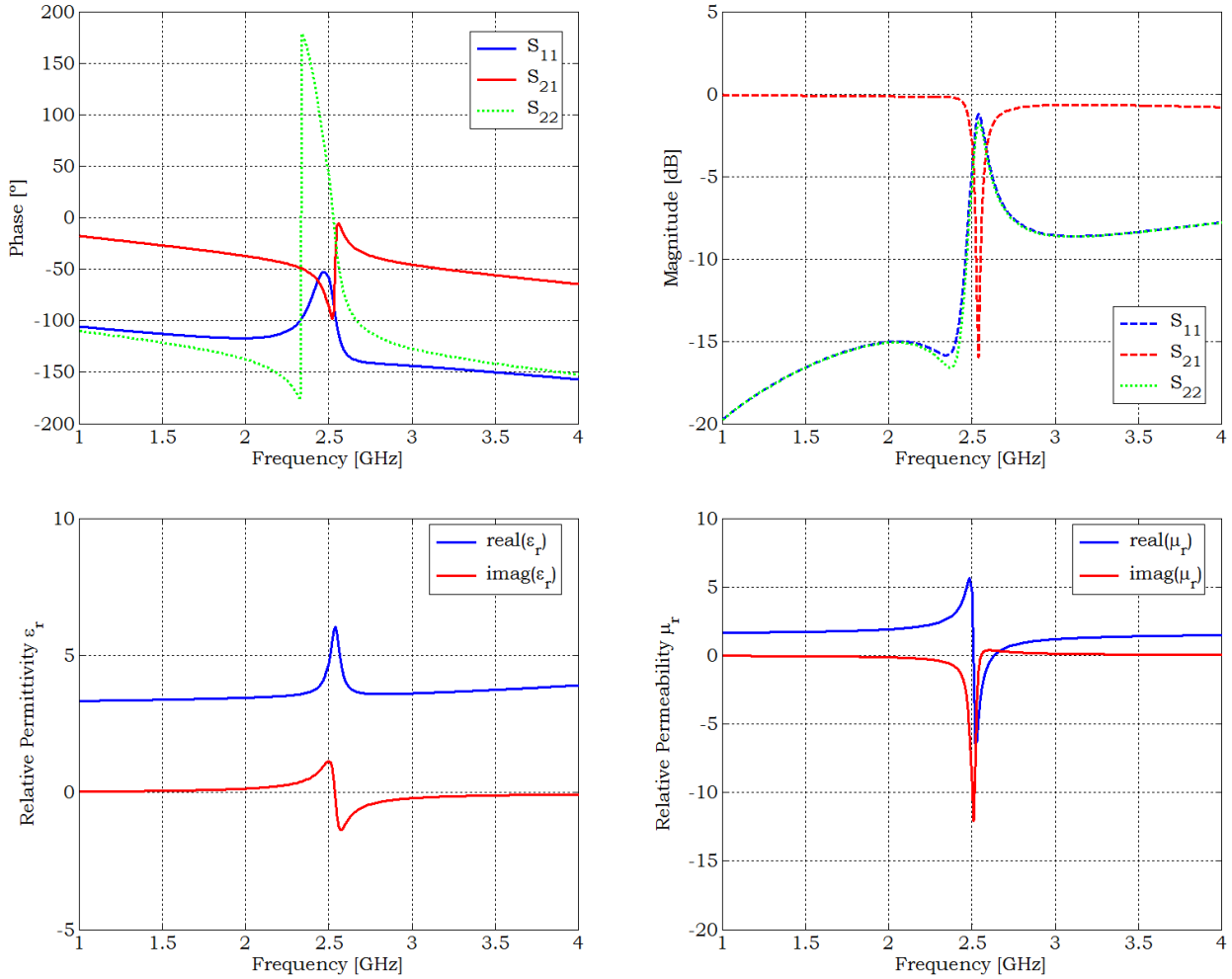

Figure 4.6: Simulated S11, S21 and S22 parameters of the SR resonators: phase (top left) and magnitude (top right). Extracted ε_{reff} (bottom left) and μ_{reff} (bottom right) for the s2d case.

It is known that to obtain higher FBW antenna values the appropriate part of the $\varepsilon_r - \mu_r$ curve in which the antenna must operate is neither too far from the resonance (μ_r values too low) nor too close to the resonance (in the material resonance the material bandwidth is very narrow). Therefore, the ideal is to have a smooth permeability value variation (having low losses), in a dispersive medium [21].

Looking at the zero crossing frequency of the S22 phase (S22 because is the side behaving as a PMC; S11 has a PEC behaviour), the material resonance is found 2.51GHz, which is further from 2.45GHz than the initial unit cell considered in [35]. At 2.45GHz the μ_{reff} is higher than one, and the material resonance is situated at a higher frequency. However, the permeability does not have a smooth value variation and this will probably lead to a FBW reduction because of the strong dispersive behaviour of $\mu_{reff}(f)$.

Another unit cell (Fig. 4.7) is designed in order to reduce the resonant frequency of the material. The

new SR is shortened leading to a higher SR resonant frequency: 3.27GHz. This SR has 1.25 loops and it is denoted as s125d.

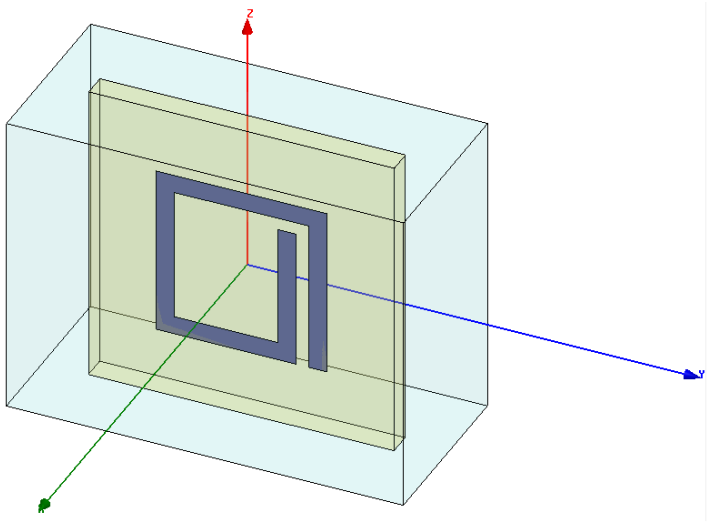

Figure 4.7: Sketch of the s125d unit cell design.

The simulated coefficients can be seen in Fig. 4.8. From the zero crossing of the S22 phase, the material resonance is found 3.29GHz. So the objective of having the resonance further is achieved with the new unit cell.

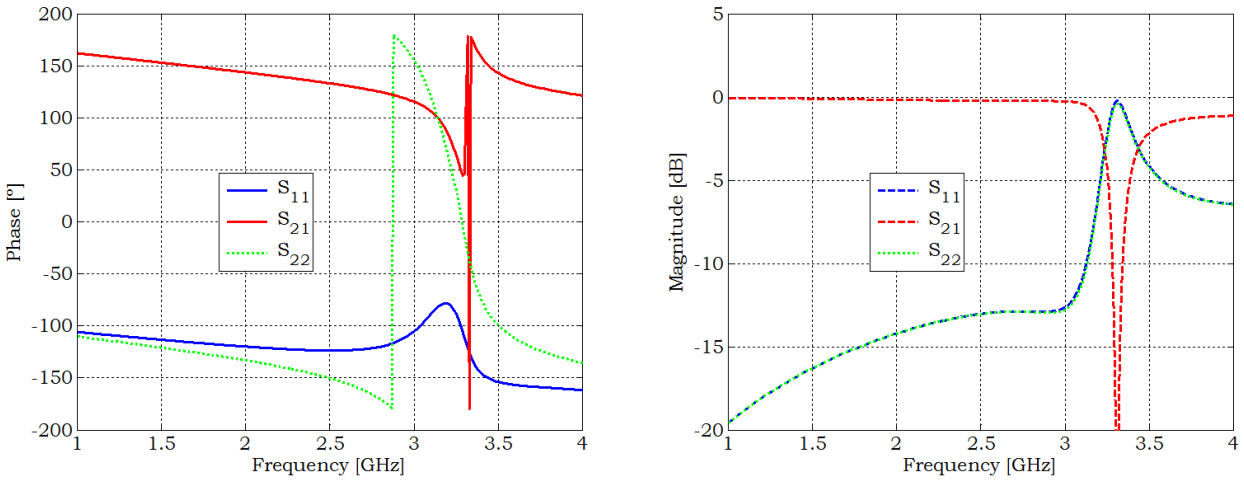

Figure 4.8: Simulated S11, S21 and S22 parameters of the SR resonators: phase (top left) and magnitude (top right). Extracted ε_{reff} (bottom left) and μ_{reff} (bottom right) for the s125d case.

Finally, two more unit cells are also considered (s2o and s125o), with a 90^{o} rotation with respect to the x axis. Nevertheless, the extracted parameters are very similar to the non-rotated unit cells.

4.3 Simulation results

After a preliminary study of which has to be the antenna size in order to be matched around 2.45GHz, a patch of 40mm x 40mm has been simulated. The ground plane size is 250mm x 250mm. Four feeding positions are considered, since the antenna substrate is h=10mm and the pin length (12mm) is considerable and will affect the matching of the antenna. The distances to the patch centre and the corresponding name of each feeding position are the following:

x_0 [mm]	Name
1.5	1
6.5	2
11.5	3
16.5	4

Table 4.1: Feeding position names; x_0 represents the distance to the centre of the patch.

The simulated model is designed the most similarly possible to the realizable antenna setup. The metasubstrate is formed by 6 strips 40mm long and 10mm high, with 4 metal SRs printed on the RO4003C dielectric strip separated 10mm between them. The strips are 6mm separated one from another. Two types of SRs are used: SRs of 2 loops (named s2) and SRs of 1.25 loops (named s125). In addition two different positions of the SRs inside the slab are simulated: SRs facing down (s2d and s125d) and SRs facing outside (s2o and s125o). The difference is shown in Fig. 4.9. However, since the results for the s125d and s125o and the s2d and s2o are highly similar respectively, only the s12d and s2d cases are considered in this work.

The number of SR loops, the SR physical size, the strips height and the metasubstrate strips density in the present work have been chosen for the ease of fabrication.

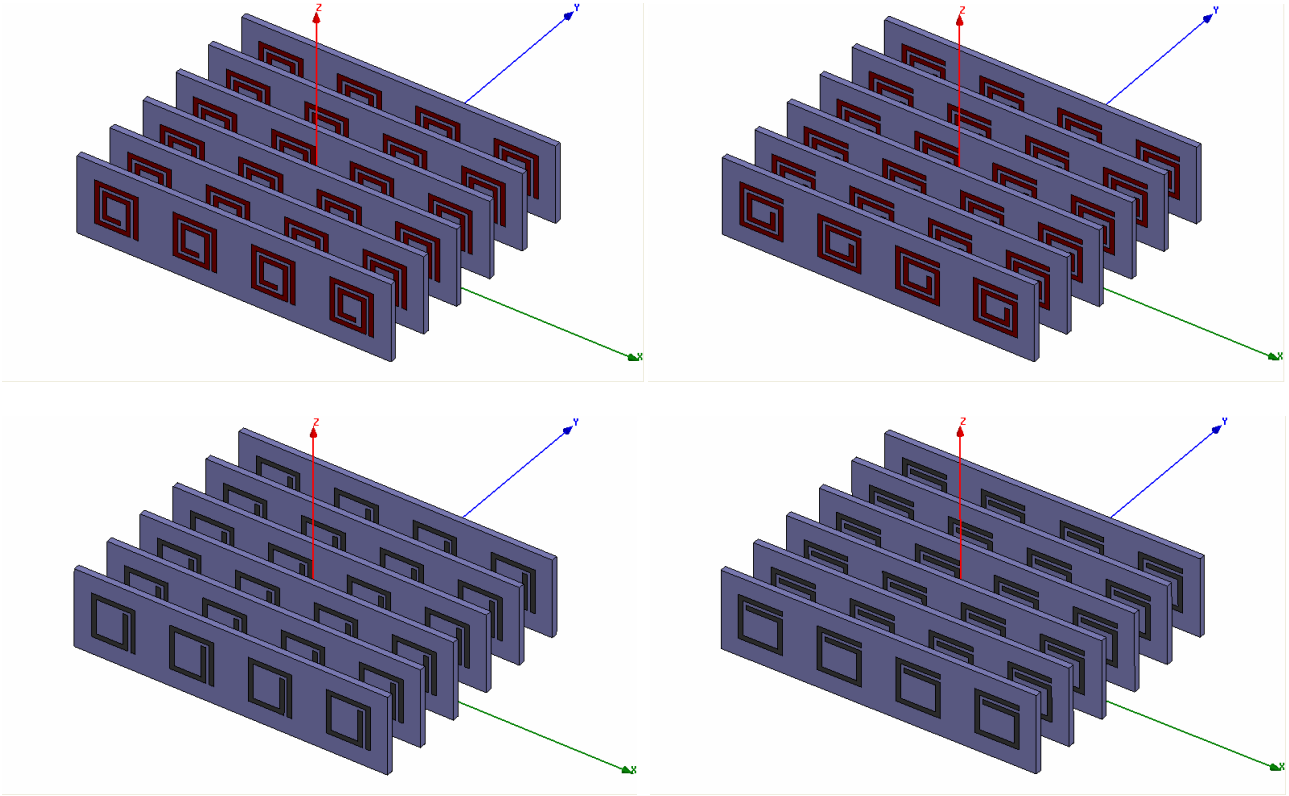

Figure 4.9: Four kinds of simulated metasubstrates: s2d (top left), s2o (top right), s125d (bottom left) and s125o (bottom right). All these metasubstrates are composed of 6 strips containing the SR.

A sketch of the simulated antenna can be observed in Fig. 4.10.

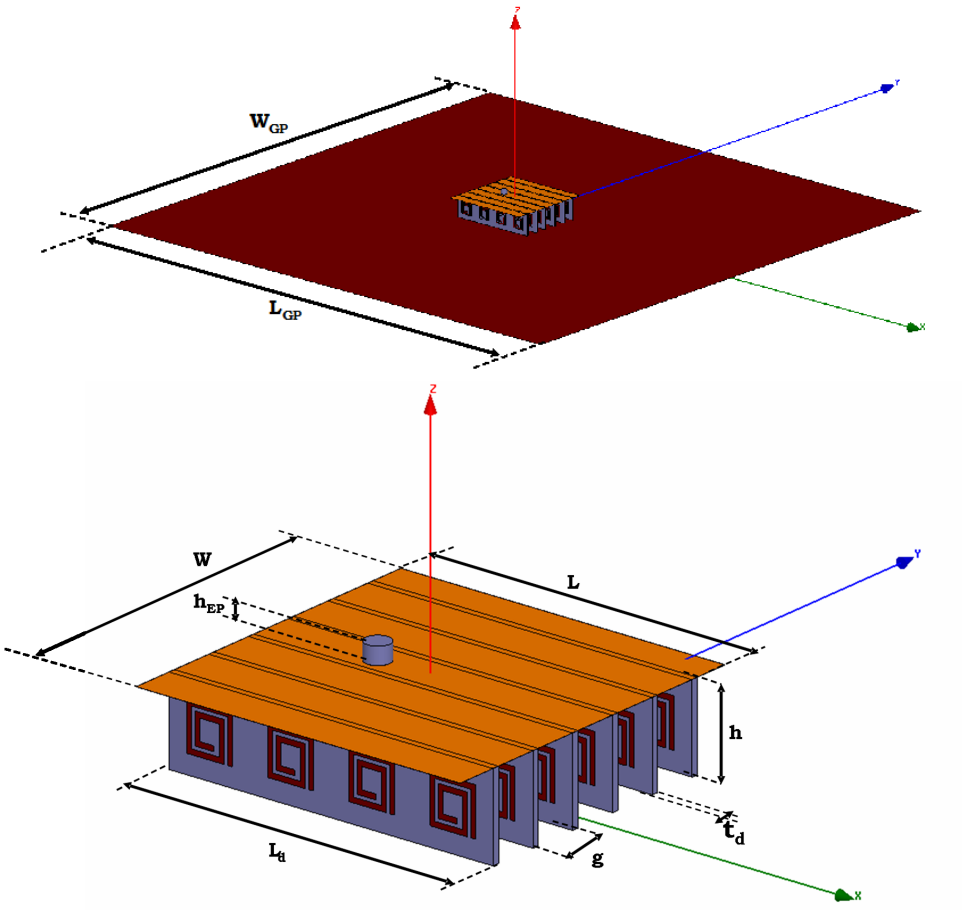

Figure 4.10: Sketch of the simulated antenna (top) and detail of the antenna metasubstrate under the copper patch (bottom). In the depicted case the metasubstre is the *s2d*. $W_{GP} = 250mm$ and $L_{GP} = 250mm$ are the ground plane width and length respectively, whereas $W = 40mm$ and $L = 40mm$ are the patch width and length. The height of the substrate is $h = 10mm$, and $h_{EP} = 2mm$ is the external pin height. The dielectric thickness is $t_d = 0.8mm$, the total length of the strips is $L_d = L = 40mm$ and the gap between consecutive strips of spirals is $g = 6mm$.

The reflection parameter S11 is studied for the air case (no metasubstrate under the patch), the s125d metasubstrate and the s2d metasubstrate for the 4 feeding position cases. The results of the simulations are gathered in Figs. 4.11 and 4.12.

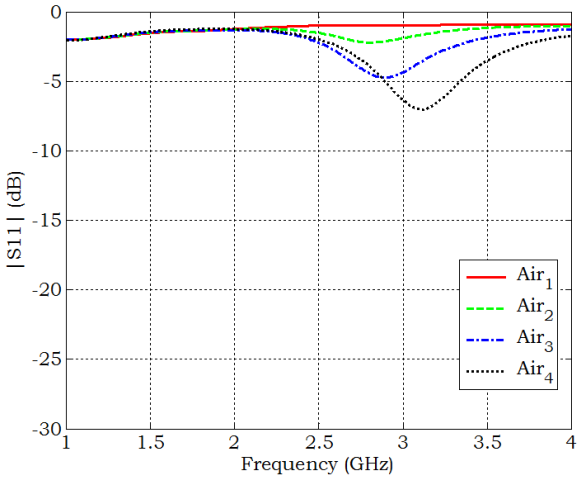

Figure 4.11: Simulated reflection coefficient when there is no substrate under the antenna.

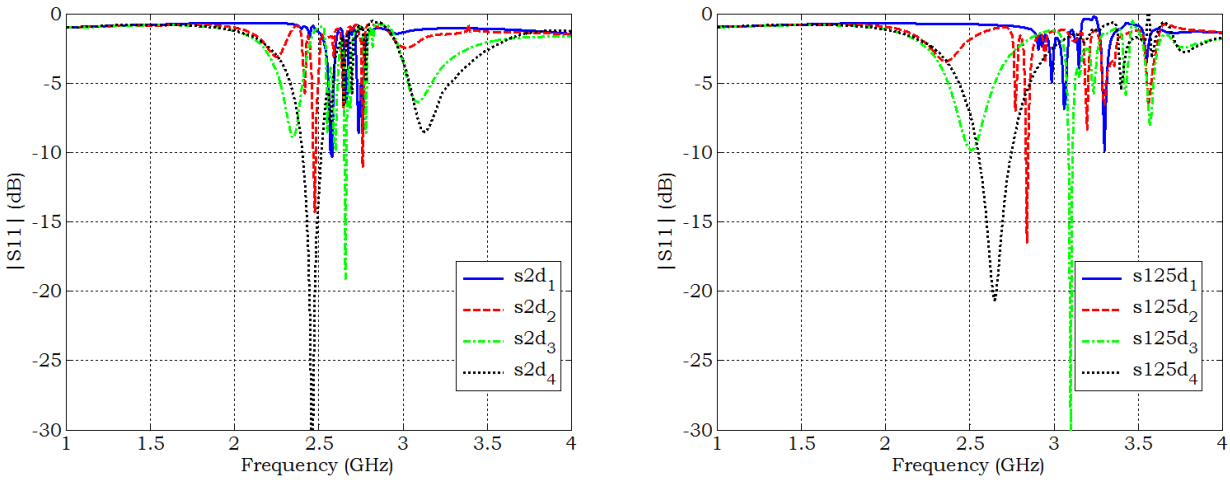

Figure 4.12: Simulated reflection coefficient when the substrate is the s125d (left) and s2d (right).

A first analysis shows how the patch filled with air has a poor matching (remember that Z_{ref} is 50Ω). This makes difficult to compare the air case with the s125d ad the s2d in terms of antenna miniaturization. The air case should have a patch of approximately 54mm x 54mm to be matched at 2.45GHz. But we must fix a common patch size in all cases in order to make a fair comparison. The matching improves with the s125d and the s2d metasubstrates, and the first frequency of resonance becomes lower, which means an electrical antenna miniaturization.

The miniaturization factor achieved with each of the metasubstrates is gathered in Table 4.2. The factor N is obtained by applying Eq. 4.3.

$$N = \left(\frac{f_{0_1}}{f_{0_2}} \right) \tag{4.3}$$

Where f_{0_1} and f_{0_2} are the resonant frequencies before and after including the metasubstrate, respectively. The miniaturization factor is shown in Table 4.2.

	Miniaturization factor	
Patch filling	N	[%]
$s2d_4$	1.21	18
$S125d_4$	1.13	11

Table 4.2: Miniaturization factor obtained with the metasubstrates referred to the resonant frequency of the air case.

A first look to the $|S11|_{dB}$ plots when choosing the matching level to -6dB[1], makes us notice that from air_4 to $s125d_4$ the bandwidth does not vary while the resonant frequency decreases. This is very important because although the miniaturization factor is not very high, The FBW is increased. In Table 4.3 the FBW_{-6dB} values obtained from the direct calculation of the reflection coefficient are gathered.

Patch filling	f_0	FBW_{-6dB}[%]
Air	3.11	8.6
$s2d_4$	2.46	7.3
$s125d_4$	2.65	12.83

Table 4.3: Direct calculation of the FBW_{-6dB} from the $|S11|_{dB}$.

As already done in Chapter 3 for the non-dispersive substrates, we apply Yaghjian to these S11 in order to obtain the maximum achievable FBW for these dispersive substrate patch antennas. Computed FBW results for the air case are plotted in Fig. 4.13, and for the s2d and s125d cases in Fig. 4.14.

[1]In this Chapter the FBW is measured at L=6dB, contrarily to the L=10dB used as a reference in Chapter 3. The reason is that the matching of the antenna when there is no substrate under the patch (air case) is too poor to allow a direct measurement of the FBW at -10dB.

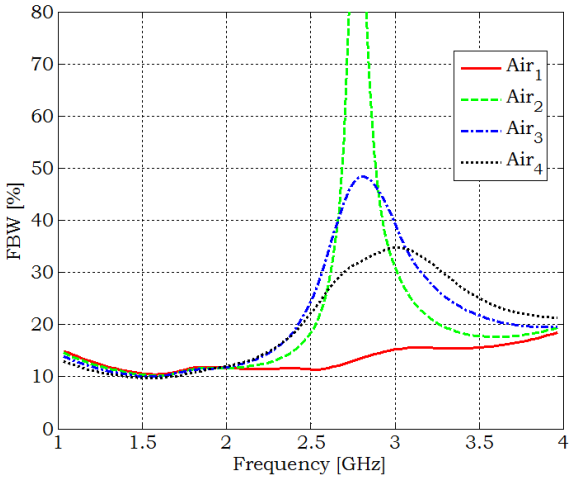

Figure 4.13: FBW_{-6dB} of the antenna for the four feeding positions defined when there is no substrate under the patch.

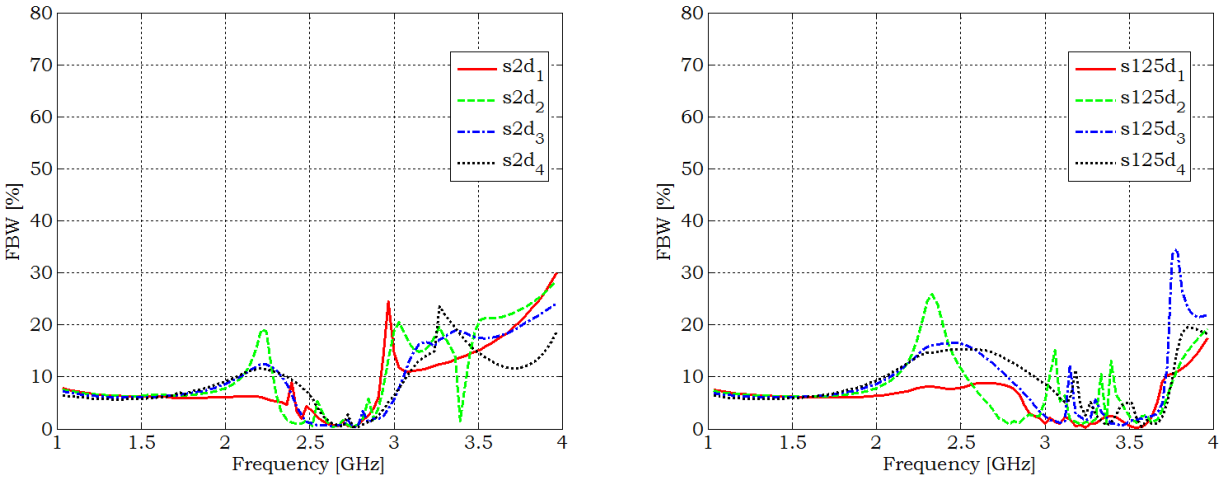

Figure 4.14: FBW_{-6dB} of the antenna for the four feeding positions defined when the metasubstrate is s125d (left) and s2d (right).

The FBW narrow peaks are unexpected post-processing results due to the resonant frequencies of the square resonators used in the simulation of the metasubstrate, and do not have to be taken under consideration. Take for example de $s125d_2$ case in the 3 to 3.5GHz frequency band which contains the s125d material resonance (3.27GHz).

In that case to see the miniaturization effect the position of the maximum FBW has to be compared. In feeding position 2, for example, the maximum is at approximately 2.75GHz, whereas in s2d the maximum is at approximately 2.2GHz. If we focus in the FBW values, it is clear that it is far from the air case, at the expense of changing the reference impedance to match it to the input impedance

of the antenna (as explained in Chapter 2, Subection 2.3). Table 4.4 gathers the FBW_{-6dB} values at the first frequency of resonance for each patch antenna filling.

Patch filling	f_0	FBW_{-6dB}[%]
Air	3.11	34.2
$s2d_4$	2.46	7.8
$s125d_4$	2.65	15

Table 4.4: Computed FBW_{-6dB} from the $|S11|_{dB}$.

These results mean that in the air case the antenna input impedance is far from the 50Ω taken as a reference to plot the $|S11|_{dB}$, because the 34.2% predicted by the Yaghjian's computed FBW is far from the 8.6% calculated directly from the reflection coefficient.

In any case, with the introduction of a dispersive material the bandwidth of the antenna decreases compared with the bandwidth of the air filling case. Nonetheless, it has to be pointed out that the bandwidth achieved with the metasubstrates is not narrow bandwidth. Values around a 10% are quite good at high frequencies. In addition, the maximum FBW achieved has a wide frequency bandwidth itself; i.e., taking as an example the $s125d_4$ case the maximum FBW can be achieved in a frequency range from 2.3GHz to 2.7GHz.

4.4 Fabrication and Measurements

In order to verify the results obtained through the simulations, the four different metasubstrates have been fabricated at our facilities using standard photo-etching techniques. The fabricated designs are composed each one of 6 strips 40mm long, containing 4 square spirals etched on RO4003C dielectric substrate. The dimensions of the SRs and the dielectric substrates are the same than the ones used in the simulations. Styrofoam boards have been used to support the dielectric strips with the printed resonators. This material is as almost transparent, like the air, at microwave frequencies and hence its use does not change the results but helps to the fabrication of the measurement setup. In Fig. 4.15 a photograph of the measurement setup is shown. In Fig. 4.16 the s2d metasubstrate slab can be seen with more detail, and in Fig. 4.17 all the fabricated strips are shown.

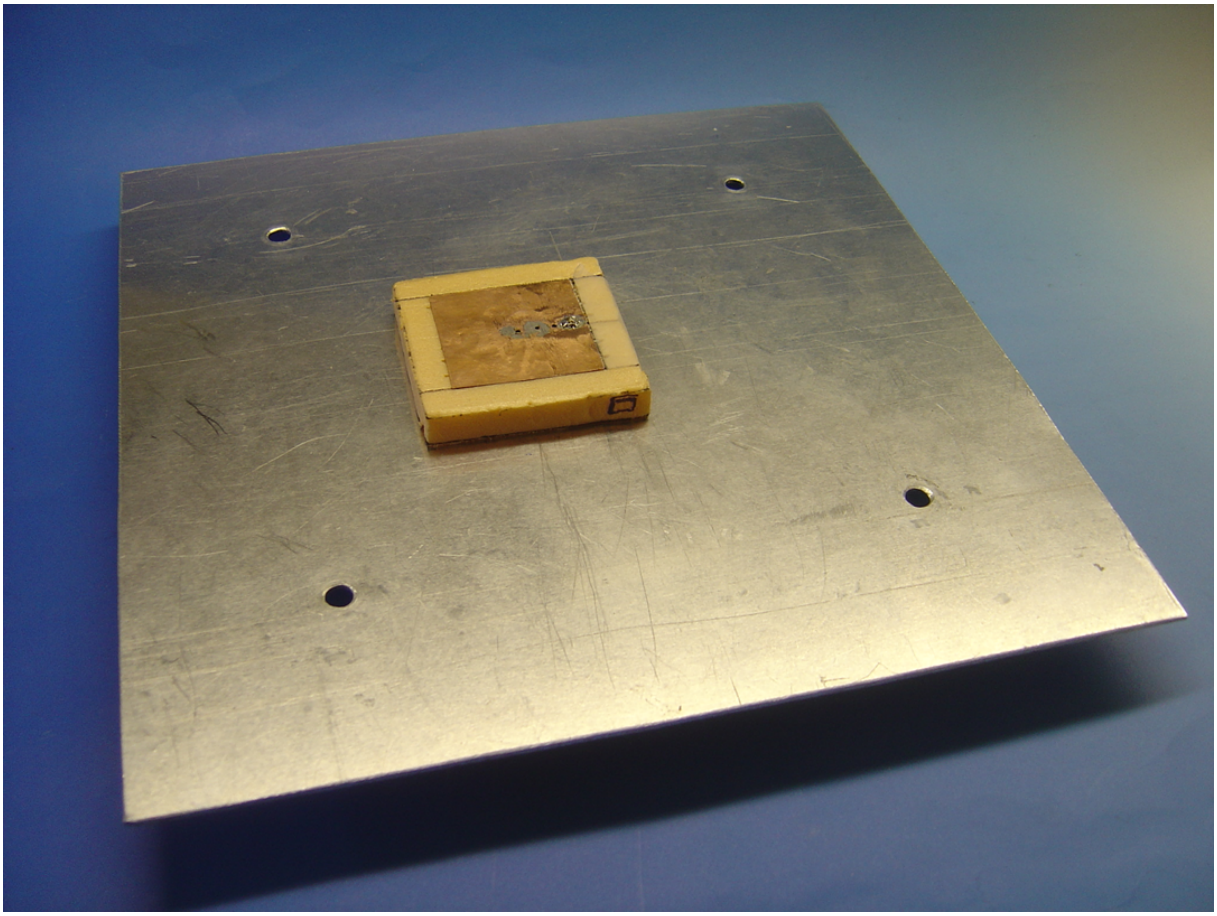

Figure 4.15: Setup with the ground plane, the copper patch and the Styrofoam containing the SR strips that form the metasubstrate.

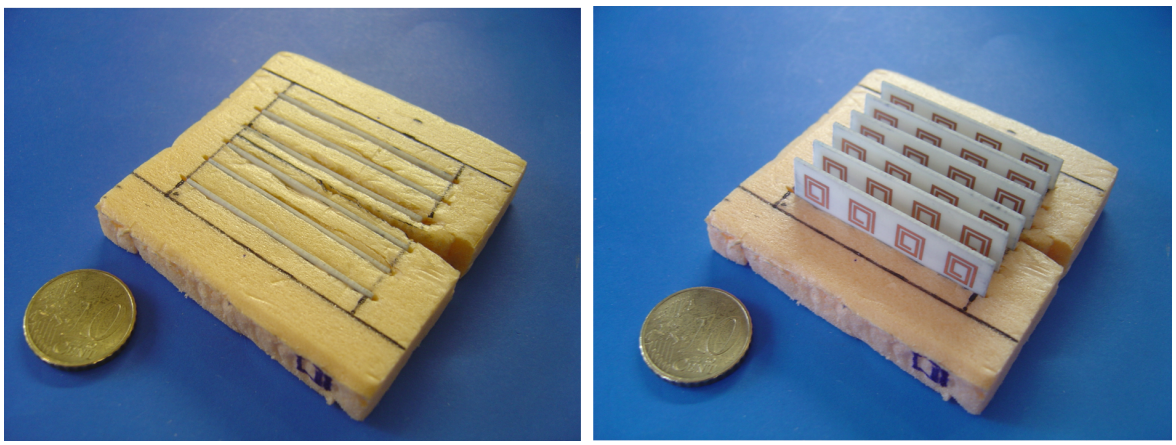

Figure 4.16: Styrofoam containing the SR strips that form the metasubstrate s2d.

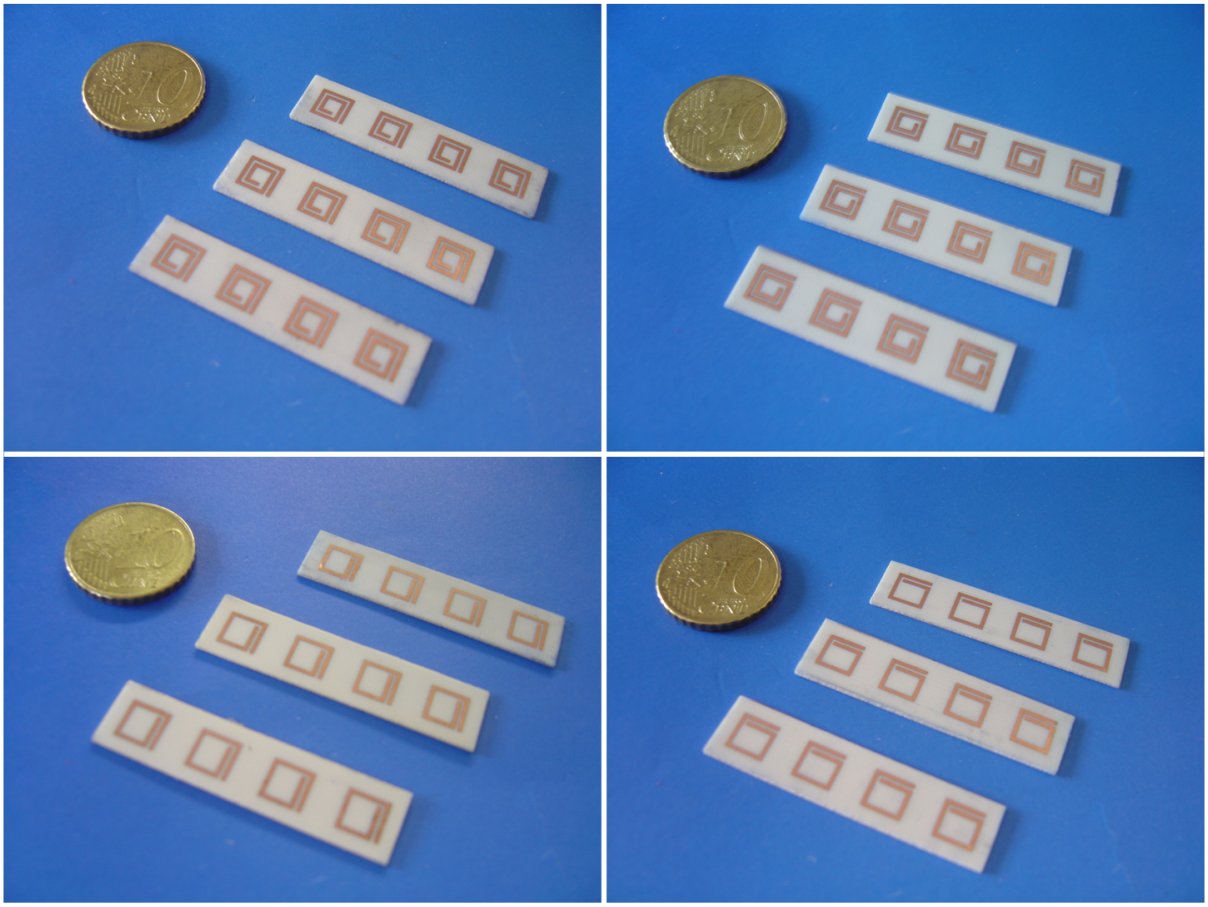

Figure 4.17: Strips which form the different measured metasubstrates: s2d (top left), s2o (top right), s125d (bottom left) and s125o (bottom right).

The ground plane is 33cm x 33cm made of aluminium, with a coaxial connector. The patch is 40mm x 40mm made of copper.

4.4.1 Measurement Setup

The setup is formed by the ground plane, the copper patch and the strips described in the former subsection. In order to measure the different reflection coefficient responses, the copper patch is soldered considering a feeding position. Then the five different patch fillings (air, s125d, s125o, s2d, s2o) are measured, changing the Styrofoam board that contains the metamaterial strips. When the five measurements are done for one of the feeding positions, the patch is unsoldered from the coaxial pin and soldered again changing the patch hole to measure another feeding position.

The fabricated patch antennas are measured using an Agilent E8362B network analyzer as seen in Fig. 4.18.

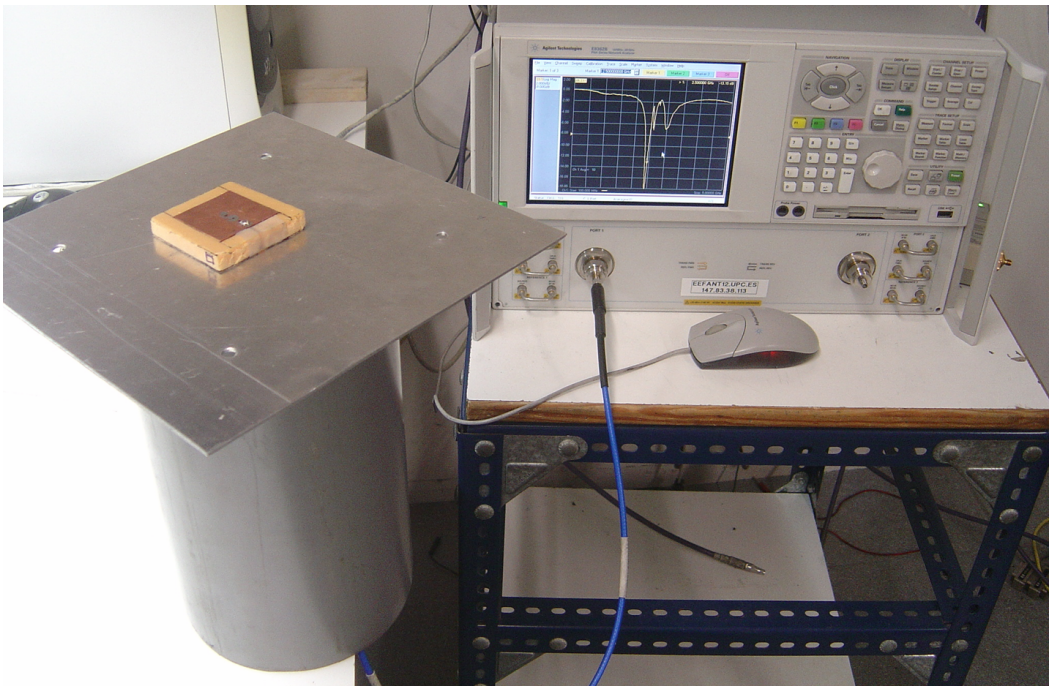

Figure 4.18: Measurement setup for the reflection coefficient of the antennas with different material fillings.

4.4.2 Reflection coefficient measurements

The S11 measurements are gathered in Fig. 4.19 and 4.20. As it can be observed, simulations and measurements agree quite well, especially for the fourth case (feeding position 4). The matching at 2.65GHz for the s125d4 is different in magnitude but not in frequency when comparing measurements (Fig. 4.20-left) and simulations (Fig. 4.12-left). The same happens with the s2d4 case (Figs. 4.20-right and 4.12-right) when comparing the matching at 2.46GHz.

As explained before, the results for the s2o and s125o cases are not shown because of their similarity with the s2d and s125d cases.

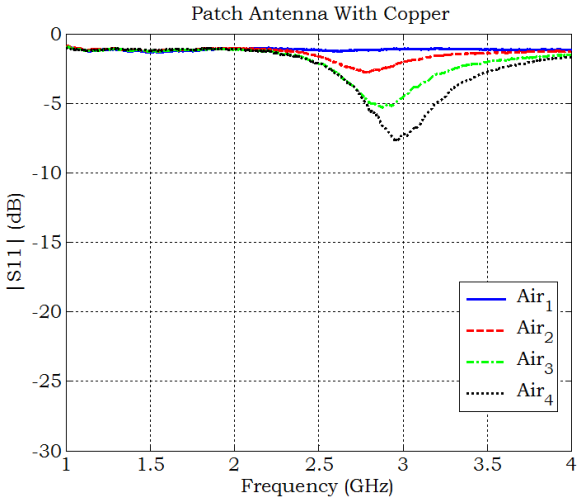

Figure 4.19: Measured reflection coefficient when the antenna has no metasubstrate under the patch. Air case.

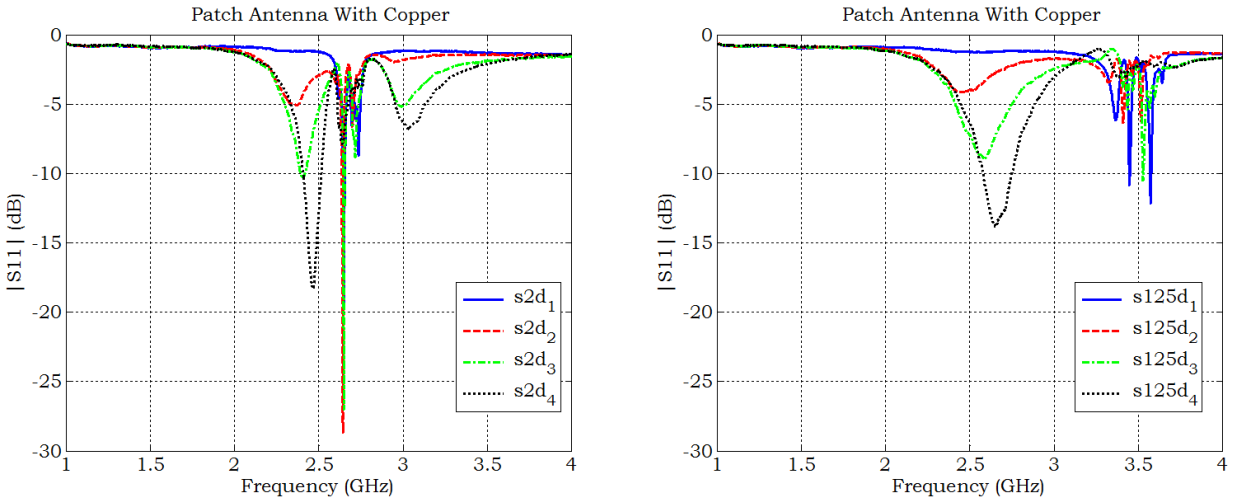

Figure 4.20: Measured reflection coefficient when the antenna is filled with the metasubstrate s125d (left) and s2d (rigth).

Since the measured results agree with the predicted by the simulations, the same observations than in Section 4.3 can be done: a small miniaturization factor is achieved, when comparing the poorly matched air case with the ones having the antenna loaded with the metasubstrates (see Table 4.5).

Patch filling	Miniaturization factor	
	N	[%]
$s2d_4$	1.20	16
$S125d_4$	1.11	10

Table 4.5: Miniaturization factor obtained with the metasubstrates referred to the resonant frequency of the air case. Feeding position 4.

However, at least for the feeding position 4, the bandwidth when using a -6dB matching level (50Ω refference impedance) is almost the same in the air case and in the s125d case. The FBW results obtained from the reflection coefficients obtained are gathered in Table 4.6.

Patch filling	f_0	FBW_{-6dB}[%]
Air	2.95	9.0
$s2d_4$	2.47	7.2
$s125d_4$	2.65	13.7

Table 4.6: Direct measurement of the FBW_{-6dB} from the $|S11|_{dB}$. Feeding position 4.

Hence, a certain miniaturization is achieved while maintaining or even improving the FBW.

4.4.3 Computed FBW Results

Since the measure method is very sensitive to the impedance variation, the curves of the measured impedances have little variations. Applying a derivative to compute the Yaghjian's FBW to these measured impedances results in sharp variations in the computed FBW. In order to apply the Yaghjian's method to extract the maximum FBW achievable with the measured antennas, the measured data has to be processed before computing the FBW. The filter applied to smooth the measurements is based in the sliding mean average. The results in Figs. 4.21, 4.23 and 4.22 (left part of the figures) compare the S11 simulated with the measured one before and after applying the moving average. The results in Figs. 4.21, 4.22 and 4.23 (right part of the figures) compare the FBW predicted by the simulations with the one predicted through the filtered measurements. For the sake of brevity, the cases shown are only the air, s125d and s2d in the feeding position 4.

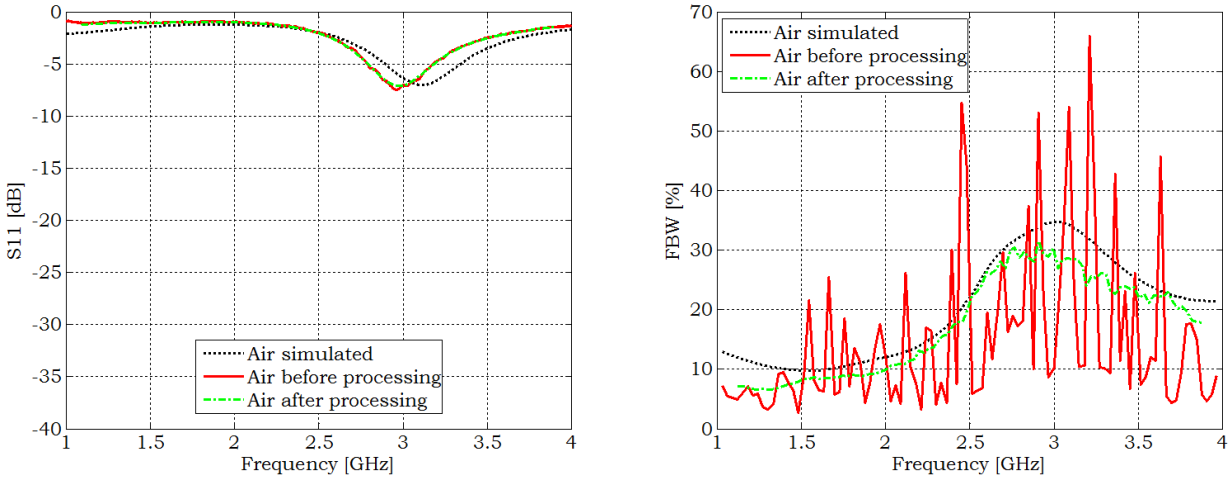

Figure 4.21: Simulated and measured reflection coefficient (left). A moving average of 101 samples is applied to the measured reflection coefficient in the air case. FBW_{-6dB} (right) computed from simulations and from measurements.

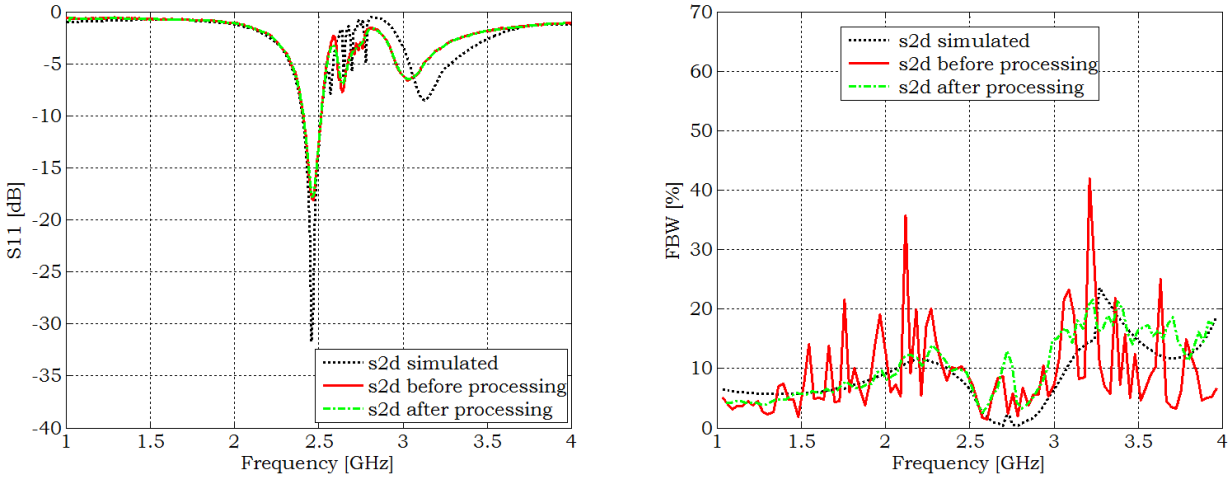

Figure 4.22: Simulated and measured reflection coefficient (left). A moving average of 26 samples is applied to the measured reflection coefficient in the air case. FBW_{-6dB} (right) computed from simulations and from measurements.

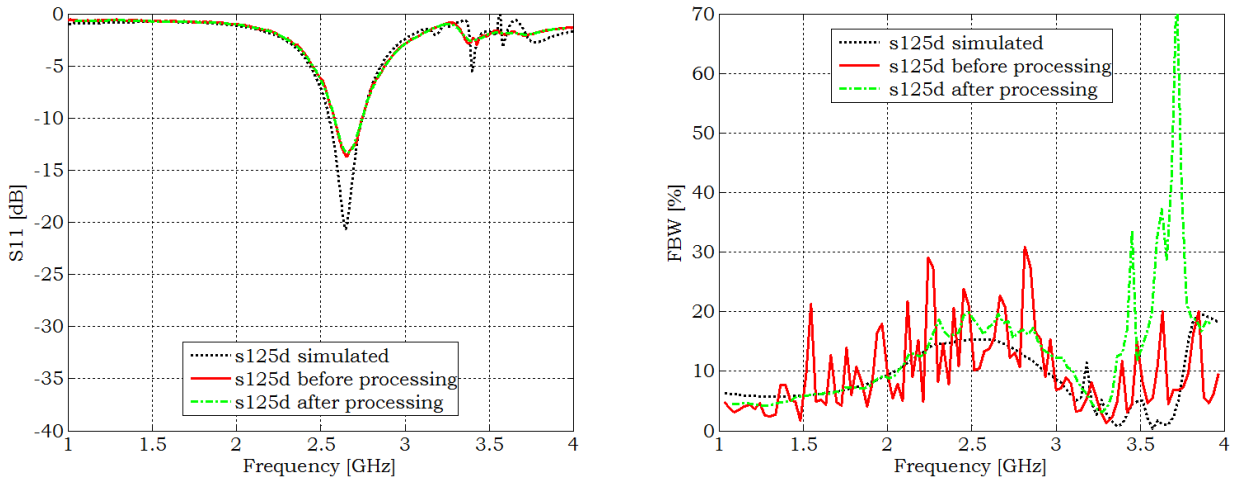

Figure 4.23: Simulated and measured reflection coefficient (left). A moving average of 51 samples is applied to the measured reflection coefficient in the air case. FBW_{-6dB} (right) computed from simulations and from measurements.

It is clear that the FBW computed from the measurements to which the mean average is applied are quite similar to the FBW computed from the simulated reflection coefficient. As expected from the comparison between simulated and measured reflection coefficients, the computed FBW obtained from simulations and from measurements agree quite well.

4.4.4 Efficiency measurement

The efficiency of the antennas is measured in order to check that the improvement in the matching obtained with the metasubstrates is not due to lossess introduced by these metasubstrates.

The efficiency has been measured using the Wheeler's cap method. The Wheeler's cap is a conducting semi-sphere with which the antenna is covered. With the antenna enclosed in this semi-sphere the radiation resistance, R_{rad}, is eliminated from the antenna input impedance, Z_0, without modifying the loss resistance R_{loss} in a significant way. Hence, to apply the original Wheeler's cap method, the real part of the antenna input impedance with and without the cap has to be measured and then one can obtain the radiation efficiency applying Eq. 4.4.

$$\eta_{rad}[\%] = \left(\frac{R_0(f_0) - R_{wc}(f_0)}{R_0(f_0)}\right) 100 \tag{4.4}$$

$$\eta_{rad}[\%] = \left(\frac{R_0(f_0)}{R_0(f_0) - R_{wc}(f_0)}\right) 100 \tag{4.5}$$

Where $R_{wc}(f_0)$ is the real part of the input impedance of the covered antenna at resonance, and $R_0(f_0)$ is the real part of the antenna impedance without the covering, at the resonance. Eq. 4.4 is useful

when the antenna input impedance can be modelled by a series RLC circuit, while Eq. 4.5 is useful when it can be modelled by a parallel RLC circuit.

Instead of applying the original Wheeler cap method we have used an improved version of the Johnston-Geissler method [42] [43].

4.4.4.1 Wheeler cap method application

Three different caps are used to measure the reflection coefficient parameters with the antenna radiating in free space and with the short-circuited antenna. The caps are shown in Fig. 4.24 while the measurement setup can be seen in Fig. 4.25.

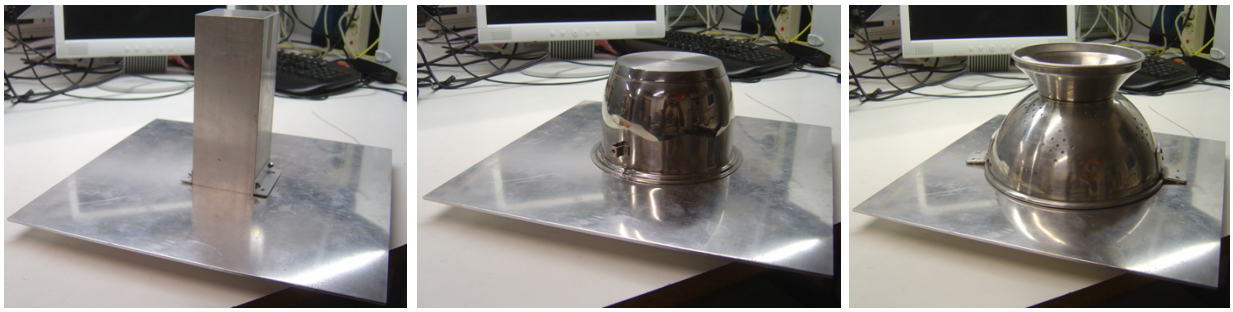

Figure 4.24: Three caps used to measure the short-circuited antenna reflection coefficient: W1, W2 and W3.

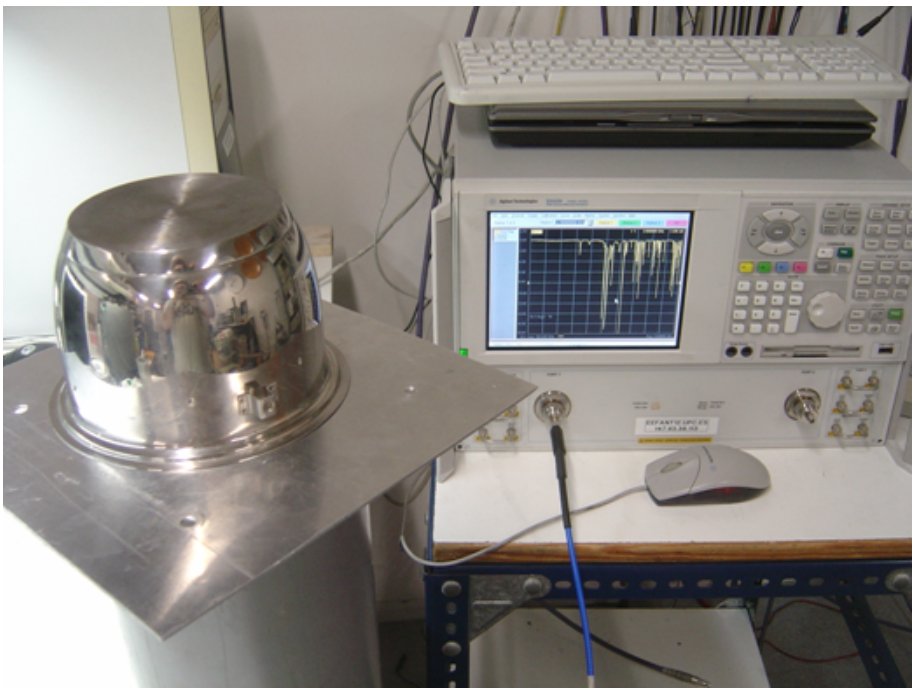

Figure 4.25: Radiation efficiency measurement with Wheeler Cap method.

In Fig. 4.26 the reflection coefficient of a monopole tuned to 2.45GHz in free space is compared with its reflection coefficient when inside the different caps. In this way the modes which propagate inside the cap can be seen. Ideally there would have to be the fewer modes as possible in order to have a good measurement.

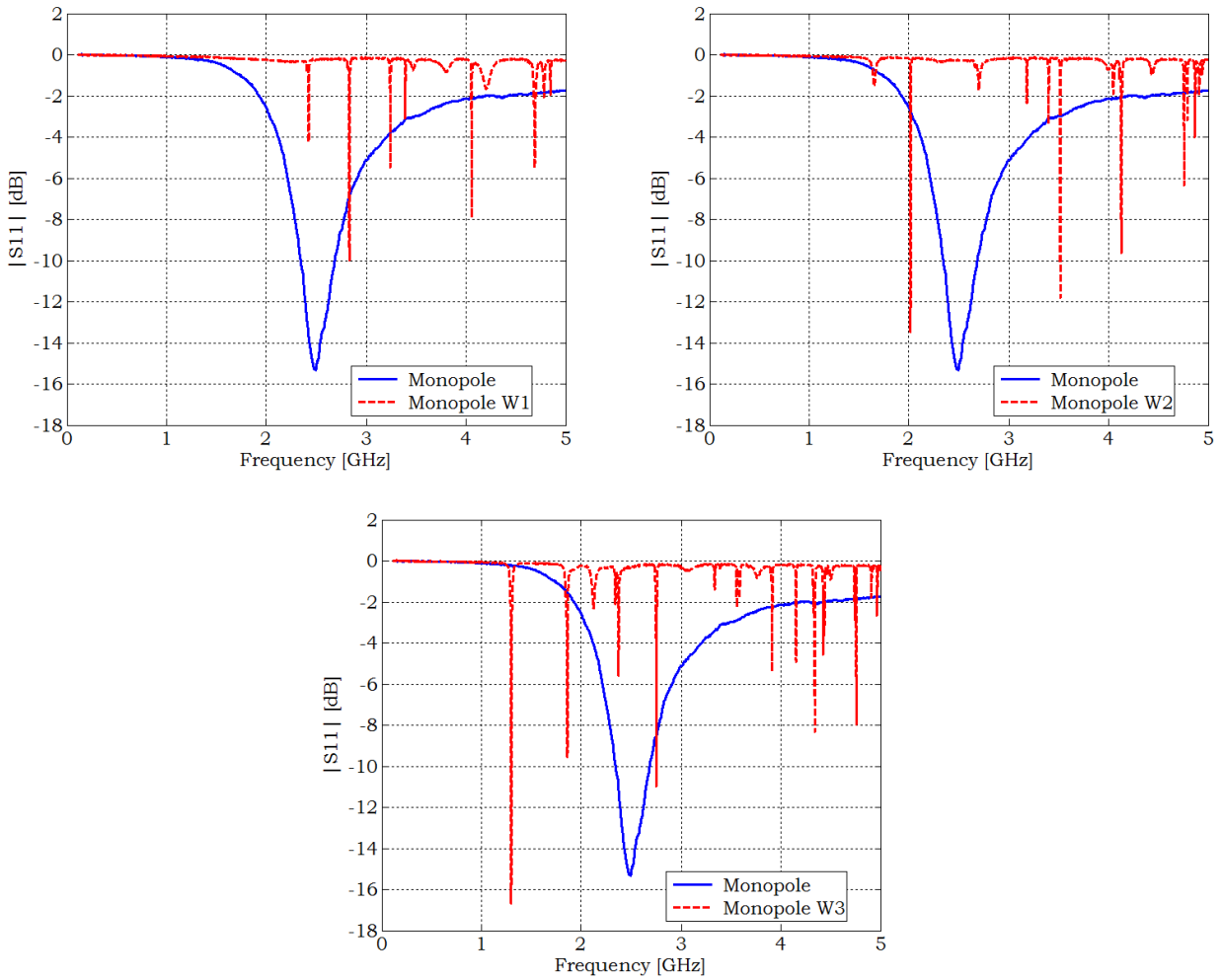

Figure 4.26: Measured reflection coefficient of the monopole antenna with and without the caps: W1, W2 and W3.

It is clear that the best cap will be the first one, W1, because less modes propagating in it will mean less interference with the resonances of the antenna under test.

4.4.4.2 Efficiency Results

Using the procedure described in P. Miskovsky et al. [43], the radiation efficiency of the antenna is obtained for a wide frequency range. The first cap used (the smaller one) provides the smoother results, as shown in Fig. 4.27.

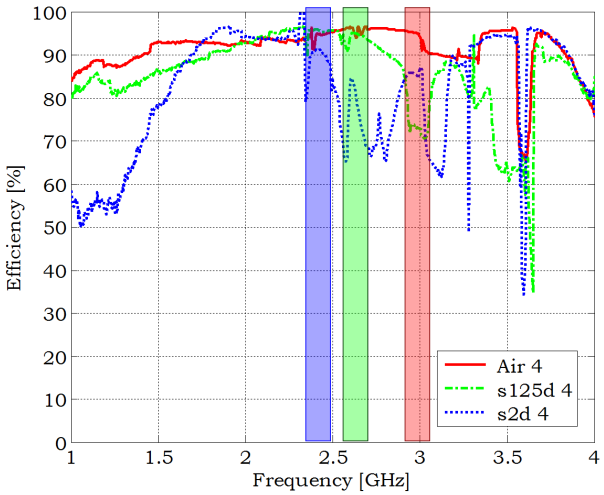

Figure 4.27: Antenna efficiency for the three cases with the cap W1: air, s125d and s2d. Feeding position: 4.

The antenna resonates approximately at 3GHz for the air case, and at this frequency the efficiency is $\eta_{rad_{air}} \sim 95\%$. The efficiency of the s125d case at its matching frequency, 2.65GHz, is $\eta_{rad_{s125d}} \sim 93\%$. For the s2d case the efficiency at its matching frequency is $\eta_{rad_{s2d}} \sim 90\%$, about a 5% below the one of the air case.

4.4.5 Radiation patterns measurement

The antenna is placed in the anechoic chamber to measure its radiation pattern. The setup can be seen in Fig. 4.28. The antenna marked with a 1 is the antenna under test, while the antenna marked with a 2 (ridged horn antenna) is used to measure the antenna under test.

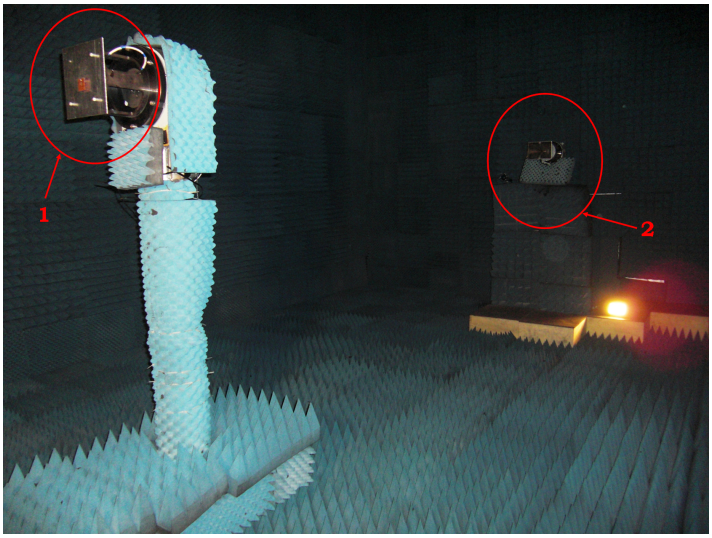

Figure 4.28: The antenna being measured in the anechoic chamber at D3 building, Campus Nord, Universitat Politècnica de Catalunya.

In Fig. 4.29 the measured components of the normalized electric field for the E and H plane patterns are shown. Each of them has been measured at its respective frequency of resonance.

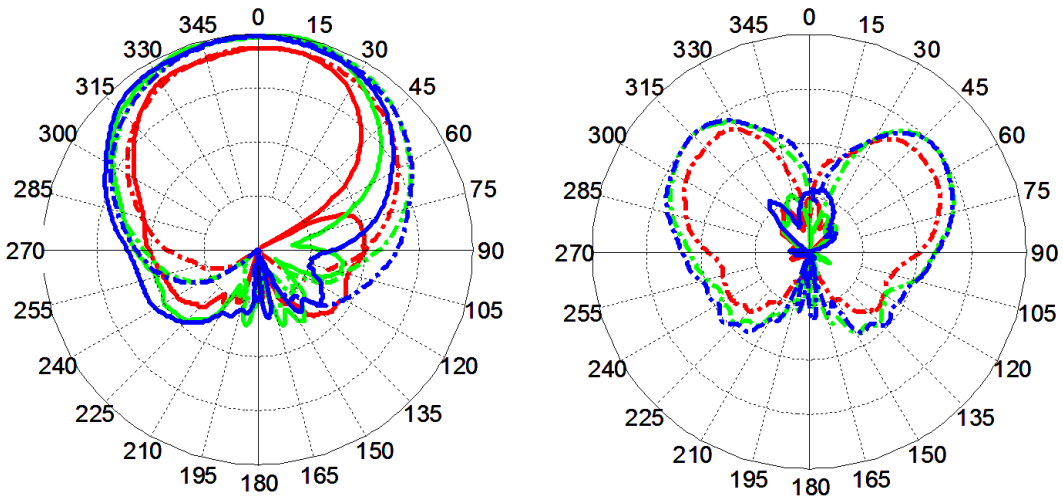

Figure 4.29: Measured $E^E{}_{copolar}$ (solid lines) and $E^H{}_{copolar}$ (dash-dot lines) (left). Measured $E^E{}_{crosspolar}$ (solid lines) and $E^H{}_{crosspolar}$ (dash-dot lines) (right). Different antenna fillings: air (red), s125d (green) and s2d (blue). Each division represents 10dB. $E^E{}_{copolar}$ and $E^E{}_{crosspolar}$ for $\varphi = 0$, $E^H{}_{copolar}$ and $E^H{}_{crosspolar}$ for $\varphi = 90$.

Simulated results are plotted in Fig. 4.30. Each of them has been simulated at its respective frequency of resonance A good agreement is achieved between measured and simulated patterns.

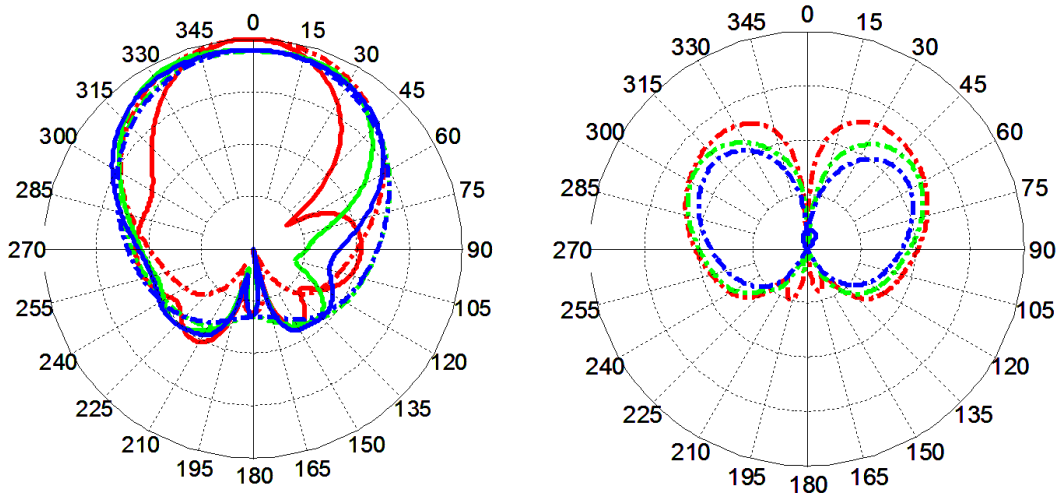

Figure 4.30: Simulated $E^E{}_{copolar}$ (solid lines) and $E^H{}_{copolar}$ (dash-dot lines) (left). Simulated $E^E{}_{crosspolar}$ (solid lines) and $E^H{}_{crosspolar}$ (dash-dot lines) (right). Different antenna fillings: air (red), s125d (green) and s2d (blue). Each division represents 10dB. $E^E{}_{copolar}$ and $E^E{}_{crosspolar}$ for $\varphi = 0$, $E^H{}_{copolar}$ and $E^H{}_{crosspolar}$ for $\varphi = 90$.

The value used to normalize the patterns has been the maximum of the maxima of all the copolar components. The crosspolar component is higher for the H-plane case than for the E-plane case. However, it is around 30dB lower in the maximum radiation direction (broadside).

The radiation patterns have a very similar shape to the theoretical for a square patch antenna. The minimum around 60^o of the copolar E-Plane is due to the pin of the coaxial feeding, which is long enough to radiate and interferes in the patch radiation.

4.5 Discussion

From previous results, we can say that the achieved miniaturization factor is not high (N∼1.2). However, there is a miniaturization while the FBW does not suffer significantly, and at the same time the efficiency is sufficiently high.

It is possible to achieve higher miniaturization factors of the antenna size if using more than 6 metamaterial strips in the substrate. In Fig. 4.31 the measured results of the reflection coefficient and the computed FBW when using 10 metamaterial strips as metasubstrate are shown, compared with the ones obtained when using 6 metamaterial strips.

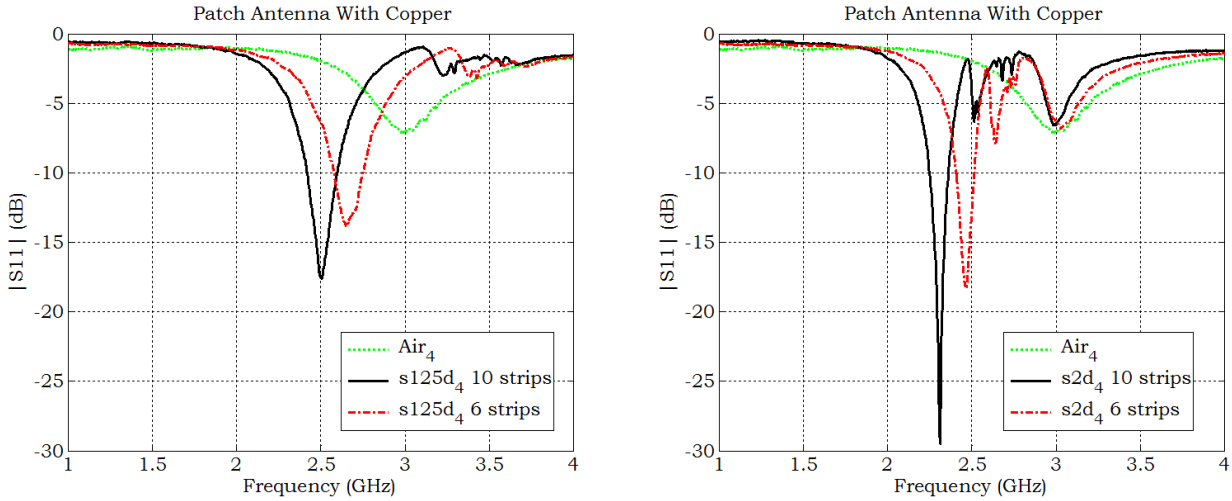

Figure 4.31: Measured reflection coefficiet (left) and computed FBW_{-6dB} (right) for two metasubstrate configurations: 6 or 10 strips. Metasubstrate s125d (left) and s2d (right).

One can see that the miniaturization has increased. A comparison of the new miniaturization factors obtained with the ones obtained with 6 strips can be found in Table 4.7.

Patch filling	Miniaturization factor 6 strips		Miniaturization factor 10 strips	
	N	[%]	N	[%]
$s2d_4$	1.20	17	1.28	22
$S125d_4$	1.12	10	1.18	15

Table 4.7: Comparison between miniaturization factors obtained with 6 or 10 strips.

Finally, the reflection coefficients are processed to obtain the maximum achievable FBW of a metasubstrate of 10 strips. In Fig. 4.32, the FBW predicted through simulation is compared with the predicted through measurements before and after processing the noisy reflection coefficient measurements. This results are compared, at the respective resonant frequency, with the ones obtained from the $|S11|_{dB}$ measurement in Table 4.8.

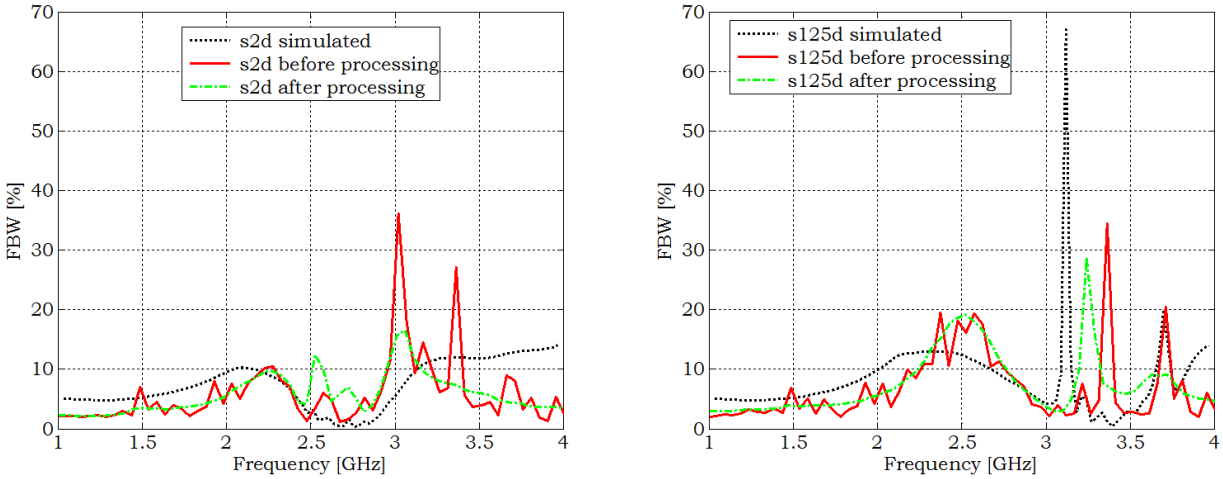

Figure 4.32: Computed FBW_{-6dB} from simulations, measurements and measurements processed (a moving average filter is applied to them before computing the FBW). Metasubstrate $s2d_4$ (left) and $s125d_4$ (right). Metasubstrates with 10 strips.

Patch filling	f_0	FBW_{-6dB}[%] $\lvert S11 \rvert_{dB}$	FBW_{-6dB}[%] Yaghjian
$s2d_4$	2.3	8	8.32
$s125d_4$	2.5	12.8	12.8

Table 4.8: Comparison between the FBW measured from the reflection coefficient and the FBW computed through the Yaghjian's formula for the 10 strip metasubstrates $s2d_4$ and $s125d_4$.

It can be affirmed that with more strips the miniaturization factor increases while the FBW is almost the same.

When measuring the efficiency of the metasubstrate with 10 strips with the Wheeler cap method (cap W1 in Fig. 4.24), $\eta_{rad_{air}} = 95\%$ at its matching frequency of 3GHz, the $\eta_{rad_{s125d}} = 94\%$ at 2.5GHz and $\eta_{rad_{s2d}} = 93\%$ at 2.3GHz. These values are extracted from Fig. 4.33.

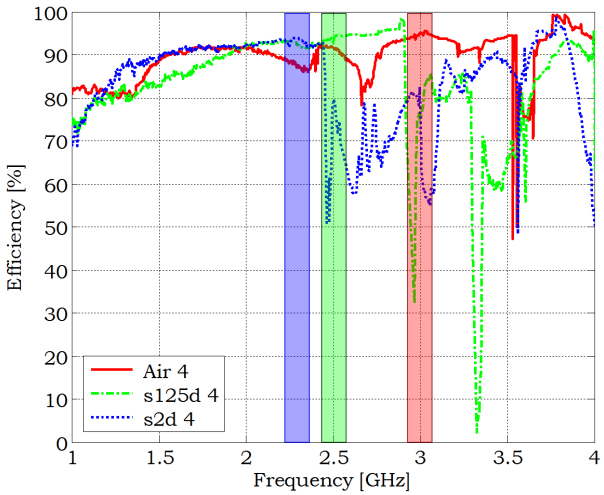

Figure 4.33: Antenna radiation efficiency for the three cases: air, s125d and s2d. Feeding position: 4. Using 10 strips.

Using the cap W1 around the matching frequencies of each antenna filling case the efficiency has a sufficiently smooth behaviour. The differences with the 6 strip cases are negligible. This is a promising result, because increasing the density of SR in the metasubstrate the efficiency is maintained. However, in future investigations other metasubstrates with a higher SR density have to be measured in order to assess which is the limit in strips density under the patch that allows an efficiency value maintainance.

Finally, the radiation patterns are measured. As shown in Fig. 4.34, the shape of the patterns does not vary substantially when increasing the number of strips in the metasubstrate.

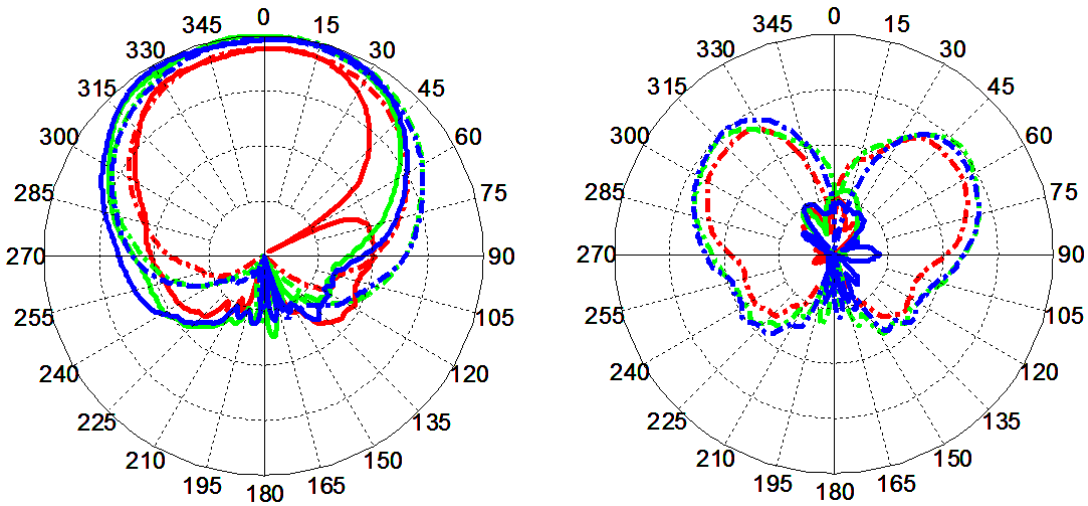

Figure 4.34: Measured $E^E{}_{copolar}$ (solid lines) and $E^H{}_{copolar}$ (dash-dot lines) (left). Measured $E^E{}_{crosspolar}$ (solid lines) and $E^H{}_{crosspolar}$ (dash-dot lines) (right). Different antenna fillings: air (red), s125d (green) and s2d (blue). Each division represents 10dB. $E^E{}_{copolar}$ and $E^E{}_{crosspolar}$ for $\varphi = 0$, $E^H{}_{copolar}$ and $E^H{}_{crosspolar}$ for $\varphi = 90$.

The fractional bandwidth does not vary significantly and neither the radiation efficiency. Therefore, for the number of strips considered in this work, it can be stated that the effect of increasing the number of strips in the metasubstrate is positive because allows a higher miniaturization effect without worsening important features of the antenna.

4.6 Conclusions

A microstrip patch antenna with four possible dispersive fillings has been simulated, fabricated and measured. The reduction of the bandwidth of the antenna when filled with dispersive metasubstrates has been assessed and the results predicted by authors as Ikonen et al. [20] have been confirmed. Nonetheless, the FBW reached with metasubstrates is not a narrow bandwidth. In addition, the maximum FBW achieved has a wide frequency bandwidth itself.

The antenna is both physically and electrically miniaturized achieving electrical miniaturization factors up to 1.28, which can be still improved. The antenna is physically miniaturized because the size of the prototype microstrip patch antennas used ($40mm \sim \frac{\lambda_0}{3}$) is less than the necessary when considering the air case ($\frac{\lambda_0}{2} \sim 61mm$) to be matched at $f_0 \sim 2.45GHz$.

The matching (S11), the efficiency and the radiation patterns of the four different antenna configurations have been measured. Two of the prototypes reach the higher electrical miniaturization factors, as a first objective. These prototypes are the ones using the $s2d_4$ metasubstrate composed by 6 and 10 strips. Their main characteristics are gathered in Table 4.9.

Patch filling	f_0	N	FBW $_{-6dB}$ (50Ω) [%]	η [%]
Air	3	-	9.0	95
$S2d_4$ 6 strips	2.46	1.21	7.2	90
$S2d_4$ 10 strips	2.3	1.28	8.3	93

Table 4.9: Main characteristics of the fabricated prototypes which provide the higher miniaturization factors compared with the reference air case.

At the light of the obtained results it can be said that when priorizing the FBW and to change the Z_{ref} does not suppose a problem, it is better to work with the patch without metasubstrate (the air case). However, in this case the antenna is not miniaturized. When using metasubstrates ($s2d_4$) the antenna is properly matched, miniaturized and has a good bandwidth.

To reduce the electrical size of the antennas several changes in the metasubstrates can be done:

- Increasing the SR density, for the same SRs. The SR density is increased including more SRs per strip, decreasing the height of the substrate and reducing the gap between consecutive strips of spirals.

– Changing the SR length. Adding more loops to each SR can help to decrease the antenna f_0; instead of 1.25 loops or 2 loops, 3 loops can be considered with the same outer SR dimensions.

Nonetheless, with the above mentioned changes the reduction in resonant frequency will be of only 0.1-0.4GHz.

However, the FBW is expected to decrease and the radiation efficiency will theoretically suffer because of the losses in the medium that will be increased with the SRs density. For the number of strips studied in this work, it still can not be stated which is the limiting strip density that reduces both the efficiency and the FBW. This is an interesting research line for future investigation.

Conclusions

The study of microstrip patch antennas miniaturization using metamaterials as metasubstrates has been carried out. The objective was to verify whether the miniaturization can be efficiently reached; i.e., keeping the antenna radiation characteristics: input impedance, radiation efficiency and radiation pattern. Another objective was to state whether the antenna fractional bandwidth (FBW) can be maintained or even improved at the same time that the antenna is miniaturized.

A compact formulation proposed by Yaghjian et al. to compute the FBW of antennas [9] has been successfully applied not only to antennas with theoretical homogeneous fillings but also to fabricated antennas loaded with dispersive metasubstrates. In practice, the only requirement to obtain the predicted FBW values is to change the reference impedance at the frequency of interest.

The study of patch antennas filled with homogeneous substrates with $0<(\varepsilon_r, \mu_r)<10$ values concludes that it is theoretically possible to increase the FBW while efficiently miniaturizing the antenna if substrates with high-μ_r. For high-ε_r values the FBW is dramatically reduced, as expected. An intermediate situation where $\varepsilon_r = \mu_r = a$ (where a is a constant value) achieves the same miniaturization than having a substrate with $\varepsilon_r = a^2$ but substantially improving the maximum achievable FBW. Since the ENZ (Epsilon Near Zero, $0<\varepsilon_r<1$) materials study has also predicted high FBW values, although leading to the patch antenna size increase, a more deep study could be carried out to investigate the feasibility of this kind of metasubstrate. Unfortunately, high-μ_r and $0 < \varepsilon_r < 1$ materials can not be found in nature, although they could be realized "taking advantage" of the dispersive behaviour of metamaterials (though having narrow-band response and losses).

A patch antenna filled with different dispersive metasubstrates has been simulated, fabricated and measured. Simulation and measurement results agree and show that the use of metamaterials allow the antenna miniaturization while maintaining the FBW. A recently published radiation efficiency computation method [35] has been applied for the first time to microstrip patch antennas, obtaining quite optimistic efficiency values for antennas loaded with dispersive substrates.

One of the fabricated prototypes has reached a 22% miniaturization factor improving the matching of the antenna and maintaining the radiation efficiency and FBW values. Two additional fabricated prototypes work at 2.46GHz and at 2.5GHz with a good matching level, maintaining the FBW and

efficiency values. These prototypes could be used for antenna applications in the 2.4-2.5GHz ISM band to assess its performance in a real scenario, although miniaturization is still improvable.

The results obtained when studying metamaterials as patch antenna metasubstrates is quite promising. However, it has been a prospective study, and the fabrication of new metasubstrates changing the unit cell or increasing its density should be carried out to totally characterize the relation between the effective parameters of the metasubstrate and the input impedance, FBW, efficiency and miniaturization factor.

Publications

The work presented in this thesis has contributed to an international conference publication:

P.J. Ferrer, I. Calafell, J.M. González-Arbesú, and J. Romeu, "Bandwidth and Size Behaviour Study for Patch Antennas using Metamaterial Fillings with Positive Permittivity and Permeability", *Proceedings of the 2nd International Congress on Advanced Electromagnetic Materials in Microwaves and Optics (Metamaterials'08)*, Pamplona (Spain), 21-26 Sept. 2008.

Bibliography

[1] P.J. Ferrer, "Metamaterial Designs for Antenna Applications", Master Thesis Proposal, AntennaLab, TSC, Universitat Politècnica de Catalunya, Barcelona, Spain, July 2007.

[2] R.A. Shelby, "Microwave Transmission Through a Two-Dimensional, Isotropic, Left-Handed Metamaterial", *Appl. Phys. Lett.*, vol. 78, no. 4, 2001, pp. 489-491.

[3] V.G. Veselago: "The electrodynamics of substances with simultaneously negative values of ε and μ", *Soviet Physics Uspekhi,* Jan.-Feb. 1968, 10, (4), pp. 509-514.

[4] J. B. Pendry, A. J. Holden, D. J. Robbins, and W. J. Stewart, "Magnetism from conductors and enhanced nonlinear phenomena", *IEEE Trans. on Microw. Theory Tech.*, vol. 47, (11), Nov. 1999, pp. 2075-2084.

[1] D. R. Smith, W. J. Padilla, D. C. Vier, S. C. Nemat-Nasser, S. Schultz, "Composite medium with simultaneously negative permeability and permittivity", *Physical Review Letters, May 2000,* vol. 84, no. 18, pp. 4184-4187.

[6] C. Caloz, and T. Itoh, "Electromagnetic Metamaterials: Transmission Line Theory and Microwave Applications", *John Wiley & Sons*, 1st Edn., 2006.

[7] J.M. González-Arbesú, "Resonadores Espirales como Partículas Resonantes Magnéticas para Pantallas Metamateriales DNG (con Permitividades y Permeabilidades Efectivas Negativas)", Prueba de Habilitación Nacional 2004.

[8] J.B. Pendry, D. Schurig, and D.R. Smith, "Controlling Electromagnetic Fields", *Science Magazine*, vol. 312, pp. 1780-1782, 2006.

[9] D. Schurig, J.J. Mock, B.J. Justice, S.A. Cummer, J.B. Pendry, A.F. Starr and D.R. Smith, "Metamaterial Electromagnetic Cloak at Microwave Frequencies", *Science Magazine*, vol. 314, pp. 977-980, 2006.

[10] A.D. Yaghjian, S.R. Best, "Impedance, bandwidth and Q of antennas", *IEEE Trans. Antennas Propag.*, vol.53, no. 4, pp. 1298-1324, April 2005.

[11] C.A. Balanis, "Advanced Engineering Electromagnetics", John Wiley & Sons, 1st Edn., 1989.

[12] C.A. Balanis, "Antenna Theory: Analysis and Design", John Wiley & Sons, 2nd Edn., 1997.

[13] J.R. James, and P.S. Hall, "Handbook of Microstrip Antenna", IEE Electromagnetic Wave Series, U.K., 1989.

[14] L.J. Chu, "Physical limitations of small antennas", J. Appl. Phys., vol. 19, pp. 1163-1175, Dec. 1948.

[15] G.A. Thiele, P.L. Detweiler, R.P. Penno, "On the lower bound of the radiation Q for electrically small antennas", *IEEE Trans. Antennas Propag.*, vol. 51, no. 6, pp. 1263-1269, June 2003.

[16] G.Y. Lee, Y. Kim, J.S. Lim, S. Nam, "Size Reduction of Microstrip-Fed Slot Antenna by Inductive and Capacitive Loading", *IEEE Antennas Propag. Society Int. Symp. Dig.*, pp. 312-315, Columbus, OH, USA, June 2003.

[17] H. Liu, S. Ishikawa, S. Kurachi, T. Yoshimasu, "Miniaturized Microstrip Meander-Line Antenna With Very High-Permittivity Substrate for Sensor Applications", *Microw. Opt. Technol. Lett.*, vol. 49, no. 10, pp. 2438-2440, Jul 2007.

[18] E.H. Bhuiyan, Y.H. Park, S. El-Ghazaly, V. Nair, H. Goronkin, "Active Tuning and Miniaturization of Microstrip Antennas", *IEEE Antennas Propag. Society Int. Symp. Dig.*, pp. 10-13, San Antonio, TX, USA, June 2002.

[19] R.C. Hansen, and M. Burke, "Antennas With Magneto-Dielectrics", Microw. Opt. Technol. Lett., vol. 26, no. 2, pp. 75-78, June 2000.

[20] P.M.T. Ikonen, S.I. Maslovski, C.R. Simovski, and S.A. Tretyakov, "On Artificial Magnetodielectric Loading for Improving the Impedance Bandwidth Properties of Microstrip Antennas", *IEEE Trans. Antennas Propag.*, vol. 54, no. 6, pp. 1654-1662, June 2006.

[21] H. Mosallaei, K. Sarabandi, "Design and Modeling of Patch Antenna Printed on Magneto-Dielectric Embedded-Circuit Metasubstrate", *IEEE Trans. Antennas Propag.*, vol. 55, no. 1, pp. 45-52, Jan. 2007.

[22] H. Mosallaei, K. Sarabandi, Reply to "Comments on 'Design and Modeling of Patch Antenna Printed on Magneto-Dielectric Embedded-Circuit Metasubstrate'", *IEEE Trans. Antennas Propag.*, vol. 55, no. 10, pp. 2936-2937, Oct. 2007.

[23] W. Abdouni, A.-C. Tarot, A. Sharaiha, "Simple Manufacturing Process of an Artificial Magneto-Dielectric Substrate Applied to Planar Antennas", *Proc. Metamaterials 2008*, Pamplona, Spain, Sep. 2008.

[24] F. Bilotti, A. Alù, L. Vegni, "Design of Miniaturized Metamaterial Patch Antennas with μ-Negative Loading", *IEEE Trans. Antennas Propag.*, vol. 56, no. 6, pp 1640-1647, June 2008.

[25] A. Alù, F. Bilotti, N. Engheta, L. Vegni, "Subwavelength, Compact, Resonant Patch Antennas Loaded with Metamaterials", *IEEE Trans. Antennas Propag.*, vol. 55, no. 1, pp. 13-25, Jan. 2007.

[26] CST Microwave Studio 5.0 (3D EM Simulation). Available at: http://www.cst.com.

[27] F. Bilotti, A. Toscano, and L. Vegni, "Design of spiral and multiple split-ring resonators for the realization of miniaturized metamaterial samples", *IEEE Trans. Antennas Propag.*, vol. 55, no. 8, pp 2258-2267, Aug. 2007.

[28] Y. Lee, Y. Hao, "Characterization of Microstrip Patch Antennas on Metamaterial Substrates Loaded with Complementary Split-Ring Resonators", *Microw. Opt. Technol. Lett.*, vol. 50, no. 8, pp. 2131-2135, Aug. 2008.

[29] Ansoft HFSS, 3D Full-wave Electromagnetic Field Simulation, Available at: http://www.ansoft.com/hfss/.

[30] I.S. Nefedov, A.C. Tarot, K. Mahdjoubi, "Wire Media - Ferrite Substrate for Patch Antenna Miniaturization", *International Workshop on Antenna Technology: Small and Smart Antennas, Metamaterials and Applications*, 2007.

[31] R.V. Petrov, A.S. Tatarenko, G. Srinivasan, and J.V. Mantese, "Antenna Miniaturization with Ferrite-Ferroelectric Composites", *Microw. Opt. Technol. Lett.*, vol. 50, no. 12, pp. 3154-3157, Dec. 2008.

[32] EDA Board, Available at: http://www.edaboard.com.

[33] L.I. Basilio, M.A. Khayat, J.T. Williams, S.A. Long, "The Dependence of the Input Impedance on Feed Position of Probe and Microstrip Line-Fed Patch Antennas", IEEE Trans. Antennas Propag., vol. 49, no.1, pp. 45-47, Jan. 2001.

[34] P.M.T. Ikonen, S.A. Tretyakov, "On the Advantadges of Magnetic Materials in Microstrip Antenna Miniaturization", *Microw. Opt. Technol. Lett*, vol. 50, no. 12, Dec. 2008.

[35] P.J. Ferrer, J.M. González-Arbesú, J. Romeu, and A. Cardama, "Bidirectional Artificial Magnetic Reflectors at Microwave Frequencies", *Microw. Opt. Technol. Lett.*, vol. 49, no. 8, pp. 1949-1953, Aug. 2007.

[36] P.J. Ferrer, J.M. González-Arbesú, J. Romeu, "Design and Measurement of a Spiral-Cell PMC for Metamaterial Applications", *IEEE Antennas Propag. Society Int. Symp. Dig.*, pp. 31-34, Albuquerque, NM, USA, July 2006.

[37] R.W. Ziolkowski, "Design, Fabrication, and Testing of Double Negative Metamaterials", *IEEE Trans. Antennas Propag.*, vol. 51, no. 7, pp. 1516-1529, July 2003.

[38] C. Xudong, C. Hafner, K. Tavzarashvili, R. Vahldieck, "Parameters Extraction from Homogeneous Metamaterials with Model Based Parameter Estimation", *11th Int. Conf. Mathematical Methods in Electromagnetic Theory*, Kharkiv, Ukraine, June 26-29, 2006.

[39] A. Semichaevsky, A. Akyurtlu, "Homogenization of Metamaterial-Loaded Substrates and Superstrates for Antennas", *Progress in Electromagnetics Research*, PIER 71, pp. 129-147, 2007.

[40] A. Alù, N. Engheta, "On Role of Random Disorders and Imperfections on Performance of Metamaterials", *IEEE Antennas Propag. Society Int. Symp. Dig.*, pp. 2897-2900, Honolulu, HW, USA, June 2007.

[41] EM Talk, Available at: http://www.emtalk.com/tutorials.htm.

[42] R.H. Johnston, and J.G. McRory, "An Improved Small-Antenna Radiation Efficiency Measurement Method", *IEEE Antennas Propag. Mag.*, vol. 40, no. 5, pp. 40-48, Oct. 1998.

[43] P. Miškovský, J.M. González-Arbesú, J. Romeu, "Antenna Radiation Efficiency Measurement in an Ultra-Wide Frequency Range", *IEEE Antennas Wireless Propag. Lett.*, Accepted for future publication in 2009.

[44] B.A. Austin, "Resonant Mode Limitations with the Wheeler Method of Radiation Efficiency Measurement", *IEEE Colloquium on Advances in the Direcct Measurement of Antenna Radiation Characteristics in Indoor Environments*, 1989, pp.7/1-7/4

Appendix A

Patch Antennas Filled with Air

This chapter is devoted to the study of which effects the variation of certain physical parameters of a reference patch antenna cause in the matching, bandwidth and some other basic antenna features.

Ansoft HFSS v11 [29], a finite element method (FEM) software has been used to perform the simulations.

A.1 Main Antenna Parameters Variation

As the main objective is to observe the changes which the variation of certain antenna parameters cause to its FBW, return losses and input impedance mainly, the antenna to consider as a reference in the following simulations does neither have to be perfectly adjusted to resonate at 2.45GHz nor to be perfectly matched at 2.45GHz.

Fig. A.1 shows the sketch of the patch antenna and Table A.1 the initial values of the reference antenna. The main simulation analysis conditions to obtain the results are gathered in Table A.2. The Air Box surrounding the structure is set to a quarter-wavelength of the frequency of interest (2.45GHz) distance in the direction of the radiated field [41]. The pin probe distance (x_0) from the centre of the patch to the edge is fixed to 10 mm.

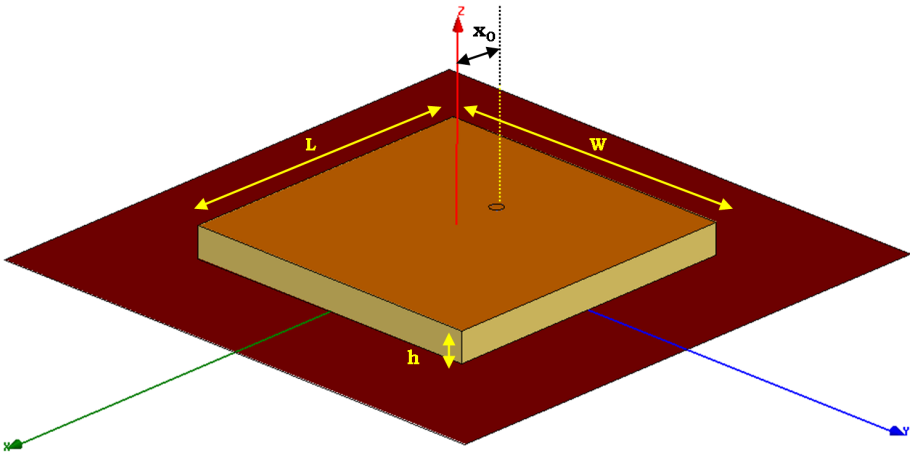

Figure A.1: Reference patch antenna.

	Patch	Substrate	Ground plane
Width [mm]	54.56	54.56	λ_0
Length [mm]	54.56	54.56	λ_0
Height [mm]	——	3	——

Table A.1: Main reference antenna parameters.

Solution Setup	
Solution frequency	3.8GHz
Sweep	
Sweep Type	Fast
Step Size (Linear Step)	0.001 GHz
Start	1 GHz
Stop	4 GHz

Table A.2: Simulation conditions used.

It has been said that the values in Table A.1 for the reference patch antenna size are *"initial"*. That is said because the antenna filled with air, which will always be our reference in all the studies that are carried out throughout the present work, will suffer some modifications in size depending on the circumstances. For instance, these initial values are slightly changed when the precise tuning of the antenna is needed (see Chapter 3, where the reference case is changed with the design criterion).

A.1.1 Ground Plane Size

The ground plane size is one of the parameters which is going to maintain its reference size through all the chapters. That reference value is a free-space wavelength at the desired antenna operational frequency, f_0=2.45GHz. This value is considered sufficiently large to avoid possible resonant effects that may appear when having a finite ground plane.

The ground plane size is varied from 70% of λ_0 (55mm) to a 175% of λ_0 (215mm). The simulated results have been plotted in Fig. A.2.

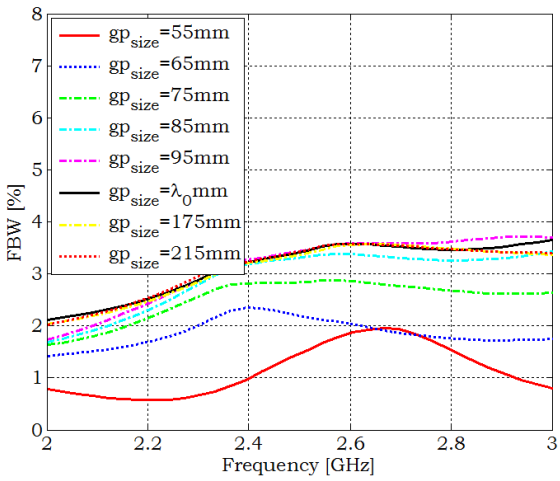

Figure A.2: Antenna FBW_{-10dB} when the ground plane size is increased.

The effect that the ground plane size has in the maximum FBW achievable is clear: for smaller ground planes the matched bandwidth decreases. However, from 85mm to 215mm the change in FBW value around f_0 is not significant.

In Fig. A.3, it can be observed how in terms of input impedance the cases which are further from the reference λ_0-sized ground plane one are the one with almost the same size than the patch (55mm) and the 65mm one. The reflection coefficient is better than -20dB (a good 50Ω-matching level) except for the same cases commented before, where the 50Ω-matching level decreases.

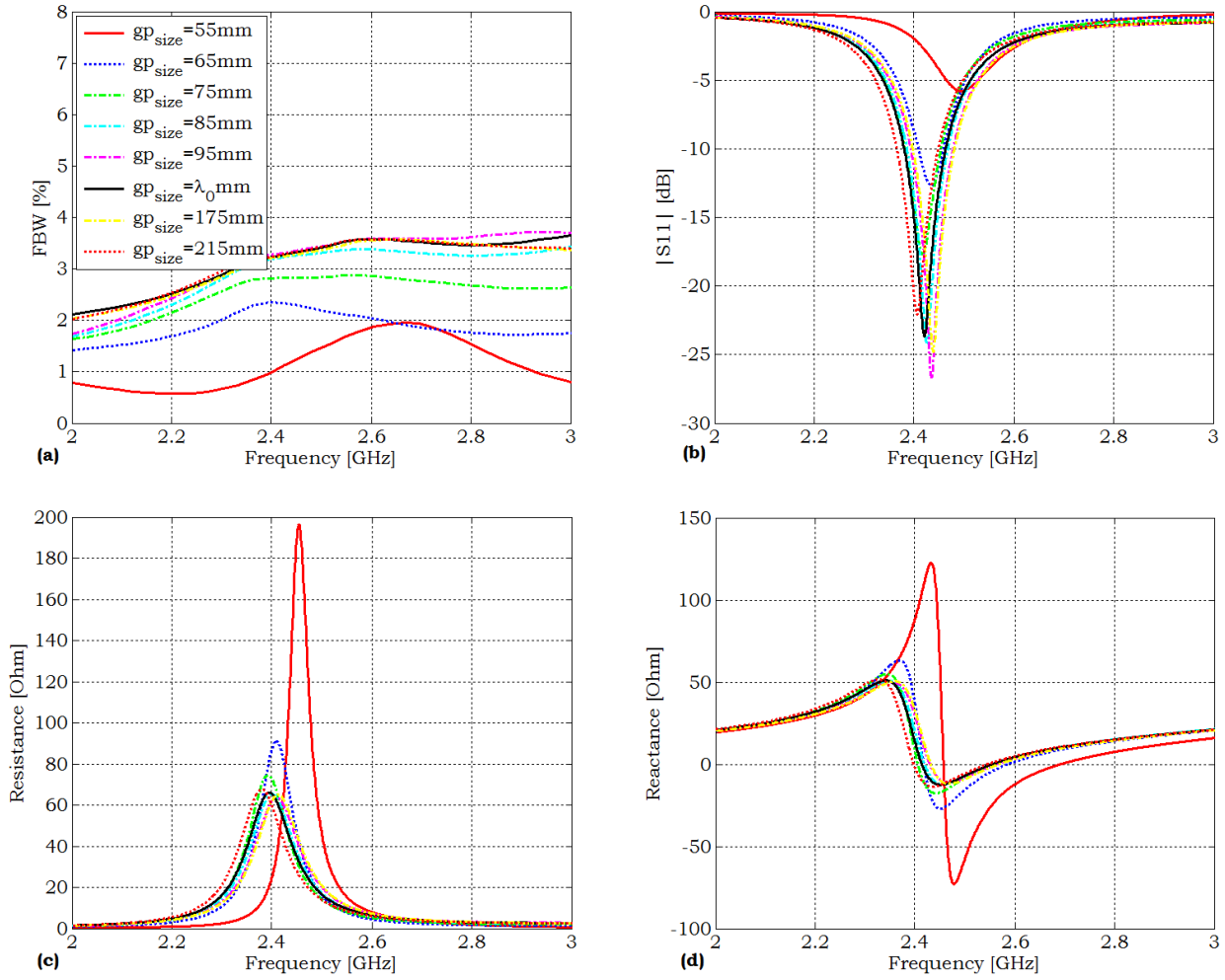

Figure A.3: Antenna (a) FBW_{-10dB}, (b) magnitude of the simulated reflection coefficient and (c and d) input impedance when the size of the ground plane is varied.

In order to check whether the antenna is radiating properly, three plots of the directivity radiation pattern are shown in Fig. A.4. All of them are computed at the resonant frequency (2.45GHz) of the antenna. As it can be observed, the antenna radiates effectively like a patch antenna for the (b) and (c) cases. In (a) the ground plane is too shrunk, thus affecting the radiation in the broadside direction. The 85mm-sized ground plane demonstrates to have a good radiation behaviour altogether with a good FBW, hence proving that the criterion to take a λ_0-sized ground plane is a criterion taken by excess.

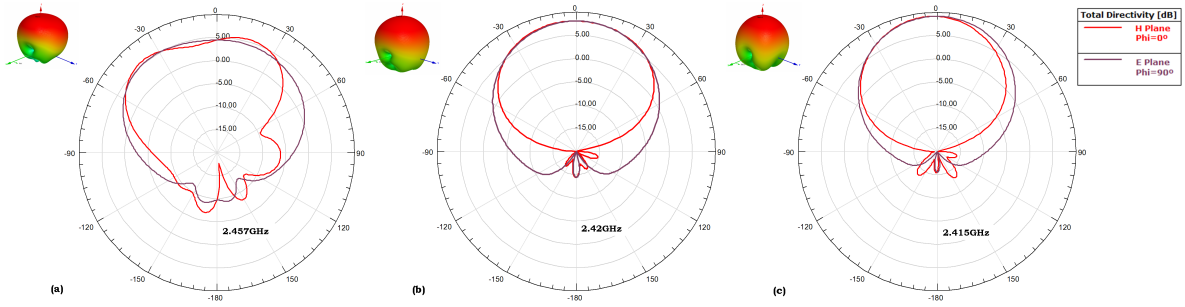

Figure A.4: Directivity radiation pattern for (a) patch-sized ground plane, (b) 85mm-sized ground plane and (c) ground plane of $\lambda_0$mm.

A.1.2 Substrate Height

A microstrip line conducts better (radiates less) when the substrate height decreases, however in antenna applications the objective is precisely to radiate. When the separation between the patch and the ground plane increases the fringing fields at the edge of the patch are stronger and the electric field under the patch becomes weaker. A consequence is that the energy trapped in the patch antenna becomes lower thus leading to lower Q values. This yields an improvement in the impedance FBW.

The substrate thickness is varied from 1mm to 8mm. The maximum computed FBW on each case can be observed in Fig. A.5.

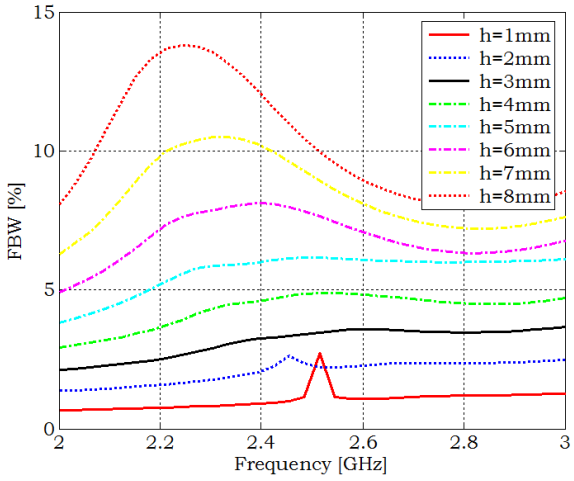

Figure A.5: Antenna FBW_{-10dB} when the substrate height is varied.

As expected, the substrate height increase produces higher FBW values. However, if the input impedance is observed (Fig. A.6), the 5mm-high substrate antenna does not resonate and neither the ones with higher substrates. Nevertheless, the FBW computed through the matched bandwidth formula informs us about the maximum achievable FBW if the antenna was tuned.

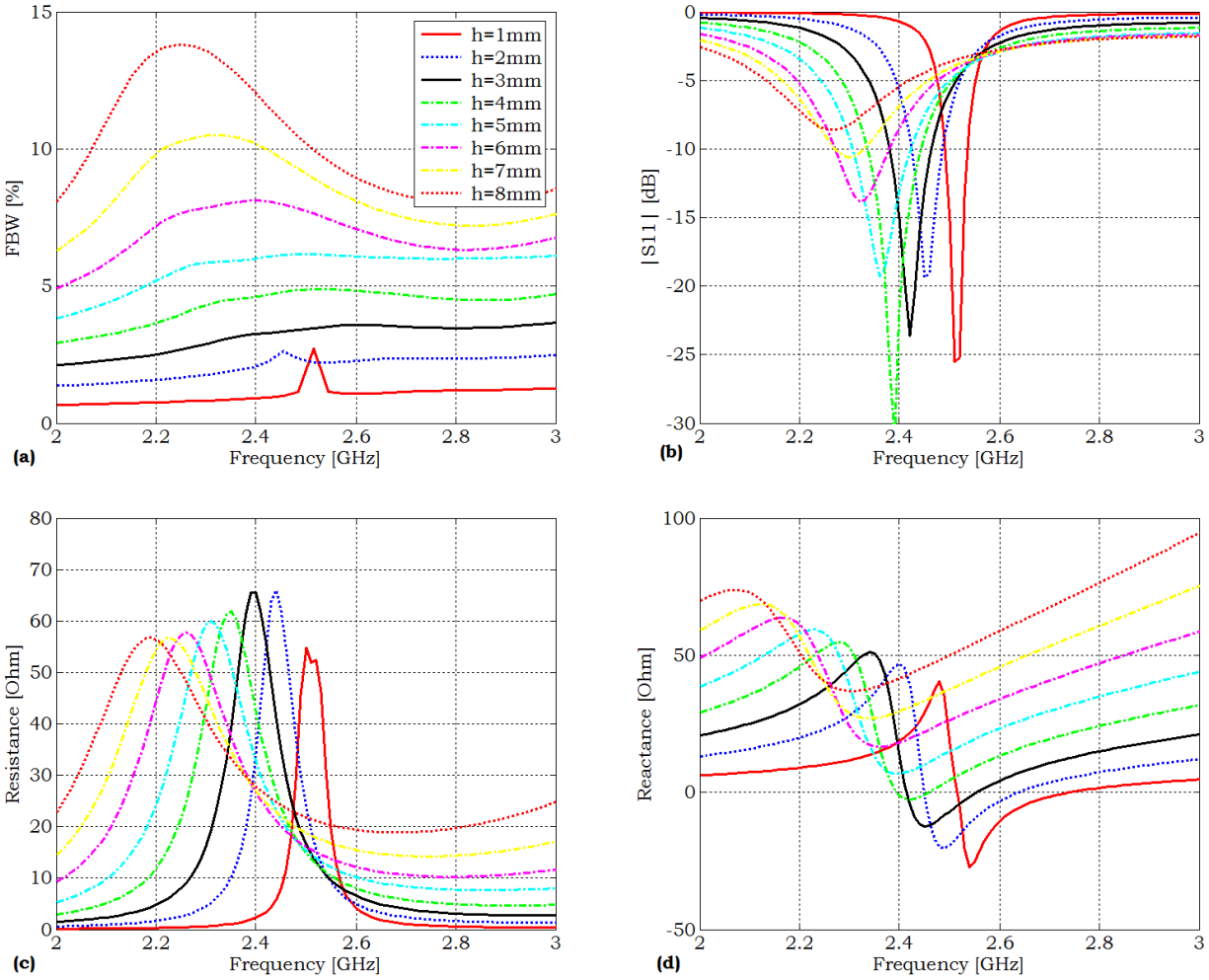

Figure A.6: Antenna (a) FBW_{-10dB}, (b) magnitude of the simulated reflection coefficient and input resistance (c) and reactance (d) when the thickness of the substrate is increased from 1mm to 8mm.

Among this results, a thickness of 3mm will be used as a reference for the dielectric height.

A.1.3 Feed Position

A typical current distribution on the patch surface could be the one shown in Fig. A.7 (it depends on the TM mode excited, the number of resonances[1]). The current distribution (magnetic field) is minimal

[1] In fact, this Figure shows the imaginary part of the current. At the resonant frequency the imaginary part dominates over the real one. In addition the imaginary part is independent of the coaxial position, whilst the real one mostly

near the edges of the patch, while maximum at its centre. On the contrary the electrical field (voltage) is zero in the patch centre and maximal near the edges. This way, the patch surface impedance has a cosine-over-two-like [33] distribution being minimal at the centre of the patch and maximum at the edges. So there is a point somewhere along the resonant length of the patch where the impedance is near to 50Ω.

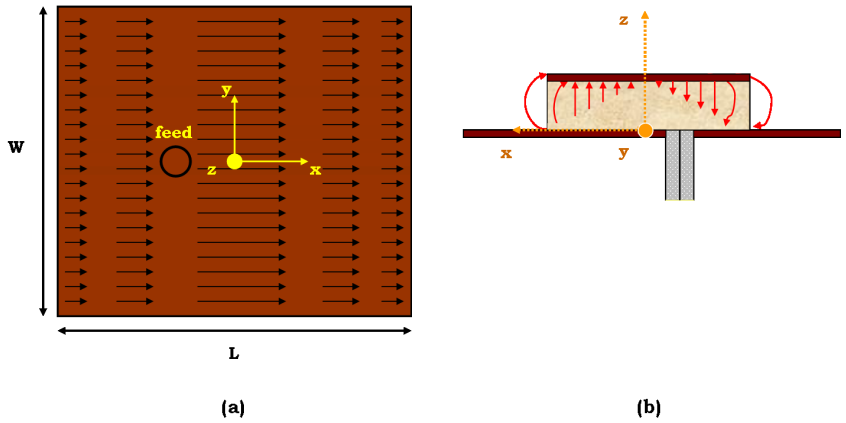

Figure A.7: Typical (a) current distribution on the patch surface and (b) electric field inside the patch.

Precisely because the patch impedance varies along the patch length, by moving the feed point the input impedance seen after de-embedding (the input impedances shown in the figures correspond with the ones seen right on the patch surface) changes its value. The results for the maximum achievable matched bandwidth is shown in Fig. A.8.

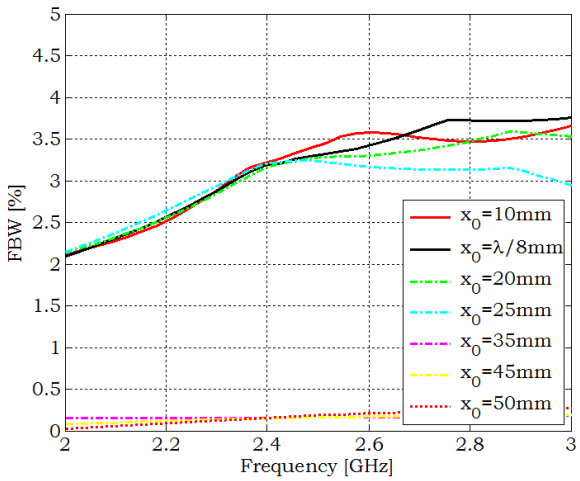

Figure A.8: Antenna FBW_{-10dB} when the pin probe coaxial varies its position along the patch length.

depends on this [13].

Significant changes in the final matched bandwidth are not observed. It can not be said the same for the return losses (Fig. A.9). But as it has been said and remembered many times, the Yaghjian's FBW formulation considers the antenna tuned and matched at each and every frequency.

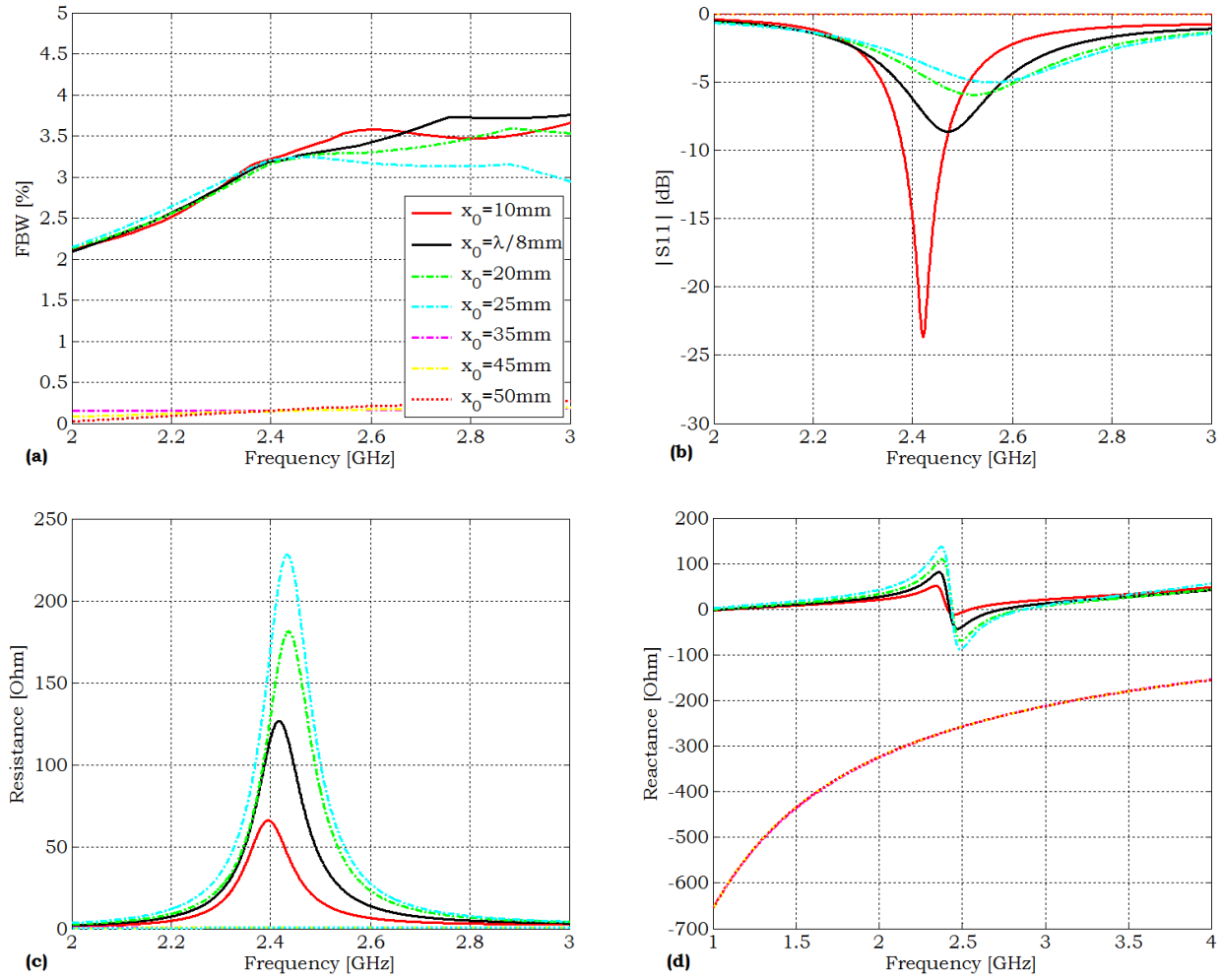

Figure A.9: Antenna FBW_{-10dB} (a), magnitude of the simulated reflection coefficient (b) and input resistance (c) and reactance (d) when the position of the antenna feeding is varied from the center to the edge of the patch.

Directivity radiation patterns are obtained for two feed positions: (a) pin at $\frac{\lambda}{8}$ from the centre of the patch and (b) pin at the centre of the patch (Fig. A.10). It is easy to see that when the feeding is correctly placed the antenna radiates properly, while when the feeding is wrongly placed (at the centre of the patch) the antenna radiates like a monopole rather than like a patch antenna.

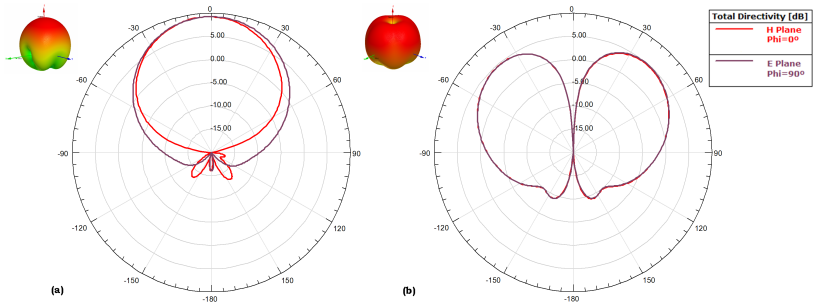

Figure A.10: Directivity radiation patterns for two different feeding positions: (a) pin at $\frac{\lambda}{8}$ from the patch and (b) pin at the centre of the patch.

A.2 Reference Patch Antenna

The reference patch antenna with air filling is defined in order to compare the results that will be obtained varying the substrate properties.

In Chapter 3 the antenna size and probe pin position will vary depending on whether the parameter adjusted to compare antenna designs when changing the substrate characteristics is the reactance (to make the antenna resonat at f_0) or the return loss value (to match the antenna to a given reference resistance value).

In Chapter 4, where dispersive values of μ_r and ε_r will be considered, the reference patch antenna may suffer physical modifications if the comparison with the metamaterial loaded ones has in mind to compare the frequency where the maximum FBW achievable is maximum, or the resonant frequency, for example. It will also change when the height of the metamaterial loaded antenna will vary from the height considered in Chapter 3.

In any case, the reference patch antenna will have: patch-sized substrate, coaxial feeding and rectangular shape.

Appendix B

Patch Antenna Filling: Homogeneous Substrates

B.1 Substrate Parameters Variation

In order to understand more deeply the statements found in Chapter 3, some of the Figs. which have been omitted for the sake of brevity are exposed in the following sections.

The first simulation results are obtained applying the S_{11} *minimum at* f_0 *method*.

B.1.1 ε_r variation

The complete set of Figs. obtained for the first criterion applied to design the antenna (to adjust the matching to 50Ω with a level of approximately -20dB of reflection coefficient value and centred at 2.45GHz) when $0 < \varepsilon_r < 1$ is shown in the Fig. B.1.

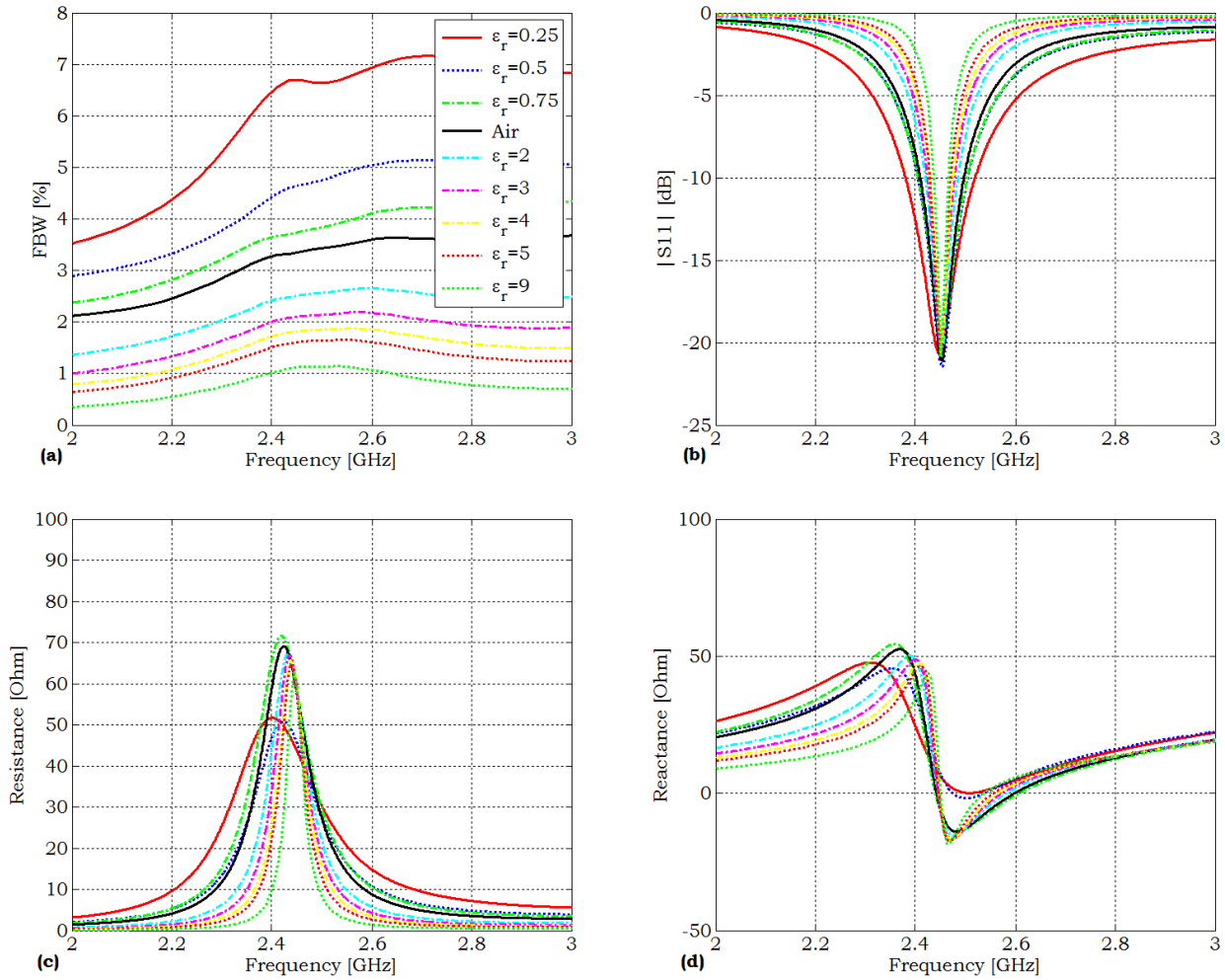

Figure B.1: Antenna (a) FBW_{-10dB}, (b) magnitude of the simulated reflection coefficient, (c) input resistance and (d) input reactance.

B.1.2 μ_r variation

Maximum achievable FBW, return losses and antenna input impedance when $0 < \mu_r < 10$ are depicted in the following figure:

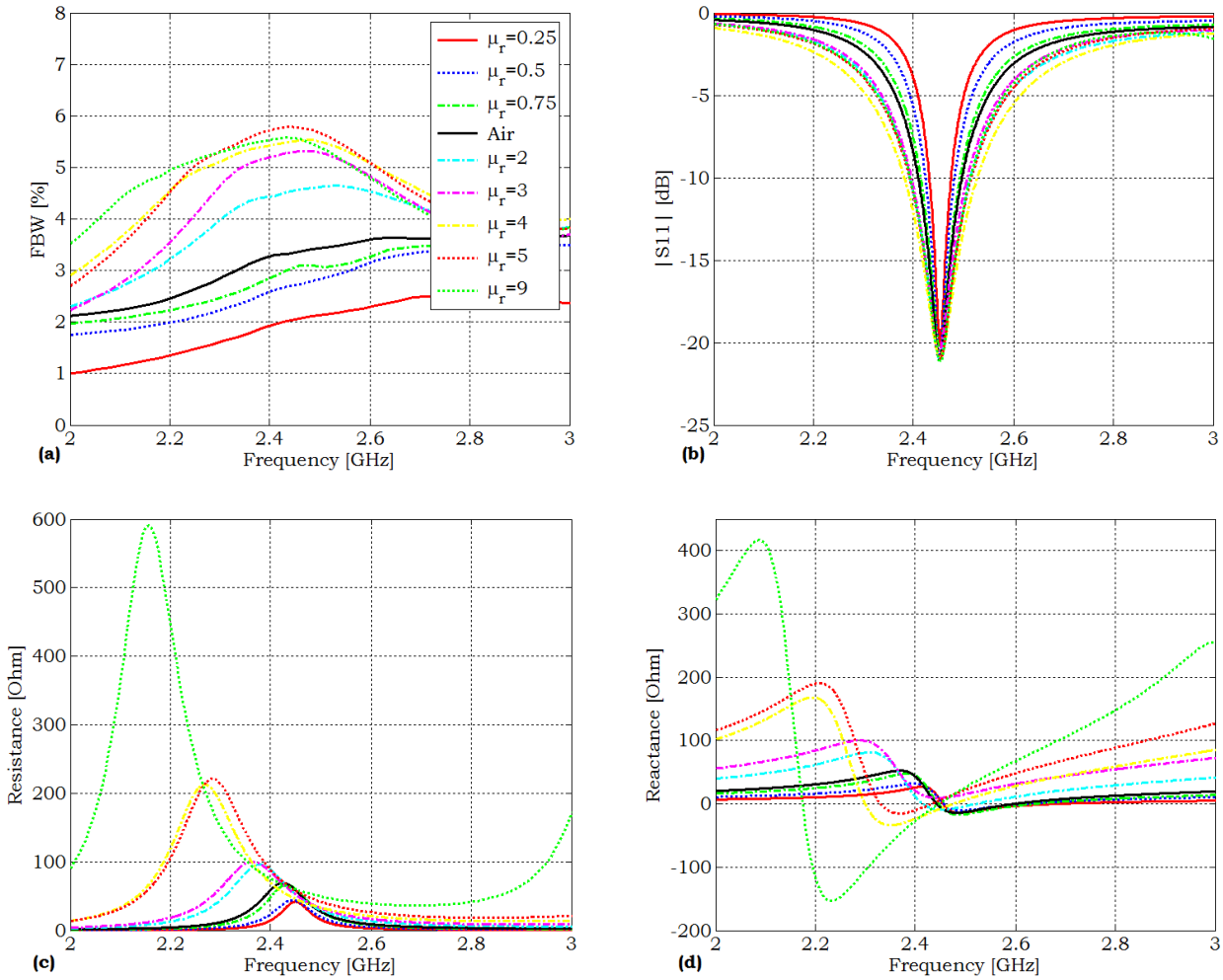

Figure B.2: Antenna (a) FBW_{-10dB}, (b) magnitude of the simulated reflection coefficient, (c) input resistance and (d) input reactance.

B.1.3 Product $\varepsilon_r \cdot \mu_r$ variation

Both ε_r and μ_r are varied, with $\varepsilon_r = \mu_r$:

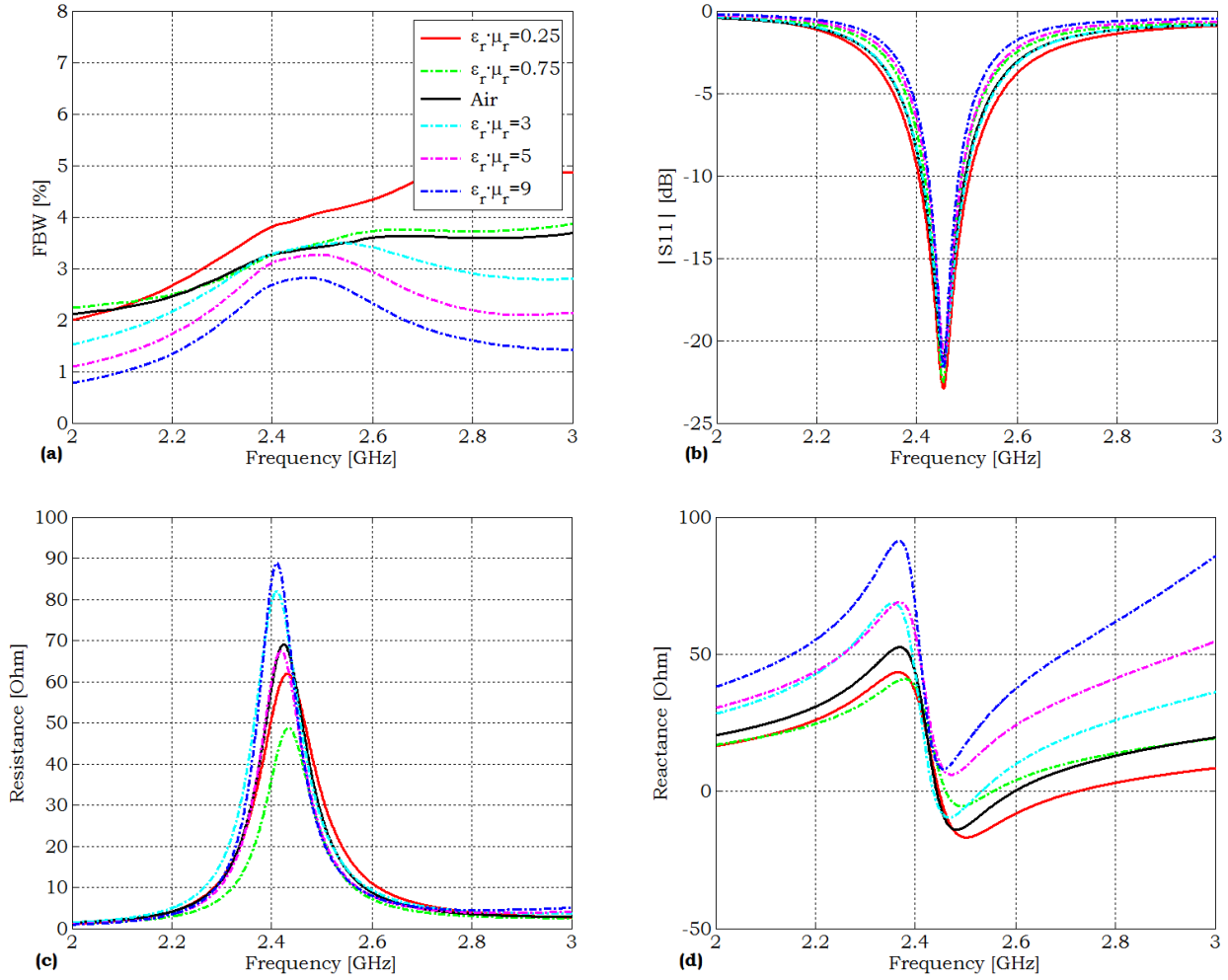

Figure B.3: Antenna (a) FBW_{-10dB}, (b) magnitude of the simulated reflection coefficient, (c) input resistance and (d) input reactance.

B.2 Lossy Substrates

Fig. B.4 and B.5 are clear: when the losses in the substrate increase, the FBW values become higher. The trade-off is that the radiation efficiency decreases, and having the same radiation pattern shape the gain of the antenna is reduced.

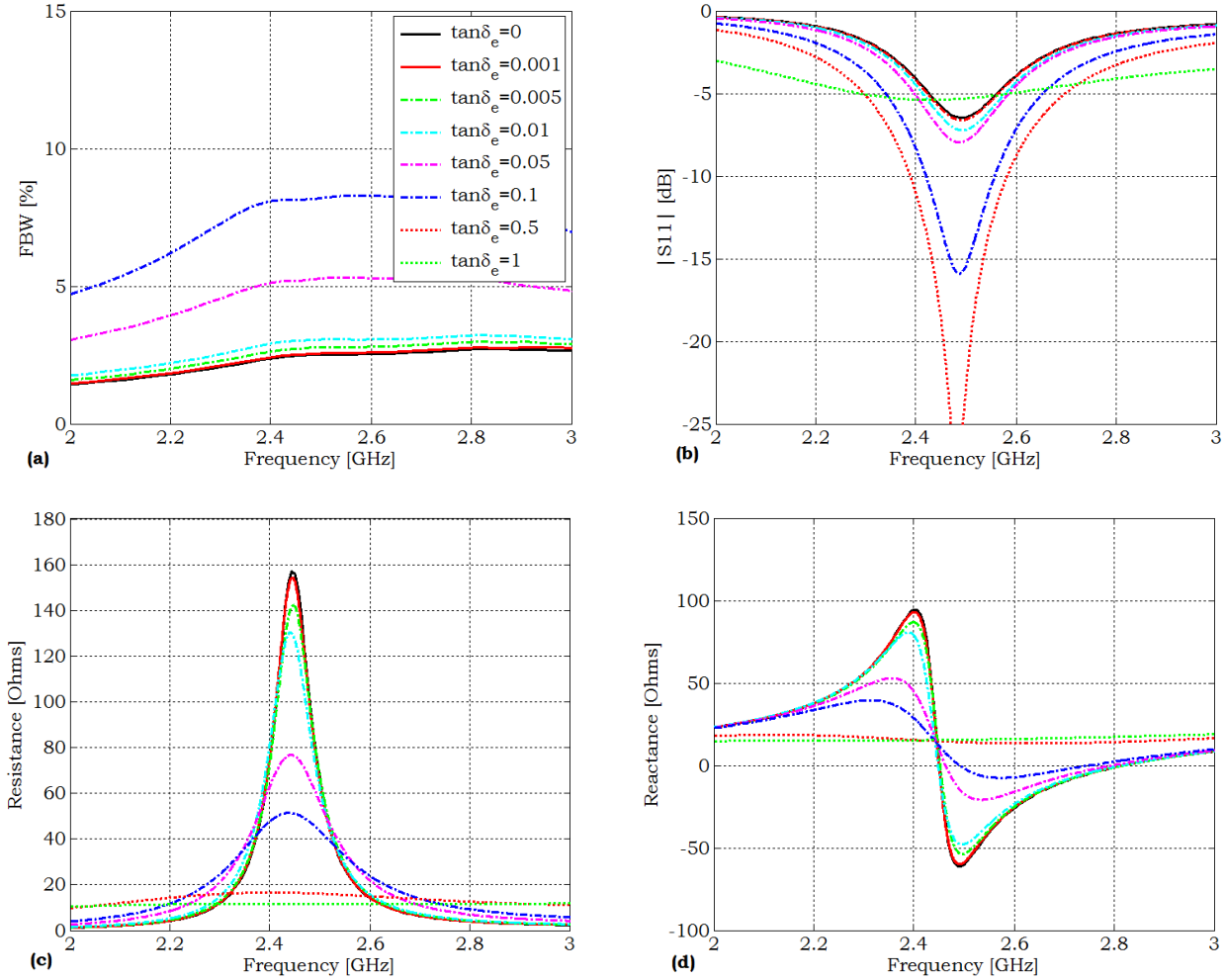

Figure B.4: Antenna FBW_{-10dB} (a), magnitude of the simulated reflection coefficient (b) and input impedance (c,d) when increasing $\tan\delta_e$.

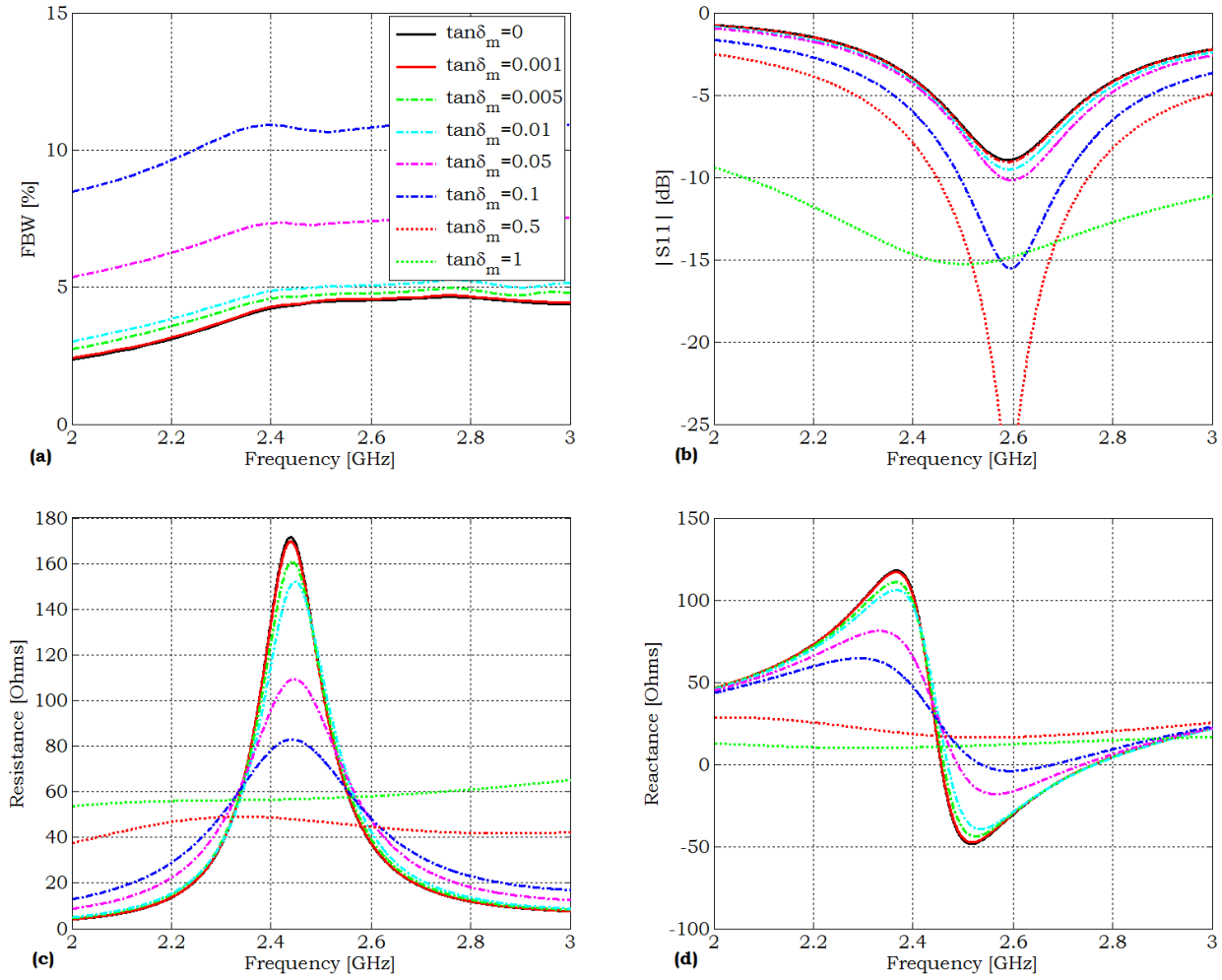

Figure B.5: Antenna FBW_{-10dB} (a), magnitude of the simulated reflection coefficient (b) and input impedance (c,d) when $\tan\delta_m \uparrow\uparrow$.

B.3 Antenna Design Methods

The results obtained are not the same when the criterion of design is to make the antenna resonant at a desired frequency than when the method followed has being to adjust the return loss value to a fixed threshold around the frequency of design. For that reason, different antenna design methods are analysed.

B.3.1 Im{Z_0}=0 at f_0

When the antenna is designed to have a natural resonance at f_0 (2.45GHz), the trend of the FBW and other characteristic parameters can be observed in: Fig. B.6 when ε_r is incresed, Fig. B.7 when the μ_r is increased and Fig. B.8 when $\varepsilon_r = \mu_r$ are increased.

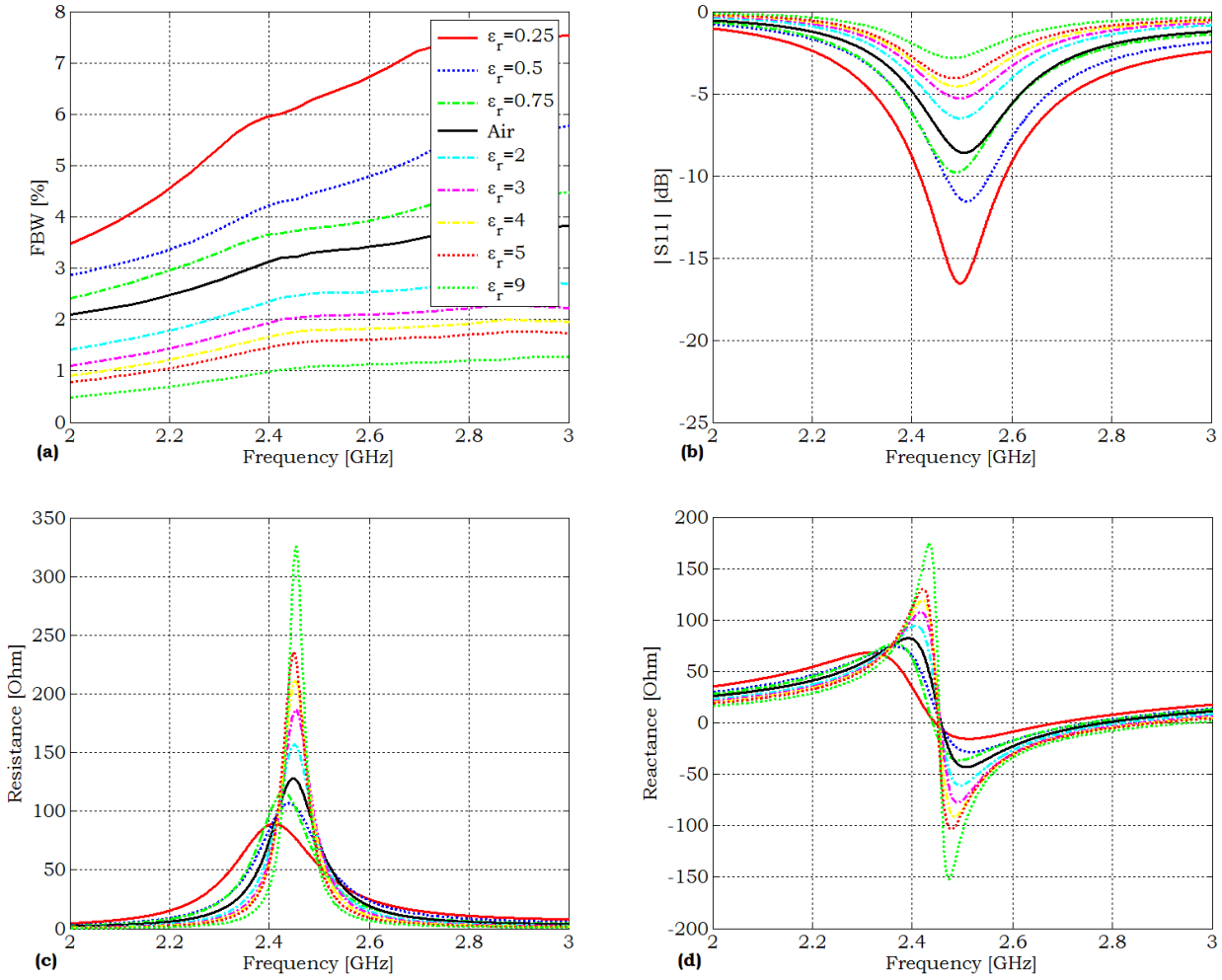

Figure B.6: Antenna (a) FBW_{-10dB} , (b) magnitude of the simulated reflection coefficient and (c,d) input impedance when $0 < \varepsilon_r < 10$.

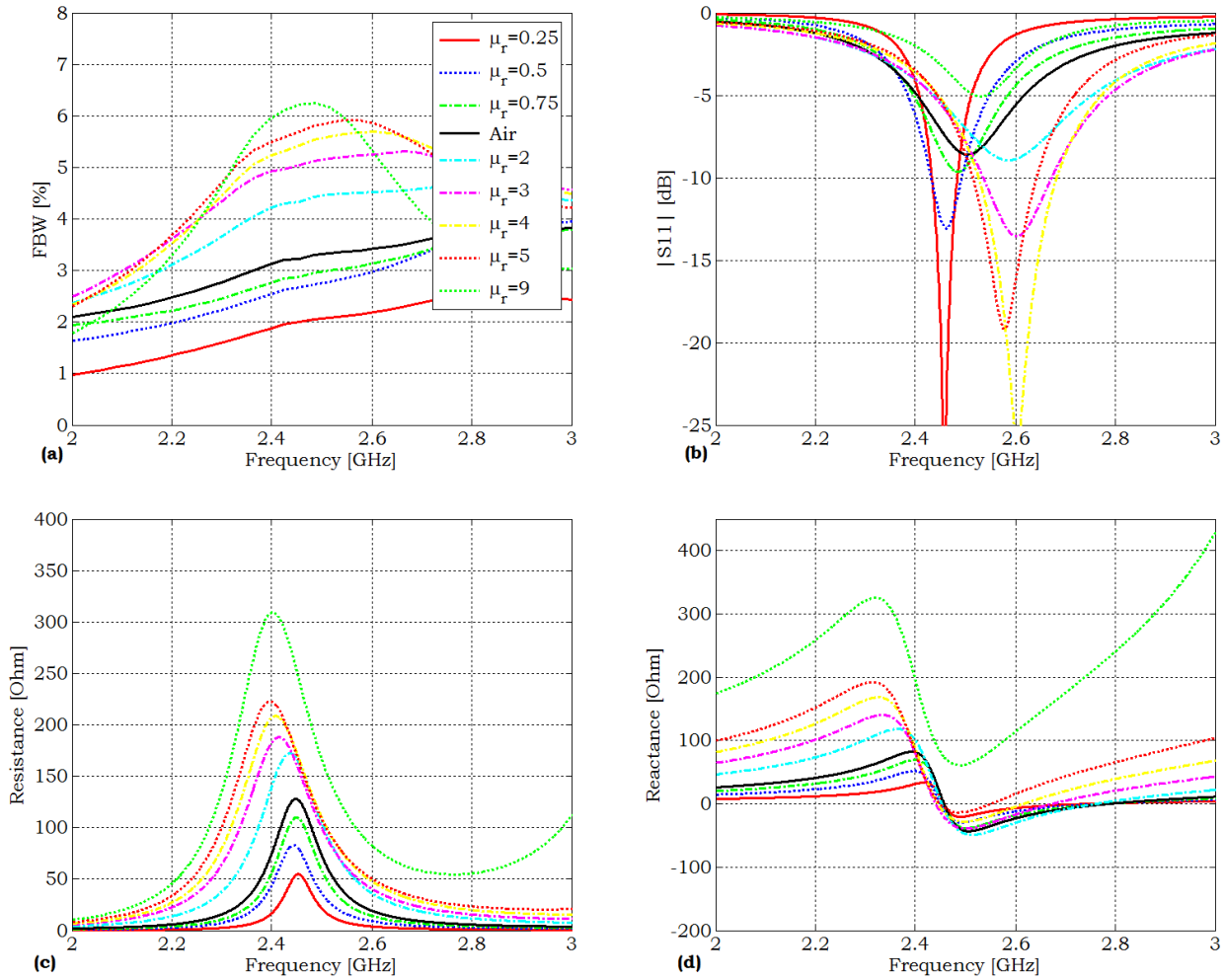

Figure B.7: Antenna (a) FBW_{-10dB}, (b) magnitude of the reflection coefficient and (c,d) input impedance when $0 < \mu_r < 10$.

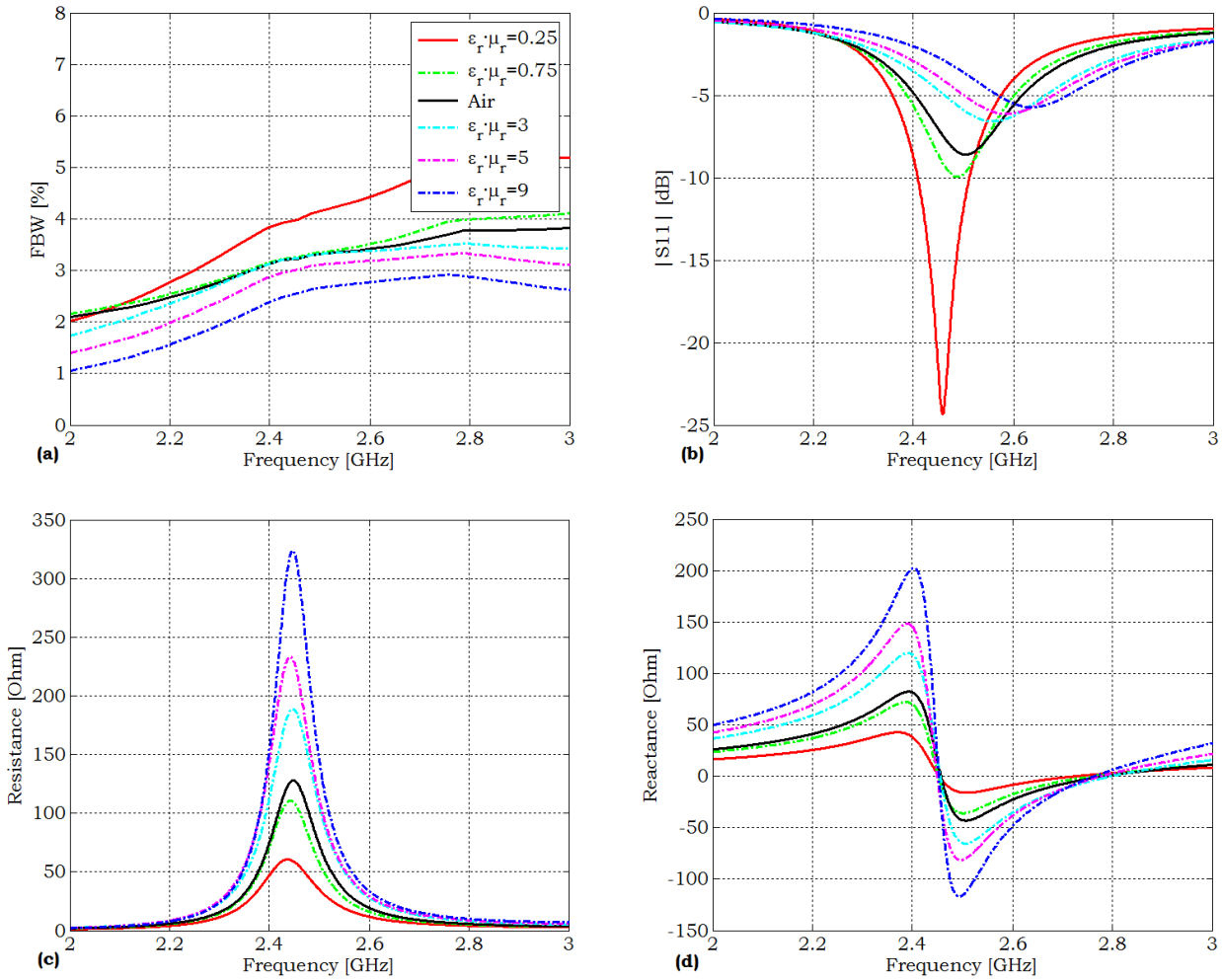

Figure B.8: Antenna FBW_{-10dB} (a), magnitude of the simulated reflection coefficient (b) and input impedance (c,d) when $\varepsilon_r \cdot \mu_r \uparrow\uparrow$ being $\varepsilon_r = \mu_r$.

B.3.2 Blind method

This is the also called *academic method*, because the resonant length of the patch is directly taken from a formula and any other adjustments are done. The figures when increasing the ε_r, the μ_r and both values (with $\varepsilon_r = \mu_r$) along with the table of input impedance at 2.45GHz values can be found in this section (Figs. B.9, B.10 and B.11).

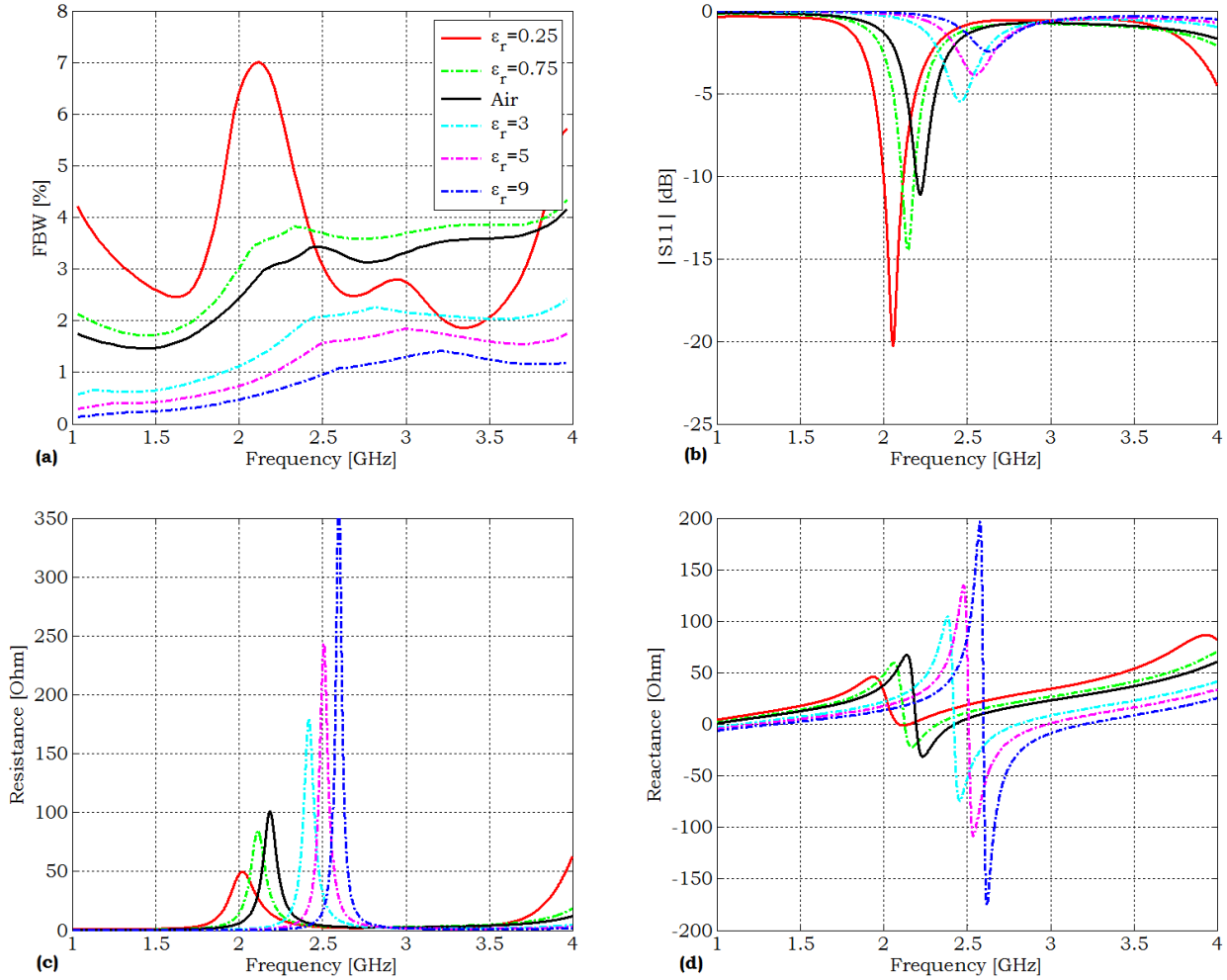

Figure B.9: Antenna FBW_{-10dB} (a), magnitude of the simulated reflection coefficient (b) and input impedance (c,d) when $\varepsilon_r \uparrow\uparrow$.

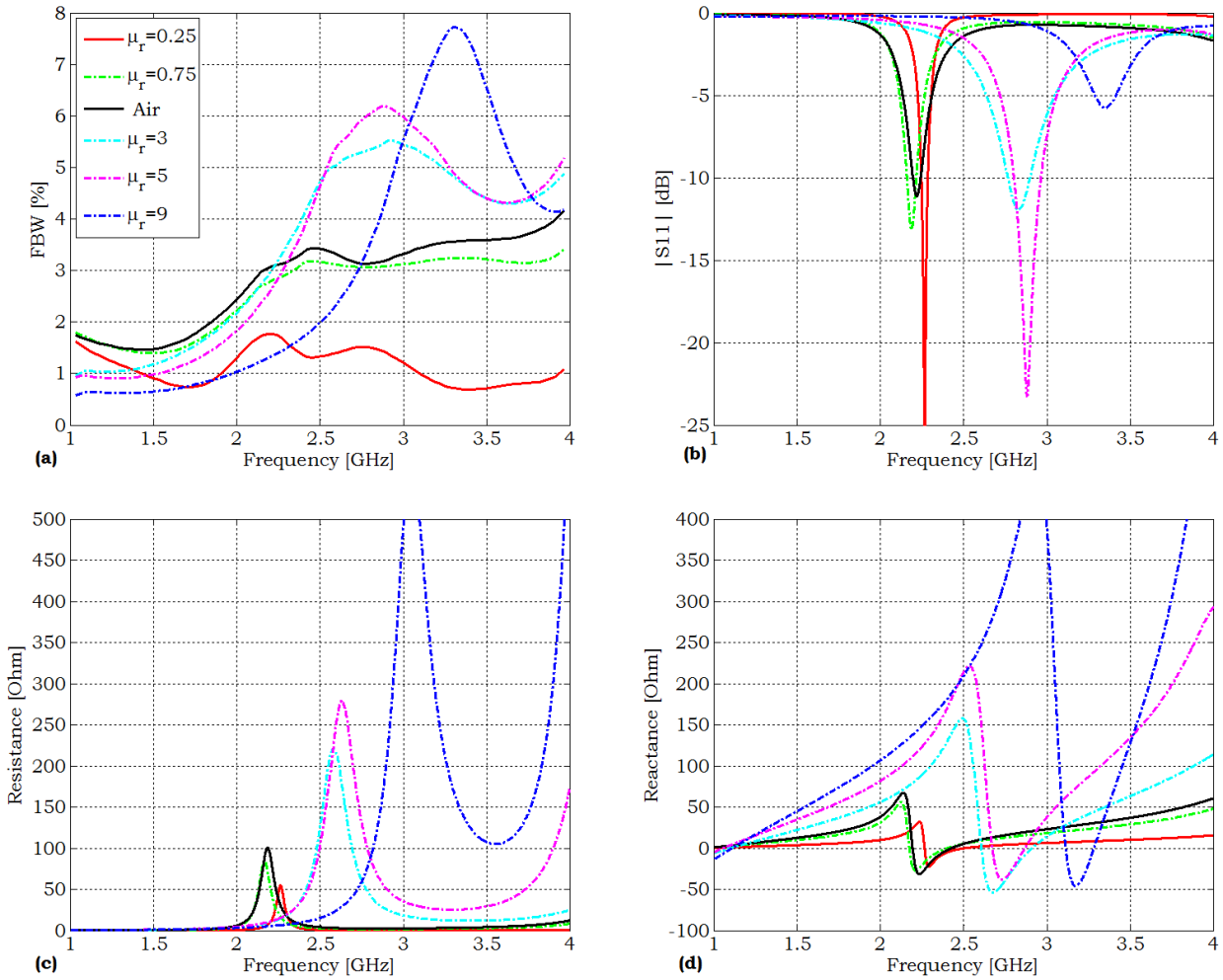

Figure B.10: Antenna FBW_{-10dB} (a), magnitude of the simulated reflection coefficient (b) and input impedance (c,d) when $\mu_r \uparrow\uparrow$.

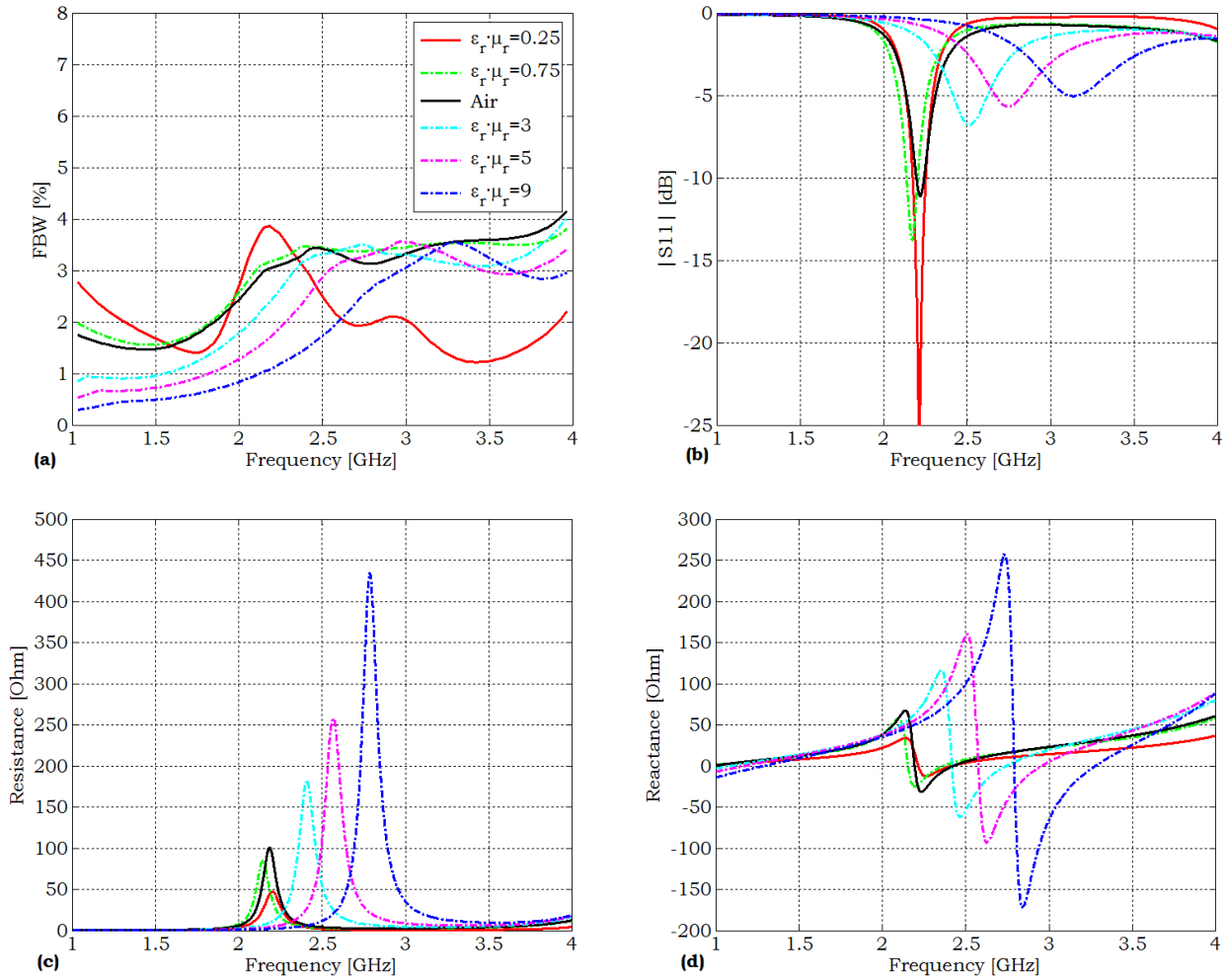

Figure B.11: Antenna FBW_{-10dB} (a), magnitude of the reflection coefficient (b) and input impedance (c,d) when $\varepsilon_r \cdot \mu_r \uparrow\uparrow$ being $\varepsilon_r = \mu_r$.

Appendix C

Patch Antenna Filling: Dispersive Substrates

C.1 Efficiency measurement

In Chapter 4, Subsection 4.4.4, the efficiency of the antenna is measured using the three caps shown in Figure C.1.

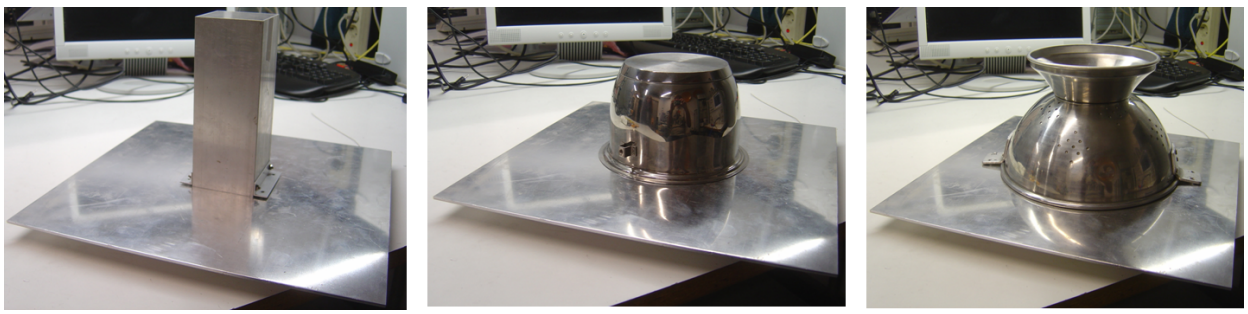

Figure C.1: Caps used to measure the antenna efficiency. W1 (left), W2 (centre) and W3 (right).

The results are shown for the cap 1 because in the bandwidth of interest this is the cap which introduces fewer resonances inherent to the cap cavity. In Figure C.2 there are the reflection coefficients of the three different caps used when the antenna covered by the cap is a monopole. The $\frac{\lambda}{4}$ monopole is used in order to investigate the frequency operating ranges and the influence of shape and size of the Wheeler cap in the results. The caps are made of aluminium.

The monopole used is approximately 3cm long (first resonance at 2.45GHz), mounted in the centre of the ground plane and at an angle of approximately 10^{o} towards a corner of the cap [44]. In Figure C.2 various of the resonant modes inherent to each cavity are visible.

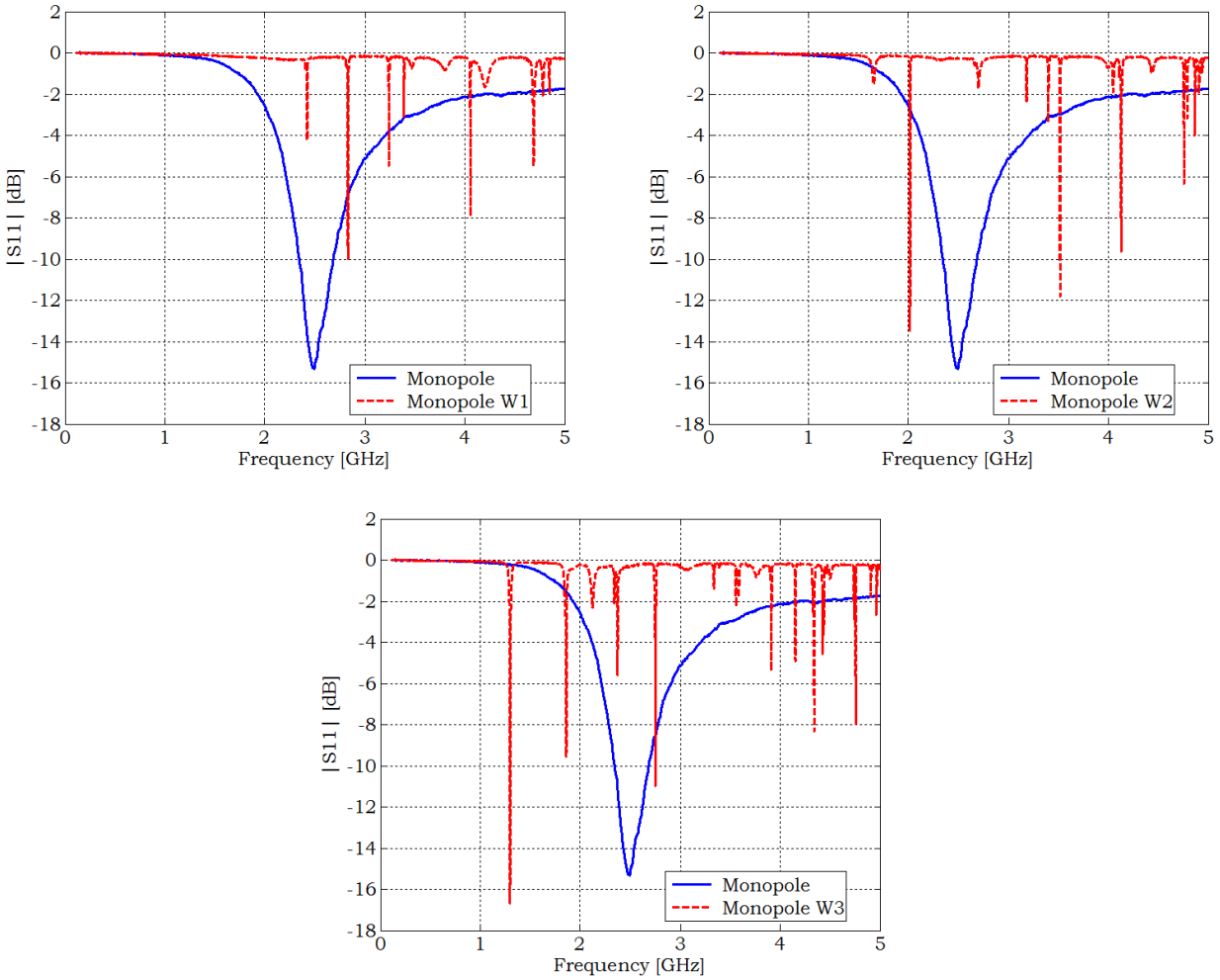

Figure C.2: Measured reflection coefficient of the monopol antenna with and without the caps: W1, W2 and W3.

The reflection coefficient post-processing for the two antenna prototypes considered in Chapter 4, Subsection 4.4.4 are shown in Figures C.3, C.4 and C.5, which are obtained when using the caps 1, 2 and 3 respectively.

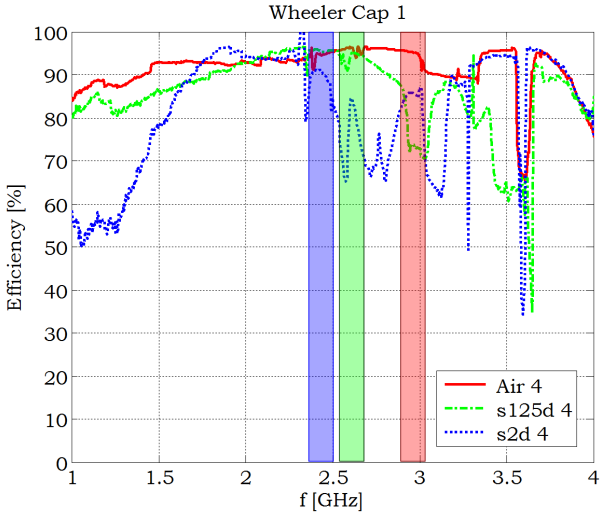

Figure C.3: Efficiency obtained when using the cap W1.

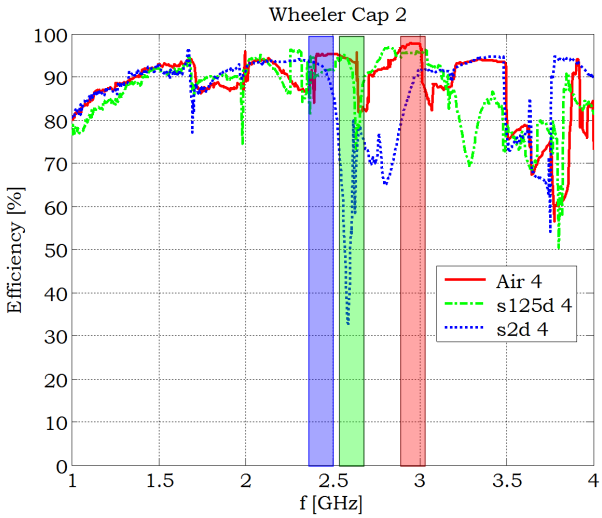

Figure C.4: Efficiency obtained when using the cap W1.

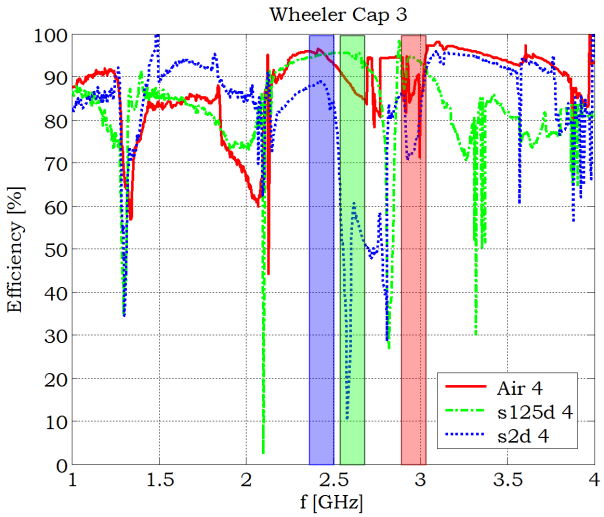

Figure C.5: Efficiency obtained when using the cap W1.

It is clear that when the cap resonances are interfering with the antenna resonances the error in the estimation of the efficiency is higher. For that reason the third cap, W3, is the one which obtains noisier efficiency results. However, from W1 and W2 it is very clear that the trend is that the antenna efficiencies with the different fillings are between 80% and 95%.

C.2 Effective Parameter Extraction

All the antennas in Chapter 4 are simulated using a full-wave simulation. This means that all the elements of the metasubstrate are modelled; from the dielectric slabs to the SRs. This kind of simulation has proved to be very accurate because the simulated results agree quite well with the measurements. However the simulations can be done introducing in HFSS the models of the permittivity and the permeability resulting from the effective parameter extraction. The results are shown in Figures C.6, C.7 and C.8 comparing the simulated reflection coefficients when the full-wave simulation is considered with the simulations taking into account the parameters extracted.

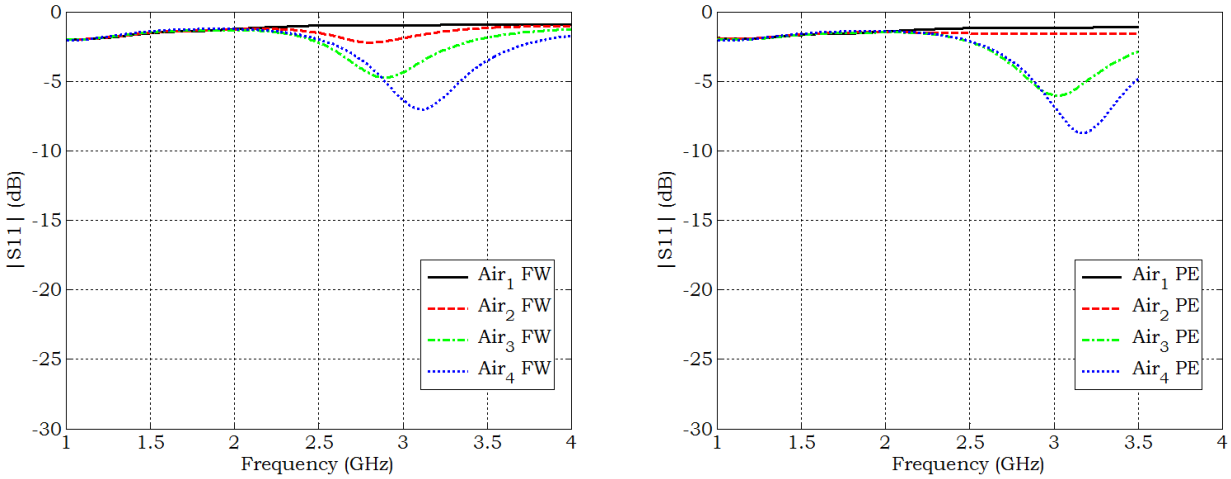

Figure C.6: Simulated reflection coefficient: full-wave model (left) and parameter extraction model (right)

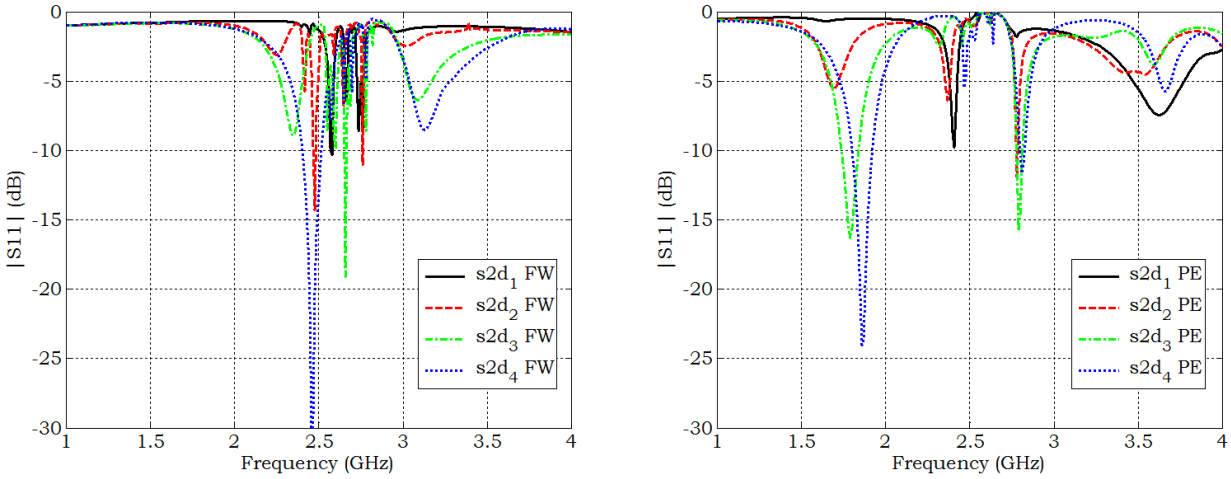

Figure C.7: Simulated reflection coefficient: full-wave model (left) and parameter extraction model (right)

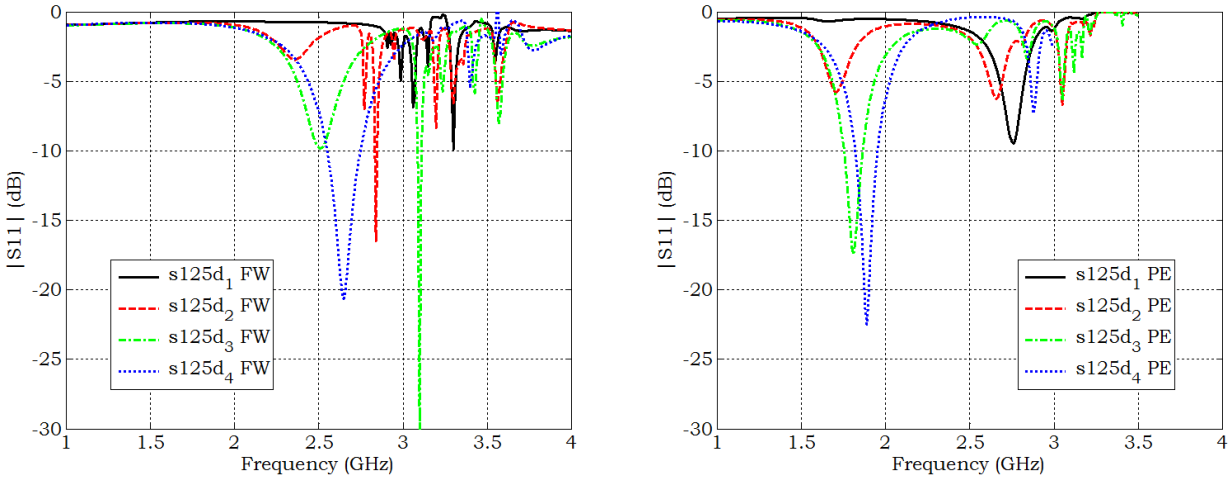

Figure C.8: Simulated reflection coefficient: full-wave model (left) and parameter extraction model (right)

In that case the parameter extraction is not suitable to predict which will be the antenna behaviour. This inaccuracies can be due to the fact that the parameter extraction IBC extrapolates an homogeneous material from a single layer SR.

Glossary

AMC	Artificial magnetic conductor
BW	Bandwidth
CSRR	Complementary split ring resonator
DNG	Double negative (medium), $\varepsilon_r < 0$,$\mu_r < 0$
DPS	Double positive (medium), $\varepsilon_r > 0$,$\mu_r > 0$
EM	Electromagnetic
ENG	Epsilon negative (medium), $\varepsilon_r < 0$, μ_r
ENZ	Epsilon near zero (medium), $0 < \varepsilon_r < 1$
FBW	Fractional bandwidth
FDTD	Finite difference time domain (method)
FEM	Finite element method
GPS	Global positioning system
GSM	Global system for mobile communications
IBC	Infinite boundary conditions
IEEE	Institute of electrical and electronics engineers
ISM	Industrial, scientific and medical (radio band)
LHM	Left handed materials $\equiv$ DNG materials
MNG	Mu negative (medium), ε_r, $\mu_r < 0$
MNZ	Mu near zero (medium), ε_r, $0 < \mu_r < 1$
MSRRs	Multiple split ring resonators

NIM	Negative index material, $n < 0$, $n = \sqrt{\varepsilon_r \mu_r}$
NRW	Nicolson Ross Weir (retrieval approach to extract material effective parameters)
PDA	Personal digital assistant
PEC	Perfect electric conductor (boundary condition)
PMC	Perfect magnetic conductor (boundary condition)
RHM	Right handed materials $\equiv$ DPS material
SR	Spiral resonator
SRR	Split ring resonator
VSWR	Voltage standing wave ratio
WiFi	Wireless fidelity (wireless quality standard)

List of Symbols

$\overrightarrow{E}$	Electric field vector
$\overrightarrow{H}$	Magnetic field vector
$\overrightarrow{k}$	Wave vector
$\overrightarrow{\beta}$	Propagating vector
$\overrightarrow{S}$	Poynting vector
ω	Angular frequency
ω_p	Electric plasma frequency
ω_{pm}	Magnetic plasma frequency
n	Refractive index, $n = \sqrt{\varepsilon_r \mu_r}$
ε	Dielectric permittivity
μ	Magnetic permeability
ε_0	Free space permittivity, $\varepsilon_0 = \frac{1}{36\pi} 10^{-9} F/m$
μ_0	Free space permeability, $\mu_0 = 4\pi 10^{-7} H/m$
ε_r	Relative permittivity
μ_r	Relative permeability
ε_{reff}	Effective (relative) permittivity
μ_{reff}	Effective (relative) permeability
Q	Quality factor
Q_{Chu}	Chu's quality factor
f_0	Operational antenna frequency (or working frequency)

k_0	Wave number at the working frequency
λ_0	Free space wavelength at the operational frequency f_0
λ_m	Wavelength in a material
ρ	Linear reflection coefficient
Γ	Reflection coefficient in dB
RL	Return lossess
$tan\,\delta_e$	Dielectric loss tangent
$tan\,\delta_m$	Magnetic loss tangent
Z_0	Antenna input impedance, $Z_0 = R_0 + j\,X_0$
R_0	Antenna input resistance
X_0	Antenna input reactance
Z_{ref}	Reference impedance
x_0	Antenna coaxial feeding position from the centre to the edge of the patch
N	Antenna miniaturization factor
η_{rad}	Radiation efficiency
$E^E{}_{copolar}$	Copolar radiation pattern E-Plane ($\varphi = 0$)
$E^E{}_{crosspolar}$	Crosspolar radiation pattern E-Plane ($\varphi = 0$)
$E^H{}_{copolar}$	Copolar radiation pattern H-Plane ($\varphi = 90$)
$E^H{}_{crosspolar}$	Crosspolar radiation pattern H-Plane ($\varphi = 90$)